

UNIVERSITAT ROVIRA I VIRGILI
DISEÑO DE CATALIZADORES PARA UNA OBTENCIÓN LIMPIA DE 2-FENILETANOL
Olga Bergadà Miró
ISBN:978-84-691-0355-5 /DL:T.2186-2007



Universitat Rovira i Virgili

Facultat de Química
Departament de Química Física i Inorgànica

Diseño de catalizadores para una obtención limpia de 2-feniletanol

Memòria de Tesi Doctoral

Olga Bergadà Miró

Tarragona, Juliol 2007

UNIVERSITAT ROVIRA I VIRGILI
DISEÑO DE CATALIZADORES PARA UNA OBTENCIÓN LIMPIA DE 2-FENILETANOL
Olga Bergadà Miró
ISBN:978-84-691-0355-5 /DL:T.2186-2007



UNIVERSITAT
ROVIRA I VIRGILI

La Dra. Pilar Salagre Carnero i la Dra. Yolanda Cesteros Fernández, professores titulars del Departament de Química Física i Inorgànica de la Universitat Rovira i Virgili,

CERTIFIQUEN:

Que la memòria de tesi doctoral “Diseño de catalizadores para una obtención limpia de 2-feniletanol”, que presenta la Sra. Olga Bergadà Miró per a optar al grau de Doctor per la Universitat Rovira i Virgili, ha estat realitzada sota la nostra direcció al Departament de Química Física i Inorgànica de la Universitat Rovira i Virgili.

Tarragona, 27 d'abril de 2007

Dra. Pilar Salagre Carnero

Dra. Yolanda Cesteros Fernández

UNIVERSITAT ROVIRA I VIRGILI
DISEÑO DE CATALIZADORES PARA UNA OBTENCIÓN LIMPIA DE 2-FENILETANOL
Olga Bergadà Miró
ISBN:978-84-691-0355-5 /DL:T.2186-2007

Aquest és el meu espai per dedicar unes paraules d'agraïment als qui m'han fet costat en una etapa molt positiva per a mi, plena de petits moments de diversió, d'emoció, de treball i alguns que altres nervis que, en conjunt, m'han enseyat molt tan a nivell professional com personal.

Voldria mostrar el més sincer agraïment a les meves directores de tesi, la Dra. Pilar Salagre i la Dra. Yolanda Cesteros, per l'oportunitat que em van donar i per la seva excepcional direcció.

Voldria agrair al Dr. Francisco Medina i al Dr. Jesús E. Sueiras la seva aportació professional en la meva formació.

Al grup de Catàlisi Homogènia per transmetre'm els seus coneixements durant els meus anys de tesi.

Agraïr als meus companys de seminari el suport mostrat i els moments que hem compartit. Molts d'ells ja són doctors, d'altres ho serán en breu i n'hi ha que acaben de començar. Marc, Isabel, Isa, Cris, Raquel, Xavi, Rosa, Marta, Ana, Ali, Clara, Yvette, Eva, Aitor, Bianca, Eduardo, Cyril, Jesús, Vanesa, Verónica, Martha, Carolina i Angelica, moltes gràcies. I dedicar un especial agraïment a la resta de companys de Catàlisi Heterogènia: Sònia, Clara, Chimentao, Ilham, Noe, Iuliana, Anton, Marco i Sandra, amb qui he compartit estones de laboratori i una bona amistat.

Voldria donar les gràcies a la M^a José, per tota l'ajuda rebuda durant aquest temps, i a tot el Servei de Recursos Científics i Tècnics de la Universitat Rovira i Virgili.

Gràcies a tots els meus companys/es de la Selva que m'heu animat a fer realitat aquest projecte.

De ben segur que em deixo d'anomenar algú. Durant aquest temps he fet amistats que d'alguna manera o d'una altre han posat el seu granet d'arena en el meu treball i dels que, potser, en aquest moment no me'n recordo. Accepteu les meves disculpes.

Les últimes paraules d'agraïment les dedico a la meva família: papa, mama, Pere i àvia, moltes gràcies pel vostre recolzament que ha fet possible el dia a dia.

A tu Antonio, totes les paraules que em vénen al cap són poques per agrair-te tot el suport que m'has donat. Tan sols et puc recordar que: "*La gota de l'aigua no desgasta la pedra per la seva força sinó per la seva constància*".

UNIVERSITAT ROVIRA I VIRGILI
DISEÑO DE CATALIZADORES PARA UNA OBTENCIÓN LIMPIA DE 2-FENILETANOL
Olga Bergadà Miró
ISBN:978-84-691-0355-5 /DL:T.2186-2007

ÍNDICE

	<u>Pág.</u>
1. Introducción	<u>Pág.</u>
1.1 Producción industrial de 2-feniletanol	3
1.2 La catálisis como alternativa para la obtención de 2-feniletanol	8
1.2.1 Catálisis homogénea	8
1.2.2 Catálisis heterogénea	10
2. Objetivos	21
3. Parte experimental	
3.1 Catalizadores estudiados	25
3.1.1 Sistemas catalíticos de Ni y Ni-MgO	25
3.1.2 Sistemas catalíticos basados en compuestos tipo hidrotalcita	27
3.1.3 Sistemas catalíticos de Ni-Mordenita	28
3.2 Técnicas de caracterización	31
3.2.1 Fisisorción de nitrógeno.	31
3.2.2 Difracción de Rayos X (XRD)	33
3.2.3 Espectroscopia FT-IR	35
3.2.4 Desorción a temperatura programada (TPD)	36
3.2.5 Espectroscopia de Absorción Atómica (AAS)	38
3.2.6 Reducción a Temperatura Programada (TPR)	39
3.2.7 Quimisorción de Hidrógeno. Determinación de áreas metálicas	40
3.2.8 Microscopía electrónica de barrido (SEM)	41
3.2.5 Microanálisis de Rayos X	42
3.2.10 Microscopía electrónica de transmisión (TEM)	43
3.2.11 Análisis termogravimétrico (TGA)	43
3.2.12 Reacciones modelo para estudios de acidez	44

Pág.

3.3 Montaje del sistema de reacción e identificación analítica para la reacción de hidrogenación de óxido de estireno	47
--	-----------

4. Resultados y discusión

4.1 Sistemas catalíticos de Ni y Ni-MgO	51
4.1.1 Introducción	51
4.1.2 Parte experimental	53
4.1.3 Discusión de resultados	56
4.1.4 Conclusiones	73
4.2 Sistemas catalíticos basados en compuestos tipo hidrotalcita	75
4.2.1 Introducción	75
4.2.2 Parte experimental	78
4.2.3 Discusión de resultados	80
4.2.4 Conclusiones	107
4.3 Sistemas catalíticos de Ni-Mordenita	109
4.3.1 Introducción	109
4.3.2 Parte experimental	112
4.3.3 Discusión de resultados	116
4.3.4 Conclusiones	135
5. Conclusiones	139
6. Referencias bibliográficas	144



1. INTRODUCCIÓN

1.1 Producción industrial de 2-feniletanol

El 2-feniletanol es un líquido transparente e incoloro con un agradable olor a rosa [1]. Esta característica hace que este compuesto sea muy apreciado como fragancia en la industria del perfume y en la producción de cosméticos. Su estabilidad en medios alcalinos hace que pueda ser utilizado para perfumar jabones. También se usa como materia prima en la producción de derivados de este alcohol, los cuales se emplean, añadidos en pequeñas cantidades, como aditivos alimentarios para dar sabor y olor. Cabe destacar que el 2-feniletanol se encuentra presente de forma natural en alimentos cuyos procesos de producción incluyen una etapa de fermentación como en hojas de té, cacao, café, pan, vino, sidra, cerveza, queso y en la salsa de soja.

El 2-feniletanol tiene también aplicación en la industria farmacéutica como anestésico local, antiséptico y como solvente. Es considerado como repelente de mosquitos y tiene propiedades fungicidas.

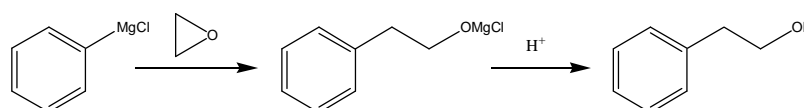
Aparte de todos estos usos, cabe comentar sus aplicaciones en la industria química. El 2-feniletanol se utiliza en procesos de obtención de diferentes productos como pueden ser el estireno, el éster fenilacético, el fenilacetaldehído, los ácidos benzoico y fenilacético y el bifenil éter entre otros. Además, como este alcohol tiene un anillo aromático, en éste se pueden dar reacciones de nitración, sulfonación y halogenación que permiten la obtención de diferentes compuestos de gran importancia industrial.

En las aplicaciones alimenticias en las que el 2-feniletanol se necesita en pequeñas cantidades y libre de componentes tóxicos, éste se obtiene por extracción de fuentes naturales como los aceites esenciales de muchas flores y plantas [1,2]. En general, las concentraciones que se encuentran en estas fuentes naturales son muy bajas, excepto en el aceite de rosas en donde se encuentra entorno al 60 % (dependiendo de la variedad de rosa escogida). De hecho, sólo se puede obtener mediante la extracción con un solvente y posterior destilación, pero mediante este proceso el rendimiento en el

Introducción

producto deseado es muy bajo. Con la finalidad de obtener mayores cantidades de 2-feniletanol se han utilizado diferentes métodos de síntesis química aunque, como veremos a continuación, todos ellos generan importantes problemas medioambientales y/o tienen elevados costes económicos.

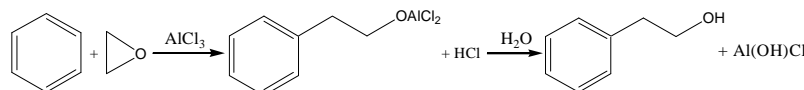
La síntesis con reactivos de Grignard es uno de los métodos industriales tradicionalmente utilizados para la obtención de 2-feniletanol [2]. En esta síntesis el clorobenceno se transforma en cloruro de fenilmagnesio, que por reacción con el óxido de etileno se convierte en cloruro de magnesio feniletóxido. Éste se descompone en medio ácido para dar el 2-feniletanol (Esquema 1).



Esquema 1. Síntesis de 2-feniletanol utilizando reactivos de Grignard.

Este proceso presenta como principales inconvenientes la generación de una gran cantidad de residuos, la utilización de disolventes extremadamente peligrosos en su manipulación como el dimetileter y la baja pureza del 2-feniletanol obtenido, ya que se forman subproductos difícilmente separables, siendo estos hechos un grave inconveniente para su utilización en la industria del perfume.

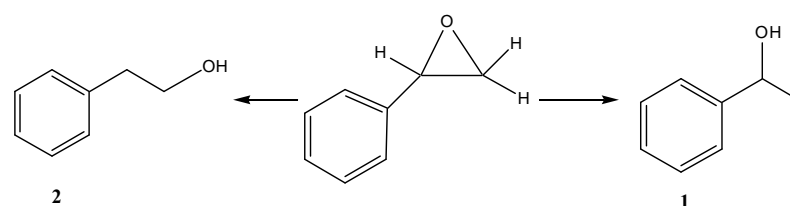
La reacción de alquilación de Friedel-Craft es otro método utilizado a nivel industrial. En esta reacción se hace reaccionar benceno con óxido de etileno utilizando como catalizador tricloruro de aluminio anhidro (Esquema 2) [3,4].



Esquema 2. Reacción de Friedel-Craft para la obtención de 2-feniletanol.

Un inconveniente que presenta este método es el elevado contenido de catalizador que se necesita, ya que se introduce en cantidades estequiométricas, resultando ser, a la práctica, un reactivo más que un catalizador. Además, se utilizan especies altamente corrosivas (AlCl_3) por lo que se hace necesaria la utilización de reactores y conexiones resistentes a la corrosión, elevando considerablemente los costes de producción. El catalizador no se recupera, por lo que se generan grandes cantidades de residuos. Por último, la difícil separación de los compuestos de aluminio resultantes del producto final hace que la utilización del 2-feniletanol obtenido mediante este método en perfumería no sea factible.

Otro método descrito ampliamente en la bibliografía es la apertura del epóxido con un agente reductor (Esquema 3). Los agentes reductores utilizados en esta síntesis son de tipo hidruros o metales alcalinos [5-18]. En general está favorecida la formación del alcohol más sustituido (1), siendo difícil la obtención selectiva del alcohol primario, el 2-feniletanol, (2).



Esquema 3. Productos de la reacción de reducción del óxido de estireno.

No obstante, durante los años 60 y 70 se empezaron a publicar comunicaciones en las que el 2-feniletanol se obtenía con buenos rendimientos por reducción de óxido de estireno con la utilización de compuestos reductores de tipo LiAlH_4 y LiEt_3BH en presencia de AlCl_3 o AlBr_3 [12,15]. La problemática existente en estos procedimientos es la utilización de especies altamente corrosivas de tipo AlX_3 (donde X = Cl o Br).

Años después, se describió la apertura del epóxido utilizando como agente reductor el borohidruro de zinc soportado en sílica gel y fosfato de aluminio, obteniéndose el alcohol menos sustituido (el 2-feniletanol) como

Introducción

producto mayoritario (90 %) [19,20]. Éstos son unos resultados interesantes ya que, como se observa experimentalmente, el uso de sólidos inorgánicos como soportes del agente reductor puede permitir el control de la selectividad en la reacción de apertura del epóxido. Un inconveniente es que la preparación de estos reactivos reductores introduce una etapa adicional en el proceso de obtención de 2-feniletanol, elevando los costes de producción. Otro inconveniente es que la utilización de este tipo de reactivos da lugar a la formación de una mezcla de alcoholes primarios y secundarios y otros subproductos, por lo que se necesitan diferentes etapas de separación posteriores.

Más recientemente, se ha estudiado la reducción de epóxidos con un agente reductor más específico, el triisopropóxido de boro, el cual permite la reducción tipo Meerwein-Ponndorf-Verley para dar los correspondientes alcoholes [21]. Se cree que esta reducción tiene lugar a través de un complejo de coordinación, que permite la transferencia de un hidruro mediante un estado de transición cíclico (Figura 1).

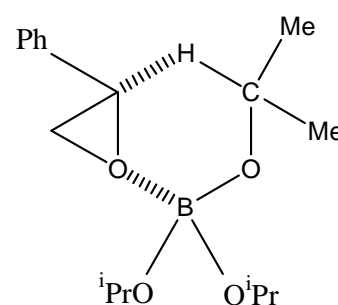


Figura 1. Estado de transición cíclico del triisopropóxido de boro.

La problemática que presenta este último método es el largo tiempo de reacción que se necesita para la obtención de 2-feniletanol (mínimo 7 días) y la baja conversión que se obtiene (30 %), aunque presenta una elevada selectividad (relación 2-feniletanol/1-feniletanol de 99/1).

Un último método de obtención de 2-feniletanol mediante síntesis química es su formación como subproducto en el proceso de obtención

conjunta de estireno y de óxido de propileno. En este proceso, primero se hace reaccionar el etilbenceno con aire con la finalidad de obtener hidroperóxido de etilbenceno. Posteriormente, éste reacciona con propileno para obtener óxido de propileno y 1-feniletanol. Finalmente, el 1-feniletanol se deshidrata y se obtiene estireno generándose un residuo de elevado punto de ebullición que contiene metales y otros subproductos de condensación [22]. De este residuo se puede recuperar el 2-feniletanol [23]. No obstante, se obtiene con un bajo grado de pureza, hecho que dificulta su utilización en perfumería.

Introducción

1.2 La catálisis como alternativa para la obtención de 2-feniletanol.

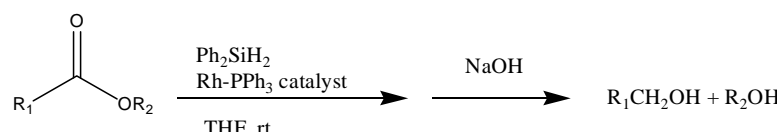
En las últimas décadas se han realizado estudios paralelos utilizando catálisis homogénea y catálisis heterogénea para la obtención selectiva de 2-feniletanol. A continuación se destacan los estudios más relevantes.

1.2.1 Catálisis homogénea

En los procesos en los que mediante catálisis homogénea se obtiene 2-feniletanol se han utilizado catalizadores metálicos, tanto catiónicos como aniónicos [24,25].

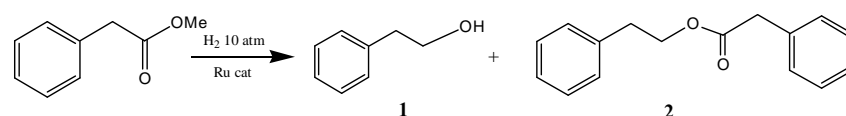
Los primeros estudios en catálisis homogénea se encuentran en 1977, en el que la utilización de complejos catiónicos de rodio dan actividad en la hidrogenación de óxido de estireno hacia los alcoholes correspondientes, mientras que el catalizador más estudiado en aquella época, el catalizador de Wilkinson, no da actividad en dicha reacción [26] . A partir de entonces se realizan estudios con complejos de rodio y diferentes ligandos para aumentar la selectividad hacia 2-feniletanol, no superándose el 70 % [24]. En 1981, se publica otro estudio en el que se utilizan complejos de rutenato fosfina hidruro como catalizador en la hidrogenación en fase homogénea de una gran variedad de compuestos insaturados [25].

En 1995 se presenta un estudio en el que se muestran estructuras de Difracción de Rayos X de complejos de tipo $[\text{Ru}(\text{CO})_2(\mu\text{-OOCCH}_3)\text{L}]$, donde $\text{L}=\text{P}^t\text{Bu}_3$, P^rBu_3 , $\text{P}^{\text{Pr}}\text{Pr}_3$, para establecer correlaciones entre la estructura del complejo con diferentes ligandos y la actividad catalítica en reacciones de hidrogenación homogénea [27]. Otro estudio muestra la reducción de ésteres carboxílicos para dar el correspondiente alcohol utilizando un agente reductor del tipo silano en presencia de un complejo de rodio (Esquema 4) [28]. Este último trabajo es de gran interés debido a la gran dificultad de reducción que presentan los ésteres.



Esquema 4. Reducción de ésteres carboxílicos a alcoholes utilizando un agente reductor de tipo silano en presencia de un complejo de rodio.

En los estudios comentados anteriormente se obtiene el 2-feniletanol utilizando altas temperaturas y elevadas presiones de reacción. Más recientemente, en 2001, se publica un estudio en el que se obtiene 2-feniletanol utilizando bajas presiones de hidrógeno (Esquema 5) [29]. Los productos de esta reacción son el 2-feniletanol (**1**) y el fenilacetato de feniletilo (**2**), a partir de fenilacetato de metilo.



Esquema 5. Hidrogenación de fenilacetato de metilo con Ru-fosfina como catalizador.

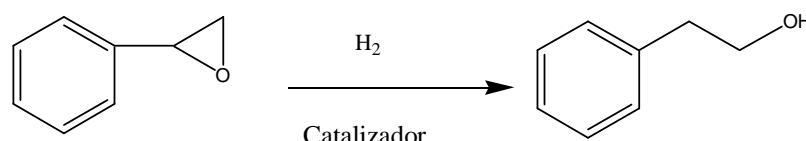
Sorprendentemente, sólo se han detectado pequeñas trazas del correspondiente aldehído. Aunque es posible la obtención de 2-feniletanol mediante este proceso homogéneo, existen dos inconvenientes: la bajas conversiones y selectividades hacia el alcohol de interés y los largos tiempos de reacción necesarios (15 h).

En general, la obtención de 2-feniletanol mediante catálisis homogénea presenta un grave problema de separación y recuperación del 2-feniletanol y, de separación y recuperación del catalizador. Esta problemática hace que algunos estudios se centren en la separación y recuperación del producto de interés y del catalizador [30].

Introducción

1.2.2 Catálisis Heterogénea

La hidrogenación de óxido de estireno mediante catálisis heterogénea para la obtención selectiva de 2-feniletanol (Esquema 6) se presenta como un proceso alternativo para solucionar problemas de recuperación y separación del producto de reacción y del catalizador, minimizando costes y los problemas medioambientales.



Esquema 6. Hidrogenación catalítica de óxido de estireno.

En el año 1930 encontramos la primera patente en la que se utiliza la hidrogenación catalítica de óxidos de olefinas para la obtención de alcoholes primarios [31]. Estos óxidos de olefinas, la estructura de los cuales se muestra en la figura 2, dónde R₁ es un grupo alquilo y, R₂ es un átomo de hidrógeno, grupo alquilo, arilo o aralquilo, pueden transformarse en alcoholes primarios tratados con hidrógeno en presencia de determinados catalizadores.

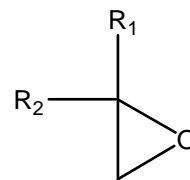


Figura 2. Fórmula general de los óxidos de alquenos.

Los catalizadores utilizados en este estudio son los catalizadores de hidrogenación tradicionales, que corresponden a metales como el níquel, cobalto, hierro, platino y paladio, entre otros, finamente divididos. Estos

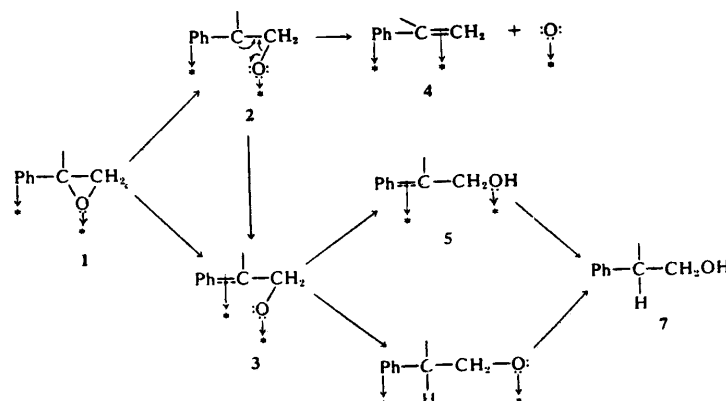
componentes se pueden utilizar como fase única o dispersos en un soporte inerte de tipo carbonato de calcio, sílica gel, piedra pómex o carbón vegetal. La actividad se ve incrementada cuando se adicionan pequeñas cantidades de promotores, como por ejemplo agentes alcalinos u óxido de aluminio, a los precursores del metal antes de su reducción. La reacción catalítica se lleva a cabo en fase líquida o en fase gas.

Otra patente del año 1950 se centra ya en la obtención de 2-feniletanol a partir de óxido de estireno, concretamente en la hidrogenación catalítica de óxido de estireno a bajas temperaturas (0-50 °C) y bajas presiones (6-15 atm) [32]. En estas condiciones los resultados no son del todo satisfactorios ya que se obtiene un bajo rendimiento hacia el producto de interés debido a la formación de cantidades importantes de etilbenceno y productos de polimerización. Para minimizar la formación de estos productos secundarios en 1958 se presenta un estudio donde la presencia de agua en el medio de reacción implica un aumento de rendimiento en la formación de 2-feniletanol gracias a la minimización de los subproductos de reacción [33]. Además, se observó que la adición al medio de pequeñas cantidades de sustancias alcalinas (hidróxido de sodio, carbonato de sodio, hidróxido de potasio, carbonato de potasio, hidróxido de calcio, óxido de calcio, óxido de bario o hidróxido de bario) permite un mejor control de productos secundarios no deseados. El producto de la reacción no depende de la sustancia utilizada pero si del pH resultante (preferiblemente entre 7 y 8).

La acción positiva de las sustancias alcalinas sobre la actividad del catalizador se intenta explicar en el año 1973 por el grupo de Mitsui y colaboradores mediante un estudio de la influencia sobre la actividad de diferentes catalizadores al añadir disoluciones acuosas de NaOH como medio básico [34].

Con el catalizador Ni-Raney se obtienen etilbenceno y 2-feniletanol como productos mayoritarios. El esquema 7 muestra el mecanismo propuesto por Mitsui para esta reacción con este catalizador.

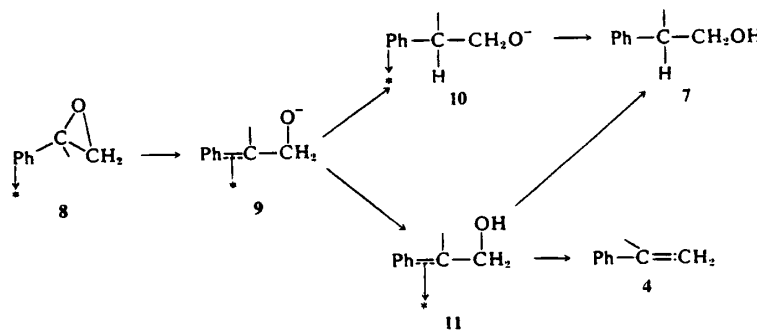
Introducción



Esquema 7. Mecanismo propuesto por Mitsui para la reacción de hidrogenación de óxido de estireno con el catalizador Ni-Raney.

La fuerte adsorción sobre el catalizador del oxígeno del epóxido o del grupo fenilo hacen aumentar la tensión del anillo del epóxido, formándose el radical (2) o el complejo π -benzílico (3), respectivamente. El radical (2) puede dar competitivamente estireno (4) o el complejo (3). La formación del radical (2) se desfavorece como consecuencia del envejecimiento del catalizador. Este hecho se confirma ya que al adicionar más cantidad de catalizador aumenta nuevamente la formación de productos desoxigenados. Además, la formación de etilbenceno aumenta al aumentar la presión de hidrógeno. La adición de hidróxido de sodio al medio de reacción hace disminuir la formación de etilbenceno por lo que se deduce que la presencia de hidróxido de sodio en el medio hace disminuir la adsorción del oxígeno del epóxido y favorece la formación del complejo π -benzílico (3).

Por contra, con catalizadores de paladio se obtiene selectivamente el 2-feniletanol sin detectar la presencia de productos desoxigenados. Esto indica que la hidrogenólisis del óxido de estireno tiene lugar mayoritariamente vía SN_2 tal como se muestra en el esquema 8.



Esquema 8. Mecanismo propuesto por Mitsui para la reacción de hidrogenación de óxido de estireno con catalizadores de paladio.

En el año 1977 se publica una patente en la que se describe unas condiciones de hidrogenación del óxido de estireno que dan lugar a una baja formación de los productos no deseados que son los causantes de la desactivación del catalizador [35]. Para este fin, se utilizaron temperaturas y presiones de hidrógeno altas, dándose así, la rápida hidrogenación del óxido de estireno y minimizando la formación de subproductos. Los catalizadores utilizados son de níquel, paladio y platino. El pH de la reacción se mantuvo entre 7 y 8 y, la principal novedad que se presenta es el control de la concentración de óxido de estireno que se mantiene baja durante toda la reacción.

Una década posterior (1988) Yadav y colaboradores publicaron un trabajo en el que se estudió en profundidad la hidrogenación de óxido de estireno utilizando Pd/C o Ni-Raney como catalizador [36]. Así, se estudió el efecto del tipo y cantidad de catalizador, el efecto de la velocidad de agitación, de la presión y de la temperatura, así como el efecto de la concentración de reactivo.

En la misma línea de los estudios presentados hasta ahora, más recientemente, encontramos una patente en la que se describe la obtención de 2-feniletanol utilizando catalizadores de metales (Ni, Pd y Pt) soportados y en presencia de una base orgánica o inorgánica que actúa como promotor [37]. Las elevadas selectividades que se obtienen hacia el alcohol de interés (99.9 % de selectividad hacia el 2-feniletanol para conversiones de 99.5 %)

Introducción

utilizando las condiciones de reacción más suaves (40-120 °C y 50-800 psig) encontradas hasta ese momento junto con la utilización de reactivos más respetuosos con el medio ambiente, hacen que esta patente sea de gran interés.

Mayoritariamente, todos los estudios encontrados en la literatura se han llevado a cabo en fase líquida. No obstante, recientemente se han publicado dos estudios realizados por nuestro grupo de investigación en el que la hidrogenación de óxido de estireno para la obtención selectiva de 2-feniletanol se ha realizado en fase gas [38,39] utilizando catalizadores de paladio y platino soportados en carbón activo, gamma-alúmina y magnesia. Se ha observado que utilizando un soporte ácido (carbón activo y alúmina) los productos mayoritarios son el fenil acetaldehído y el 1-feniletanol mientras que utilizando un soporte básico, el producto mayoritario es el 2-feniletanol, de acuerdo con los estudios publicados en fase líquida.

Hasta ahora, se ha visto que es posible controlar la selectividad por la adición de sustancias básicas al medio de reacción. Estas sustancias básicas condicionan la interacción del sustrato con los OH⁻ de forma selectiva para la obtención del alcohol de interés (2-feniletanol). Siguiendo este modelo, Divakar y colaboradores publicaron un estudio en el que se muestra como la utilización de la β-ciclodextrina favorece la apertura de óxido de estireno con Ni-Raney, Pd/C y NaBH₄ [40]. La β-ciclodextrina es un promotor molecular con forma de cono semi-truncado y que presenta grupos OH⁻ en su estructura permitiendo regular así, reacciones mediante la inclusión del sustrato en su interior. Esta inclusión del sustrato en la cavidad fue estudiada mediante espectroscopia UV-vis y RMN de ¹³C y ¹H. La interacción propuesta se representa en la figura 3.

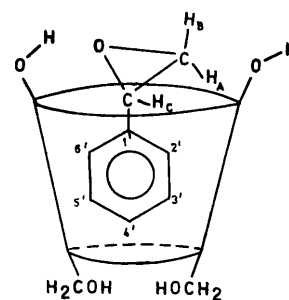
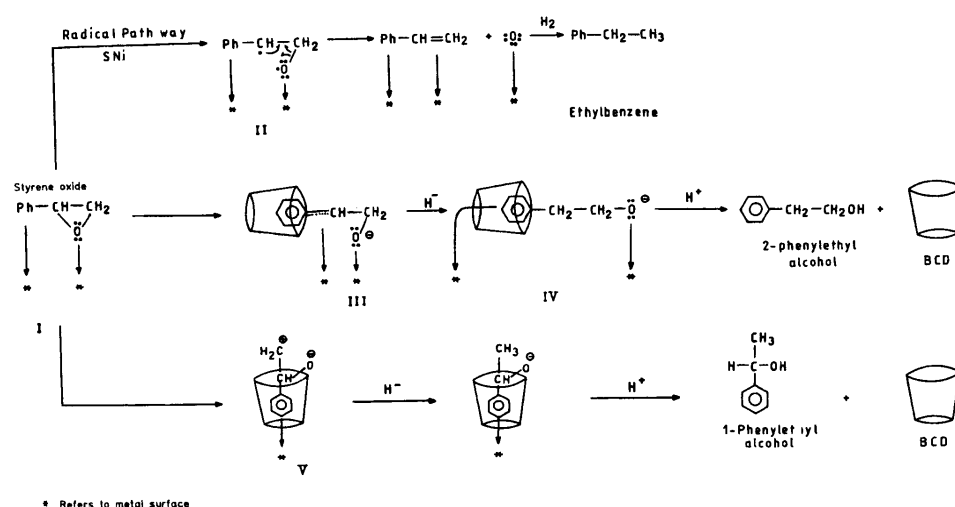


Figura 3. Colocación de óxido de estireno en el interior de la cavidad de la β -ciclodextrina.

A partir de esta interacción estos autores propusieron el siguiente mecanismo de reacción:



Esquema 9. Mecanismo de reacción propuesto con la utilización de la β -ciclodextrina.

La desoxigenación de óxido de estireno tiene lugar vía formación de estireno mediante β -eliminación por la fuerte adsorción del átomo de oxígeno y del grupo fenilo del óxido de estireno a la superficie metálica, para formar el radical **II**, de forma que pierde el átomo de oxígeno para dar estireno y, posteriormente etilbenceno. A medida que la reacción transcurre en presencia

Introducción

de la β -ciclodextrina , la formación de este radical decrece por el envenenamiento del catalizador como se confirma por la ausencia de productos de reacción desoxigenados al aumentar las horas de reacción, debido a las variaciones producidas en el enlace carbono-metal (**III-V**). Así, la formación del complejo π -bencilo **III** puede dar el anión alcóxido **IV** con posterior formación de 2-feniletanol, mientras que el complejo **V** conduce hacia la formación de 1-feniletanol. Por lo tanto, la situación del óxido de estireno en la cavidad de la β -ciclodextrina nos condiciona la interacción entre el catalizador y el sustrato y, así, la obtención del correspondiente producto de reacción.

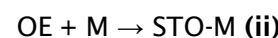
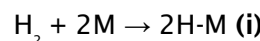
Otra forma de controlar la selectividad hacia el alcohol de interés podría ser la utilización de catalizadores que presenten selección en los diferentes productos dependiendo de su tamaño. Los catalizadores más ampliamente utilizados que presentan selectividad por tamaño son las zeolitas cuya estructura forma cavidades y/o canales que permiten inducir la selectividad por tamaño de reactivos, de productos o de intermedios de reacción. Las zeolitas son una clase de aluminosilicatos cristalinos basados en un esqueleto estructural aniónico rígido, con canales y cavidades bien definidas. Estas cavidades contienen cationes metálicos intercambiables (Na^+ , K^+ , etc.) y pueden retener moléculas huésped eliminables y reemplazables (por ejemplo agua). La fórmula estructural de una zeolita se basa en la unidad de celda cristalográfica: $(\text{M}^{n+})_{x/n}[(\text{AlO}_2)_x(\text{SiO}_4)_y]_w\text{H}_2\text{O}$, donde M es el catión intercambiable de valencia n generalmente del Grupo I o II. La relación Si/Al de la zeolita viene dada por la relación y/x mientras que w representa el agua que contiene la zeolita en el interior de los canales y/o cavidades.

Dimitrova y colaboradores propusieron la utilización de zeolitas con estructura en forma de canales tipo ZSM-5 ($\text{SiO}_2/\text{Al}_2\text{O}_3 = 38$) y ZSM-35 ($\text{SiO}_2/\text{Al}_2\text{O}_3 = 35$) con distintos grados de acidez para la apertura del epóxido de óxido de estireno en una solución de metanol [41]. Estas zeolitas se modificaron con cationes plata para poder estudiar la influencia del diferente grado de acidez sobre los productos de reacción obtenidos. También se

estudió la zeolita Beta ($\text{SiO}_2/\text{Al}_2\text{O}_3 = 36$) para ver la influencia de la variación de la estructura de los canales en la selectividad de reacción. Así los productos obtenidos con la zeolita Beta fueron el 1-feniletanol, con la ZSM-5 se obtuvo una mezcla de 1-feniletanol y 2-feniletanol y con la ZSM-35 se obtuvo como producto mayoritario el 2-feniletanol (70%). Con la ZSM-35 modificada con cationes plata se consiguieron cantidades similares de 2-feniletanol y ácido fenilacético. Un aumento de la acidez en el catalizador favorece la formación de fenilacetaldéhido el cual reacciona rápidamente para formar el ácido correspondiente y el alcohol.

Más recientemente, Hölderich y colaboradores estudiaron la formación de 2-feniletanol partiendo de estireno, en presencia de zeolitas y radiación UV obteniéndose unas selectividades muy bajas hacia el alcohol deseado [42].

Si bien, como hemos visto anteriormente, se han realizado diversas propuestas sobre posibles mecanismos de reacción, los estudios sobre la cinética de la reacción de hidrogenación de óxido de estireno para la obtención de 2-feniletanol son posteriores, de forma que en el año 2003 se propone una ecuación cinética que corresponde al siguiente modelo cinético [43]:



El óxido de estireno (OE) se adsorbe en el centro activo (M) de la superficie catalítica y la adsorción de hidrógeno es disociativa. Así, la reacción en superficie (iii) es irreversible y constituye el paso determinante de la velocidad, mientras que los pasos (i) adsorción del hidrógeno y (ii) adsorción del óxido de estireno son equilibrios rápidos. La desorción del 2-feniletanol

Introducción

(iv) es irreversible y muy rápida, lo cual es razonable ya que se ha encontrado una dependencia de orden 0 respecto a la concentración de producto.

Durante todos estos años se ha observado un progreso importante en los métodos de obtención de 2-feniletanol. No obstante, es necesario continuar investigando para conseguir catalizadores que sean más respetuosos con el medio ambiente y más resistentes a la desactivación. También, el hecho de que la adición de sustancias básicas al medio de reacción aumente la actividad del catalizador nos abre un camino hacia la investigación de catalizadores con propiedades básicas. Por último, también se ha mencionado el control de la selectividad hacia el alcohol de interés mediante la utilización de catalizadores que presenten selección para los diferentes productos dependiendo de su tamaño. Este hecho nos hace pensar en la modificación de zeolitas para la obtención selectiva de 2-feniletanol.

2. OBJETIVOS

Hemos visto que la catálisis heterogénea se presenta como una alternativa para la obtención selectiva de 2-feniletanol. Aun así, el control de la selectividad hacia nuestro alcohol de interés depende de factores tales como la naturaleza, propiedades ácido-base y estructura porosa del catalizador, así como de la interacción reactivo-catalizador. Es en estos aspectos, junto con consideraciones medio-ambientales, que centramos nuestro trabajo, en la obtención de catalizadores altamente selectivos hacia 2-feniletanol y que sean sostenibles para su utilización industrial.

Para ello nos planteamos los siguientes objetivos parciales:

- Diseñar catalizadores de níquel con diferentes características básicas.
 - Sintetizar catalizadores de níquel metálico con diferentes morfologías y tamaños de partícula y, catalizadores mixtos de níquel con magnesia, en los que la magnesia aportará las características básicas al catalizador. Éstos, se sintetizarán siguiendo procedimientos que permitan la obtención de catalizadores con diferentes propiedades básicas.
 - Preparar catalizadores a partir de materiales tipo hidrotalcita de níquel, magnesia y aluminio para obtener una elevada dispersión de los centros metálicos conservando las características básicas.
- Diseñar catalizadores de níquel con propiedades ácidas y estructura microporosa que permitan un control estructural de la selectividad hacia el producto de interés.
 - Preparar catalizadores de mordenita con diferentes contenidos y distribución de níquel.

Objetivos

- Estudiar el efecto de la utilización de microondas en el proceso de preparación sobre las propiedades de los precursores catalíticos y de los correspondientes catalizadores así como en el comportamiento catalítico de los mismos.
- Caracterizar los precursores catalíticos y catalizadores obtenidos mediante diferentes técnicas:
 - Fisisorción de nitrógeno.
 - Difracción de Rayos X (XRD).
 - Espectroscopía FT-IR.
 - Desorción a temperatura programada (TPD).
 - Espectroscopía de absorción atómica (AAS).
 - Reducción a temperatura programada (TPR).
 - Quimisorción de hidrógeno. Determinación de áreas metálicas.
 - Microscopía electrónica de barrido (SEM).
 - Microanálisis de Rayos X.
 - Microscopía de transmisión electrónica (TEM).
 - Análisis termogravimétrico (TGA).
 - Reacciones modelo para estudios de acidez.
- Probar los catalizadores preparados en la reacción de hidrogenación del óxido de estireno para la obtención selectiva de 2-feniletanol en fase líquida.
- Estudiar la vida de los catalizadores más activos y selectivos hacia la obtención de 2-feniletanol.

3. PARTE EXPERIMENTAL

3.1 Catalizadores estudiados

Se han estudiado tres grupos de catalizadores para la obtención selectiva de 2-feniletanol en la reacción de hidrogenación del óxido de estireno: catalizadores de Ni y Ni-MgO, catalizadores obtenidos a partir de precursores tipo hidrotalcita de Ni/Mg/Al y, catalizadores de Ni-Mordenita preparados a partir de NaMordenita intercambiada con níquel en fase líquida y en estado sólido. Las condiciones de preparación y caracterización se describirán ampliamente en los apartados 4.1, 4.2 y 4.3, para los precursores catalíticos y sus correspondientes catalizadores.

En este apartado se hará un resumen de los precursores y catalizadores estudiados así como de la nomenclatura utilizada para nombrarlos.

3.1.1 Sistemas catalíticos de Ni y Ni-MgO

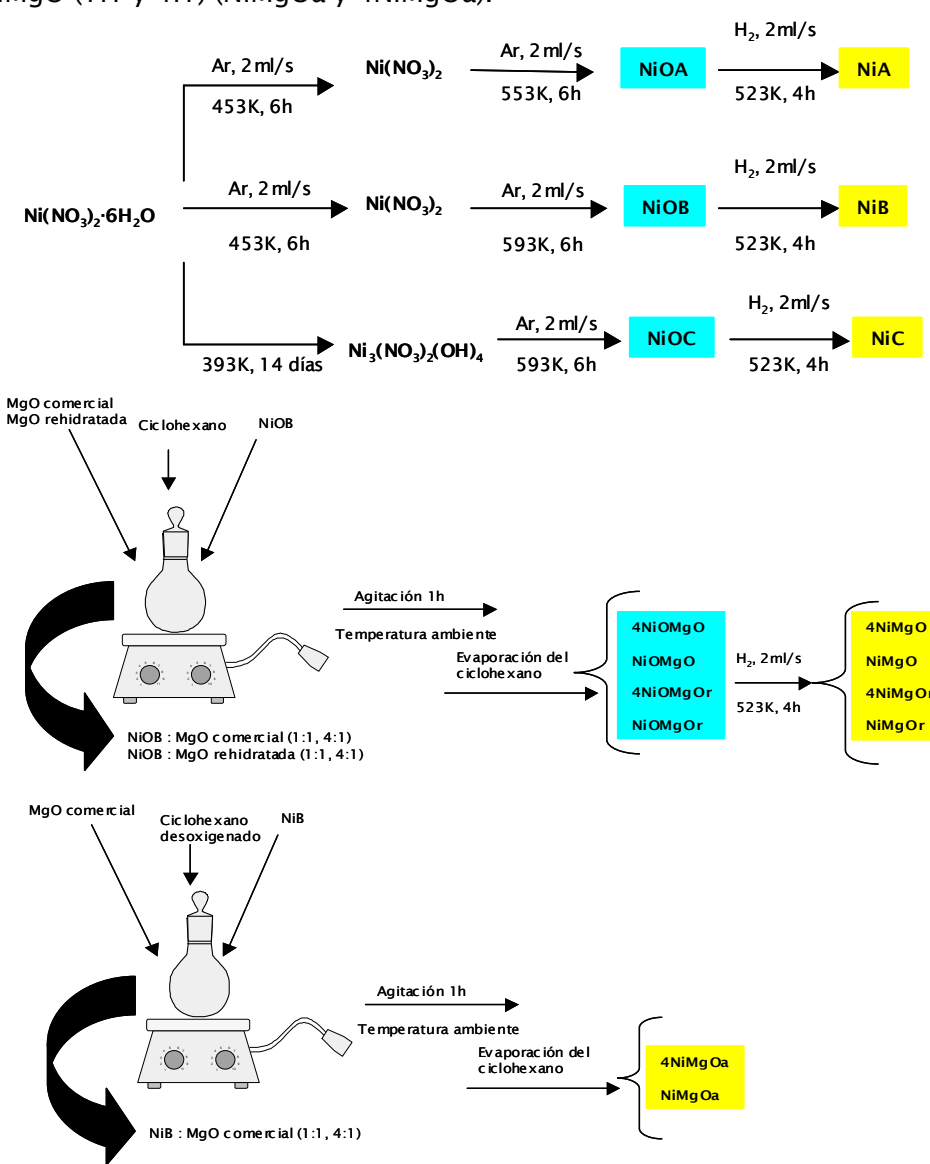
El esquema 10 nos muestra la preparación y la nomenclatura utilizada para los precursores y los correspondientes catalizadores de Ni y Ni-MgO probados en la reacción de hidrogenación del óxido de estireno.

Se han utilizado tres catalizadores de níquel básicos preparados por descomposición térmica de $\text{Ni}(\text{NO}_3)_2 \cdot 6\text{H}_2\text{O}$ (Panreac, 99%) hacia diferentes especies intermedias que posteriormente fueron calcinadas para la obtención de óxidos de níquel con diferentes características morfológicas (NiOA, NiOB y NiOC). Estos óxidos se han reducido con hidrógeno para la obtención de los correspondientes catalizadores (NiA, NiB y NiC).

Los catalizadores de Ni-MgO se han preparado mediante mezcla con agitación magnética en ciclohexano del óxido de níquel NiOB con MgO comercial (MgO) o con MgO rehidratada (MgOr) en distintas proporciones en peso NiO:MgO (1:1 y 4:1), con la finalidad de obtener óxidos con diferentes características básicas (NiOMgO, 4NiOMgO, NiOMgOr y 4NiOMgOr). Éstos han

Parte experimental

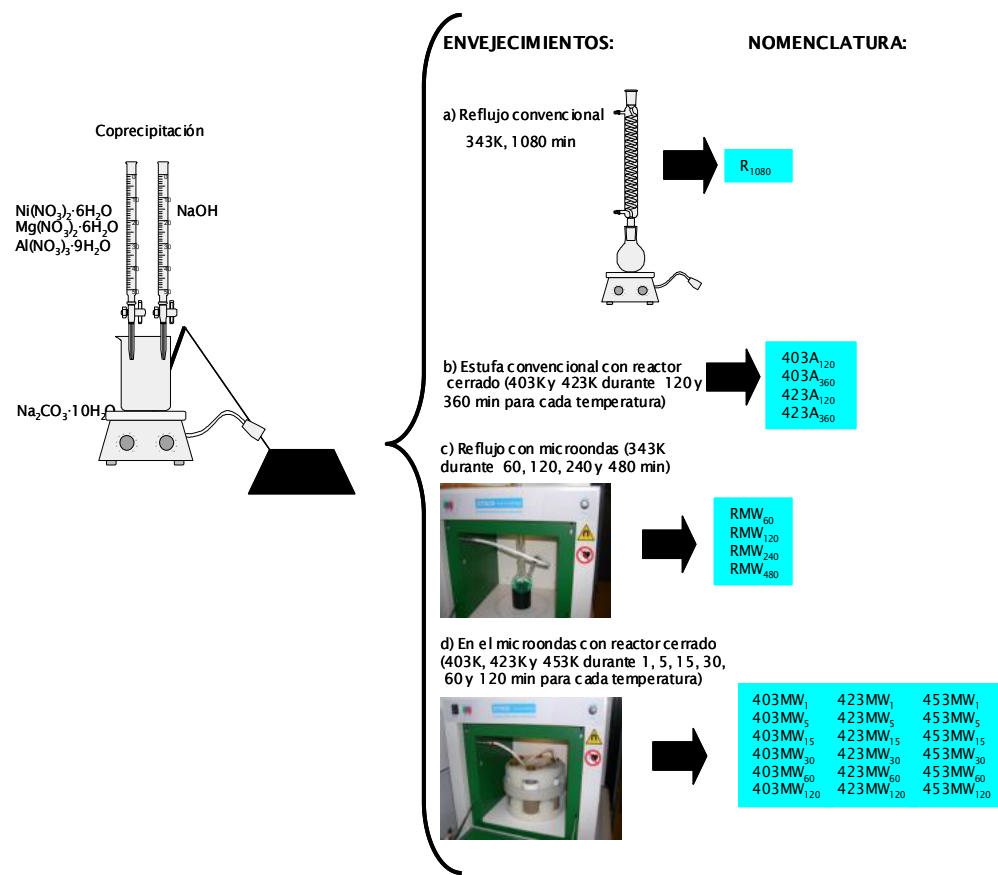
sido posteriormente reducidos para la obtención de los correspondientes catalizadores (NiMgO , 4NiMgO , NiMgOr y 4NiMgOr). Otros dos catalizadores se han preparado por mezcla mediante agitación magnética de la fase níquel ya reducida (NiB) con magnesia comercial en diferentes proporciones en peso $\text{Ni}:\text{MgO}$ (1:1 y 4:1) (NiMgOa y 4NiMgOa).



Esquema 10. Preparación de los precursores y de los correspondientes catalizadores de los sistemas de Ni y Ni-MgO.

3.1.2 Sistemas catalíticos basados en compuestos tipo hidrotalcita

El esquema 11 nos muestra la preparación y nomenclatura utilizada en los compuestos tipo hidrotalcita preparados.



Esquema 11. Preparación de los compuestos tipo hidrotalcita de Ni/Mg/Al.

El gel fue sintetizado mediante el método de coprecipitación a temperatura ambiente y pH constante ($\text{pH}=8 \pm 0.1$). El gel resultante fue envejecido mediante reflujo convencional (R_{1080}), en reactor cerrado calentando en un horno a diferentes temperaturas (403 y 423K) y tiempos (120 y 360 min) (403A_{120} , 403A_{360} , 423A_{120} , 423A_{360}), a reflujo en el microondas a 343 K a diferentes tiempos (60, 120, 240 y 480 min) (RMW_{60} , RMW_{120} , RMW_{240} , RMW_{480}) y

Parte experimental

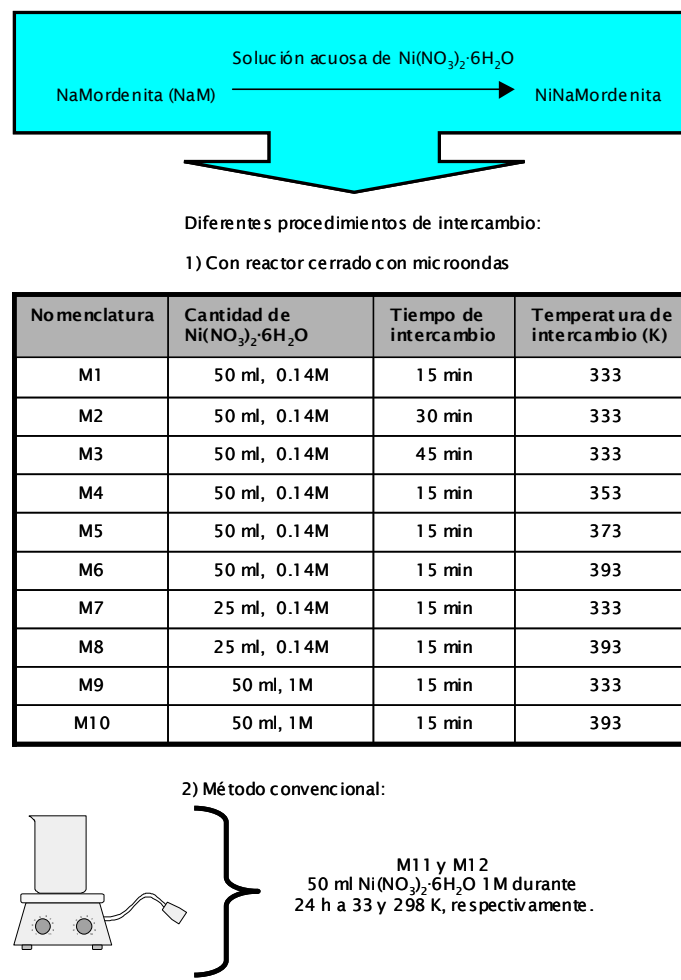
en reactor cerrado en el microondas a diferentes temperaturas (403, 423 y 453K) y tiempos (1, 5, 15, 30, 60 y 120 min) (403MW_1 , 403MW_5 , 403MW_{15} , 403MW_{30} , 403MW_{60} , 403MW_{120} , 423MW_1 , 423MW_5 , 423MW_{15} , 423MW_{30} , 423MW_{60} , 423MW_{120} , 453MW_1 , 453MW_5 , 453MW_{15} , 453MW_{30} , 453MW_{60} , 453MW_{120}). El microondas utilizado, Milestone ETHOS-TOUCH CONTROL, está equipado con un controlador de temperatura.

Los sistemas catalíticos probados en la reacción de hidrogenación de óxido de estireno se obtuvieron mediante calcinación bajo flujo continuo de N_2 (2 ml/s) a 623 K durante 3h (R_{1080}C , $403\text{A}_{360}\text{C}$, RMW_{120}C , $403\text{MW}_{15}\text{C}$ y $453\text{MW}_{120}\text{C}$) y posterior reducción con H_2 (2ml/s) a 623K durante 6h (R_{1080}R , $403\text{A}_{360}\text{R}$, RMW_{120}R , $403\text{MW}_{15}\text{R}$ y $453\text{MW}_{120}\text{R}$)

3.1.3 Sistemas catalíticos de Ni-Mordenita

El esquema 12 nos muestra la preparación de las muestras de NaMordenita intercambiadas con níquel.

NaMordenita comercial ($\text{Si}/\text{Al} = 6.5$, Zeolist) fue intercambiada con níquel mediante diferentes procedimientos para la obtención de las muestras deseadas. Las muestras M1, M2, M3, M4, M5, M6, M7, M8, M9 y M10 se obtuvieron por intercambio en el microondas con diferentes concentraciones (0.14 y 1 M) y volúmenes de solución de $\text{Ni}(\text{NO}_3)_2 \cdot 6\text{H}_2\text{O}$ (50 y 25 ml) y, diferentes tiempos (15-45 min) y temperaturas (333 y 393 K). M11 y M12 se prepararon mediante el método convencional, utilizando 50 ml $\text{Ni}(\text{NO}_3)_2 \cdot 6\text{H}_2\text{O}$ 1M durante 24h a 333 y 298 K, respectivamente. Para mejorar la difusión del Ni^{2+} y aumentar el % de intercambio se prepararon dos muestras más, M13 y M14, mediante dos intercambios en microondas con 50 ml de una disolución de $\text{Ni}(\text{NO}_3)_2 \cdot 6\text{H}_2\text{O}$ 1M durante 15 min a 333 K pero con un tratamiento térmico intermedio entre los dos intercambios: M13 se calentó en una mufla a 673 K durante 12 h y M14, en el microondas a 453 K durante 6h.



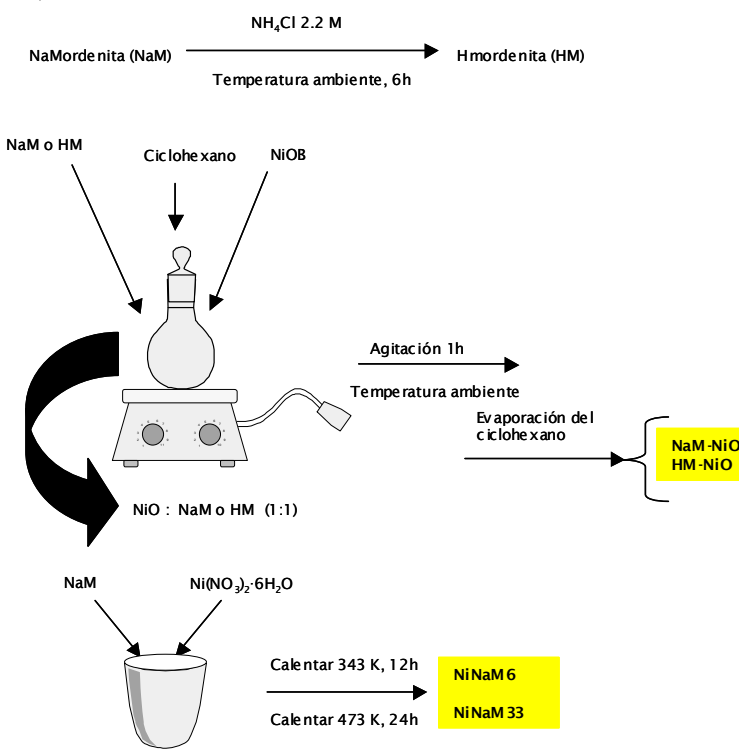
Esquema 12. Preparación de las muestras de NaMordenita intercambiadas con níquel.

Para mejorar la migración del níquel en el interior de la NaMordenita, se obtuvieron otras dos muestras en fase sólida. Una se preparó mediante 2.5 g de $\text{Ni}(\text{NO}_3)_2 \cdot 6\text{H}_2\text{O}$ y 1g de NaMordenita. Los dos sólidos se mezclaron en una cápsula de porcelana y la mezcla resultante se calentó, en una primera etapa a 343 K durante 12 h, en la que se consigue la fusión del $\text{Ni}(\text{NO}_3)_2 \cdot 6\text{H}_2\text{O}$ y después se calentó hasta 473 K durante 24 h (NiNaM33) (Esquema 13). La segunda muestra se preparó siguiendo el mismo procedimiento anterior pero se utilizó 0.4 g de $\text{Ni}(\text{NO}_3)_2 \cdot 6\text{H}_2\text{O}$. Esta cantidad fue calculada a partir del CEC

Parte experimental

(Cation Exchange Capacity) de la NaMordenita (2.32 meqNa⁺/g zeolita) y es la necesaria para obtener un intercambio total. La muestra resultante se ha llamado NiNaM6 (Esquema 13).

La muestra HMordenita (HM) se preparó previamente a partir de la NaMordenita (1 g) por intercambio con una solución 2.2 M de NH₄Cl durante 6h a temperatura ambiente. Después se lavó con agua destilada y se dejó secar a 393 K durante toda la noche. A continuación se calcinó a 673 K durante 12 h para la obtención de HM (Esquema 13). Para utilizar como referencia se obtuvieron dos muestras por agitación magnética de NaM con NiOB (su obtención se ha explicado en el apartado 3.1.1), y de HM con NiOB, con relación 1:1, en ciclohexano y posterior evaporación del disolvente. Las muestras obtenidas se han denominado NaM-NiO y HM-NiO, respectivamente (Esquema 13).



Esquema 13. Preparación de las muestras de Ni-Mordenita en estado sólido.

Los precursores probados en la reacción de hidrogenación de óxido de estireno para la obtención selectiva de 2-feniletanol se calcinaron a 623 K durante 12h y se redujeron con hidrógeno puro utilizando diferentes condiciones (623-773 K).

3.2 Técnicas de caracterización

3.2.1 Fisisorción de nitrógeno.

La técnica fisisorción de gases es la más usual en la determinación de áreas superficiales y distribución de tamaños de poros de sólidos.

Esta técnica se basa en la adsorción de nitrógeno a 77 K. Las isotermas obtenidas (representación del volumen de nitrógeno fisisorbido en el sólido respecto a la presión relativa de nitrógeno) corresponden al proceso de adsorción y desorción del gas en el sólido, produciéndose histéresis cuando la isoterma de adsorción no coincide con la de desorción. Los sólidos se pueden clasificar en función del tipo de isotermas que presenten. Las isotermas de adsorción, mayoritariamente, se pueden agrupar en cinco tipos diferentes:

- La isoterma del tipo I es característica de los sólidos microporosos con una superficie externa muy pequeña. El volumen de gas adsorbido está limitado a la accesibilidad de los microporos.
- La isoterma del tipo II la presentan los sólidos no porosos o macroporosos.
- La isoterma del tipo III nos indica que en el sistema existe una interacción de adsorbato-adsorbato más fuerte que de adsorbato-adsorbente, por lo que no se refleja una porción lineal de la formación de la monocapa.
- La isoterma del tipo IV se asocia con la condensación capilar en los mesoporosos, indicado por la pendiente elevada que se forma a altas presiones relativas, mientras que en su comienzo se parece a la isoterma III.

Parte experimental

- La isoterma del tipo V se parece a la del tipo III pero nos indica la existencia de mesoporos en el sólido.

La presencia de histéresis entre adorción y desorción es característico de las isothermas del tipo IV y V. Existen cinco tipos de histéresis según De Boer. Cada tipo de histéresis se relaciona con una forma particular de poro.

En la gráfica de la distribución de poros se representa la variación del volumen de poros en función del tamaño de poros correspondiente. Uno de los cálculos de la distribución de poros se basa en el método de B. J. H. (Barret, Joyner and Halenda) considerando el espesor de la capa adsorbida en el momento de la condensación o de la desorción capilar y se ha empleado sobre todo para calcular la distribución del tamaño de poros bajo la suposición de una forma cilíndrica del mismo.

Para la determinación de áreas superficiales, el método BET es ampliamente utilizado, aunque presenta importantes limitaciones principalmente en los sólidos microporosos. Esta teoría permite estimar el área de la superficie de la muestra a partir del volumen de la monocapa. Para la determinación del volumen de gas adsorbido de la monocapa (V_m) se utilizan los volúmenes adsorbidos correspondientes al intervalo de presiones parciales de adsorbato (N_2 en una mezcla N_2/He) comprendidas entre 5 y 20 %. Representando P/P_0 frente a $P/[V(P/P_0)]$, y a partir de un ajuste lineal y teniendo en cuenta la ecuación (1) se obtienen la pendiente, $(C-1)/V_m C$ y la ordenada en el origen, $1/V_m C$. De esta manera quedan determinados los valores de C y V_m .

$$V/V_m = C(P/P_0)/[(1-P)/P_0](1-(1-C))/(P/P_0)] \quad (1)$$

donde V es el volumen de gas adsorbido (en condiciones normales) a una presión parcial P de adsorbato, V_m es el volumen de gas requerido para formar una monocapa (en condiciones normales), P_0 es la presión de saturación de nitrógeno a 77 K y C es una constante relacionada con la energía de adsorción.

El área de la superficie (S) de la muestra (área BET), una vez conocido el volumen de gas adsorbido en la monocapa (V_m), se obtiene a partir de la ecuación 2:

$$S = (V_m AN)/M \quad (2)$$

dónde A es el número de Avogadro, M es el volumen molar del gas y N es el área ocupada por cada molécula de N_2 adsorbida (0.162 nm^2).

Para la determinación del área de microporo De Boer y Lippens desarrollaron el método de la curva-t.

Equipo utilizado:

El equipo utilizado para la determinación de áreas BET, distribución de poro y área de microporo es un analizador de superficies Micromeritics ASAP 2000.

Condiciones experimentales:

La temperatura de calentamiento durante las desgasificaciones fue de 693 K para las muestras con Mordenita y 393 K para el resto de muestras analizadas. La cantidad de muestra utilizada para los análisis fue la suficiente para tener un área BET superior a $10 \text{ m}^2/\text{g}$.

3.2.2 Difracción de Rayos X (XRD)

La técnica de difracción de Rayos X se fundamenta en la difracción de un haz de rayos X después de incidir sobre una muestra cristalina con un determinado ángulo θ .

Se produce difracción cuando se cumplen las condiciones mostradas en la ley de Bragg (3). Esta ecuación indica la relación entre el espaciado interplanar (d_{hkl}), la longitud de onda de la radiación X (λ) y el ángulo de incidencia del haz de rayos X (θ) siendo n un número entero.

$$n\lambda = 2d_{hkl} \operatorname{sen}\theta \quad (3)$$

Parte experimental

Dada la naturaleza de las muestras se ha utilizado la difracción de polvo cristalino y el difractómetro está configurado según la geometría de Bragg-Brentano. La información que puede obtenerse de un difractómetro de polvo es: a) espaciado interlaminar, b) índices de Miller de las reflexiones, c) dimensiones de la celda y del tipo de red, d) intensidad relativa de las difracciones, e) identificación cualitativa de los compuestos cristalinos, f) análisis cuantitativo de mezclas cristalinas y g) determinación del tamaño de cristal a partir de la anchura de los picos de difracción. Generalmente, para identificar las diferentes fases cristalinas obtenidas se utiliza la base de datos JCPDS (Joint Committee for Power Diffraction Sources). En este trabajo se han utilizado las fichas JCPDS siguientes: 04-0850-Ni (Níquel) ; 04-0835-NiO (Bunsenita); 45-0946-MgO (Periclasa); 089-0460-Hidrotalcita; 044-1482-Mg(OH)₂ (Brucita) y 029-1257-NaMordenita.

En el caso de las hidrotalcitas estudiadas en este trabajo se han calculado los parámetros de celda a y c a partir de las siguientes correlaciones (4) y (5):

$$a = 2d_{(110)} \quad (4)$$

$$c = 3d_{(003)} \quad (5)$$

La cristalinidad de la muestra esta relacionada en todos los casos con la anchura de los picos, de forma que, picos más estrechos corresponden a muestras más cristalinas y por tanto, con un tamaño de cristalito mayor. La anchura del pico y el tamaño de cristalito se relacionan mediante la ecuación de Scherrer (6):

$$dp = k\lambda/(B\cos\theta) \quad (6)$$

donde dp es el diámetro de partícula, λ es la longitud de onda de la radiación, θ es el ángulo de difracción, k es la constante de Scherrer, que toma un valor medio de 0.9 y B, es la anchura del pico a altura media (FWHM) expresada en radianes.

Equipo utilizado:

Los experimentos se han realizado utilizando un difractómetro Siemens D5000.

Condiciones experimentales:

El difractómetro se ha configurado según la geometría Bragg-Brentano y goniómetro vertical $\theta\text{-}\theta$. La radiación CuK_α se obtuvo a partir de un tubo de rayos X de cobre a un potencial de 40 kV y 30 mA. Se ha utilizado un monocromador de grafito para eliminar la componente K_α de la radiación. Los difractogramas se realizaron de 5 a 90° (2θ) con un paso de 0.05° y un tiempo de paso de 3s.

3.2.3 Espectroscopia FT-IR

La espectroscopia infrarroja con transformada de Fourier se utiliza principalmente en el análisis cualitativo de grupos funcionales.

Al absorber radiación infrarroja, las unidades y agrupaciones estructurales de los sólidos experimentan un cambio neto en su momento dipolar, el cual es consecuencia de sus movimientos de vibración y de rotación.

El espectro infrarrojo se divide en tres regiones denominadas infrarrojo cercano, medio y lejano, lo que corresponde a longitudes de onda entre 0.78 y 1000 μm . La mayoría de aplicaciones se han centrado en la región del infrarrojo medio comprendida entre los 4000 y los 400 cm^{-1} (de 2.5 a 25 μm). Las unidades para medir la radiación infrarroja pueden ser la longitud de onda (μm) o el número de onda (cm^{-1}).

En el presente trabajo se ha utilizado esta técnica para la identificación del grupo OH^- en la magnesia rehidratada (MgOr), para estudiar variaciones de basicidad en las hidrotalcitas a través de las bandas correspondientes de carbonato y bicarbonato y, para estudiar la posible desaluminación de la mordenita por efecto de las microondas.

Parte experimental

Equipo utilizado:

Los espectros de infrarrojo se obtuvieron mediante un espectrofotómetro Bruker-Equinox-55 FTIR.

Condiciones experimentales:

Los espectros se adquirieron acumulando 32 “scans” con una resolución de 4 cm⁻¹ en el rango entre 400-4000 cm⁻¹. Las muestras (hidrotalcitas, magnesia rehidratada y mordenitas) se prepararon mezclando los sólidos en polvo con KBr con una relación 15:85, para formar una pastilla.

Por otra parte, en los espectros en que se ha utilizado el CO₂ como molécula sonda se ha seguido el siguiente procedimiento: de cada muestra de hidrotalcita se ha hecho dos pastillas. Una se ha utilizado para registrar el espectro de la muestra mientras que, en la segunda pastilla se le ha pasado CO₂ a temperatura ambiente para registrar posteriormente el espectro infrarrojo después de la adsorción de CO₂.

3.2.4 Desorción a temperatura programada (TPD)

La desorción a temperatura programada se basa en la quimisorción de un gas o un líquido sobre un sólido y su posterior desorción mediante aumento de la temperatura. La cantidad de especies adsorbidas se puede detectar mediante diferentes tipos de detectores, ya sea el TCD (detector de conductividad térmica) o el espectrómetro de masas. En función de las características de la superficie, el gas se puede adsorber dando lugar a distintas especies, de manera que la desorción se producirá a diferentes temperaturas, según la fuerza de la interacción entre el gas y el centro en cuestión.

Cuando las posiciones activas de la superficie del sólido adsorben gas, se forman varias capas de adsorción, dándose la quimisorción entre la primera capa de gas y la superficie del sólido. Por tanto, antes de realizar un experimento, se deben eliminar las mult capas formadas por fisisorción calentando a bajas temperaturas. Posteriormente, se calienta progresivamente

la muestra de forma que se va produciendo la eliminación de las especies adsorvidas, las cuales se conducen hasta un detector, pudiendo así obtener un registro de las especies desorvidas en función de la temperatura.

En este trabajo se han utilizado distintas moléculas sonda tales como NH₃, el CO₂ o el H₂, para obtener información de la acidez, basicidad y tipos de centros metálicos del material, respectivamente.

A partir de estos estudios se ha obtenido información sobre las propiedades ácidas de las muestras de NaMordenita intercambiadas con níquel, las propiedades básicas de precursores y catalizadores de Ni, Ni-MgO y de derivados de hidrotalcita, así como sobre los diferentes centros metálicos de catalizadores obtenidos a partir de precursores del tipo hidrotalcita, mediante TPD de NH₃, CO₂ y H₂, respectivamente.

Equipo utilizado:

Se ha utilizado un equipo Thermo Finnigan TPDRO 1100 equipado con un horno de temperatura programable y un detector TCD. A la salida de gases se acopló un espectrómetro de masas cuadrupolo Pfeiffer GSD300.

Condiciones experimentales:

Para realizar los TPDs de CO₂, en primer lugar se colocaron, aproximadamente, 100 mg de muestra (Ni-MgO e hidrotalcitas) entre lana de cuarzo dentro de un reactor de cuarzo. La muestra se pretrató con Ar a 393 K durante 30 minutos y se enfrió hasta 353 K previamente a la adsorción de CO₂ a la misma temperatura. Después de la adsorción de CO₂ (3 % vol. CO₂ en He a 20 cm³/min durante 90 minutos), se pasó He (20 cm³/min) durante 30 minutos a 423 K para eliminar el CO₂ fisisorbido. Posteriormente, se procedió a la desorción de CO₂ quimisorbido calentando la muestra desde 423 K hasta 1073 K a una velocidad de calentamiento de 5 K/min.

Para los TPDs de NH₃ se siguió el siguiente método. Aproximadamente 100 mg de muestra (Mordenitas) se colocaron entre lana de cuarzo dentro de un reactor de cuarzo. La muestra se pretrató con Ar a 673 K durante 60 minutos y se enfrió hasta 373 K para realizar la adsorción de NH₃ (20 cm³/min) a esta temperatura durante 60 minutos. Después de la

Parte experimental

adsorción de NH₃, a la muestra se le pasó He (20 cm³/min) durante 30 minutos a 423 K para eliminar el NH₃ fisisorbido. Posteriormente, se procedió a la desorción de NH₃ quimisorbido calentando la muestra de 423 K hasta 1073 K a una velocidad de calentamiento de 5 K/min.

Los TPDs de H₂ se llevaron a cabo con, aproximadamente 200 mg de las hidrotalcitas reducidas. La muestra se colocó entre lana de cuarzo dentro de un reactor de cuarzo y se pretrató con H₂/Ar 5% durante 60 min a 623 K. Para eliminar la parte fisisorbida se pasó Ar a través de la muestra durante 60 min a 323 K. El análisis se realizó mediante el paso de 20 cm³/min de Ar calentando desde 323 K hasta 1073 K a 5 K/min.

3.2.5 Espectroscopia de Absorción Atómica (AAS)

La espectroscopia de absorción atómica es una técnica que se utiliza para determinar la composición química de las muestras. En este método se utiliza una cámara de nebulización para crear una niebla de la muestra y un quemador con forma de ranura que da una llama con una longitud de trayecto más larga. En un atomizador con llama la disolución de la muestra es nebulizada mediante un flujo de gas oxidante mezclado con el gas combustible y se transforma en una llama donde se produce la atomización. La temperatura de la llama es lo bastante baja para que no excite los átomos de la muestra de su estado fundamental. El nebulizador y la llama se utilizan para desolvatar y atomizar la muestra, pero la excitación de los átomos del analito se consigue con lámparas de diferentes longitudes de onda en función del analito. En la Absorción Atómica la intensidad de luz absorbida es proporcional a la cantidad de analito en la muestra. Debido a la buena sensibilidad y selectividad del método es comúnmente utilizado para analizar elementos traza en muestras acuosas y otros líquidos.

Equipo utilizado:

El equipo en el que se han realizado los análisis es un Hitachi Z-8200 Polarized Zeeman Atomic Absorption Spectrophotometer.

Condiciones experimentales:

Dado que es necesario tener los elementos a analizar en disolución ha sido necesario la digestión previa de los solutos. El tratamiento se ha realizado de diferente manera dependiendo de la naturaleza de las mismas. La digestión de las hidrotalcitas se ha realizado con HNO_3 concentrado con aproximadamente 100 mg de muestra. La digestión de las Mordenitas intercambiadas se ha realizado con HF diluido en un Anton Para Pressurized Microwave Decomposition System con aproximadamente 100 mg de muestra.

Todos los análisis se han realizado por triplicado.

3.2.6 Reducción a Temperatura Programada (TPR)

La reducción a temperatura programada es una técnica extremadamente sensible que permite estudiar el proceso de reducción de un sólido con hidrógeno. La reducción se realiza haciendo pasar una corriente de 5 % H_2/Ar sobre la muestra en las condiciones de temperatura programadas.

En este trabajo, el instrumento utilizado para llevar a cabo estos experimentos es una termobalanza que nos permite obtener en función del tiempo o de la temperatura las variaciones de peso que experimenta la muestra durante el proceso de reducción.

La reducción a temperatura programada es una técnica interesante cuando el tipo de materiales a caracterizar son óxidos que se quieren reducir para obtener el correspondiente metal, que es la fase activa de muchos catalizadores. Esta técnica nos permite conocer el grado de reducción en el catalizador y nos aporta información sobre las propiedades superficiales y de reducibilidad del precursor catalítico. Los datos obtenidos nos permiten entender el comportamiento catalítico ya que este es consecuencia de las características superficiales y éstas, dependen de las propiedades del óxido precursor del metal, si bien el procedimiento de reducción puede modificar las características superficiales y morfológicas.

Parte experimental

Equipo utilizado:

El equipo utilizado para realizar los experimentos de Reducción a Temperatura Programada es una termobalanza Perkin-Elmer TGA 7 equipada con un horno de temperatura programable de 273-1273 K. La precisión es de $\pm 1\mu\text{g}$.

Condiciones experimentales:

La cantidad de muestra (Ni mísico y sistemas Ni-MgO) utilizada en cada análisis fue de 30 mg. Se hizo una estabilización del peso con Ar a 393 K. La reducción se hizo con H_2/Ar al 5% con un flujo de 80 cm^3/min calentando desde 393 K hasta 1173 K a 15 K/min.

3.2.7 Quimisorción de Hidrógeno. Determinación de áreas metálicas.

La quimisorción se diferencia de la fisisorción en la especificidad de la interacción entre el adsorbato y el adsorbente (sólo se produce en unos centros determinados) y la formación de un enlace químico de elevada energía. Esta especificidad permite emplear la quimisorción en la determinación del área metálica de un catalizador cuando se utiliza como adsorbato una molécula capaz de interaccionar exclusivamente con los centros metálicos aunque en algunas ocasiones se pueden producir adsorciones sobre el soporte (spill-over) cuando existen fuertes interacciones metal-soporte. Para poder utilizar este procedimiento en el cálculo de las áreas metálicas es necesario conocer la estequiometría centro metálico-molécula sonda. Los gases más utilizados para la determinación de área metálica mediante quimisorción son el H_2 y el CO. Las técnicas para la obtención de área metálica a partir de la quimisorción incluyen métodos volumétricos, gravimétricos y de flujo.

Equipo utilizado:

El equipo utilizado fue un analizador de superficies Micromeritics, ASAP 2010C, equipado con una bomba turbomolecular.

Condiciones experimentales:

Las muestras fueron reducidas utilizando H₂ puro, reproduciendo las velocidades de calentamiento utilizadas en el sistema de reacción catalítica. El exceso de H₂ se eliminó mediante 15 cm³/min de He a una temperatura 10 K superior a la temperatura de reducción durante 180 minutos. Posteriormente, la muestra se enfriá a 303 K con el mismo flujo de He. El análisis se lleva a cabo con H₂ a 303 K.

Se calcula la superficie metálica (aportada por el Ni en nuestros catalizadores) asumiendo una estequiometría de una molécula de hidrógeno para cada dos átomos de níquel y una área atómica de 6.49x10⁻²⁰ m²/átomo Ni.

3.2.8 Microscopía electrónica de barrido (SEM).

La microscopía electrónica se fundamenta en el bombardeo mediante un haz de electrones de la superficie a visualizar. Este haz de electrones, enfocado por las lentes electromagnéticas a través de una columna con alto vacío, se proyecta sobre la superficie de la muestra donde los electrones rebotan o provocan la emisión de electrones secundarios de la muestra. Estos electrones dispersados o emitidos son recogidos por unos detectores y proyectados sobre una pantalla de televisión que proporciona una imagen tridimensional del objeto.

Para llevar a cabo la observación se necesita poca cantidad de muestra, la cual es depositada sobre un portamuestras que contiene una capa de doble adhesión de grafito. Así, las partículas quedan adheridas a él. Las muestras conductoras son las más fáciles de estudiar, aunque se han desarrollado muchas técnicas que permiten obtener imágenes SEM de muestras no conductoras. El procedimiento habitual consiste en el recubrimiento de la superficie de la muestra con una película delgada, normalmente de oro o grafito. El grosor de esta película debe ser el adecuado para que sea conductor y no enmascare los detalles de la superficie.

Parte experimental

Esta técnica nos proporciona información sobre la morfología y la topografía del sólido que se pretende estudiar.

Equipo utilizado:

Las micrografías se han realizado con un microscopio JEOL JSM6400.

Condiciones experimentales:

Los precursores de Ni y Ni-MgO y precursores tipo hidrotalcita se han recubierto, previamente, con una película delgada de oro.

Se ha utilizado un voltaje entre 30 y 35 kV, distancias focales entre 8-15 mm y se ha trabajado con un aumento máximo de 50000x.

3.2.9 Microanálisis de Rayos X

El microscopio electrónico de barrido, también ofrece la oportunidad de analizar la composición de la muestra. Los Rayos X emitidos por la muestra al ser bombardeada por el haz de electrones, son característicos para cada elemento y hacen posible determinar la distribución (mapas de distribución química) y composición química de una zona en particular de la muestra. En este trabajo se ha utilizado esta técnica para determinar los mapas de distribución de los átomos de Ni, Al, Na y Si presentes en las muestras de mordenita.

Equipo utilizado:

Los experimentos se han realizado en un microscopio electrónico de barrido JEOL JSM6400.

Condiciones experimentales:

Los experimentos se han realizado con un voltaje de aceleración de 15 kV y una distancia de trabajo de 15 mm. Las muestras analizadas se han recubierto con una capa de grafito para mejorar su conductividad. El tiempo de acumulación utilizado fue de 120 segundos.

3.2.10 Microscopía electrónica de transmisión (TEM).

La microscopía electrónica de transmisión se basa en un haz de electrones que manejado a través de lentes electromagnéticas se proyecta sobre una muestra muy delgada situada en una columna de alto vacío. El haz de electrones atraviesa la muestra, que ha sido contrastada con átomos pesados, y se pueden dar dos situaciones básicas: que los electrones del haz atraviesen la muestra o que choquen con un átomo de la muestra y terminen su viaje. De este modo se obtiene información estructural específica de la muestra según las pérdidas específicas de los diferentes electrones del haz. El conjunto de electrones que atraviesan la muestra son proyectados sobre una pantalla fluorescente formando una imagen visible o sobre una placa fotográfica registrando una imagen latente.

Equipo utilizado:

El equipo en el que se realizó la caracterización fue un microscopio de electrones JEOL (Modelo 1011)

Condiciones experimentales:

Se ha preparado una suspensión de los precursores de hidrotalcita a analizar en etanol y se ha dejado caer una gota de la suspensión sobre un polímero de carbón *Quantifoil* soportado en una rejilla de cobre. Se ha dejado secar a temperatura ambiente

Se ha trabajado con un voltaje de 80 kV y con unos valores de ampliación entre 100-500 k.

3.2.11 Análisis termogravimétrico (TGA).

Esta técnica se fundamenta en la variación de peso de una muestra cuando se somete a determinado tratamiento térmico en una atmósfera seleccionada (O_2 , N_2 , H_2).

A partir de la representación de variación de peso en función de la temperatura (termograma) se pueden identificar las diferentes etapas que

Parte experimental

tienen lugar durante el tratamiento, pudiéndose representar sobre la gráfica la derivada de la función que permite diferenciar con más claridad dichas etapas.

En este trabajo se utilizó el análisis termogravimétrico para conocer la cantidad de agua en la fórmula molecular de las hidrotalcitas sintetizadas.

Equipo utilizado:

Los experimentos se han realizado en una termobalanza, Perkin-Elmer TGA7 con una precisión de $\pm 1\mu\text{g}$.

Condiciones experimentales:

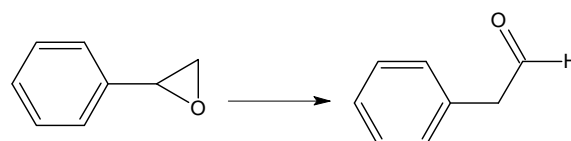
Aproximadamente 30 mg de muestra fueron calentados con una corriente de N_2 gas desde 298 K hasta 873 K a una velocidad de 5 K/min.

3.2.12 Reacciones modelo para estudios de acidez.

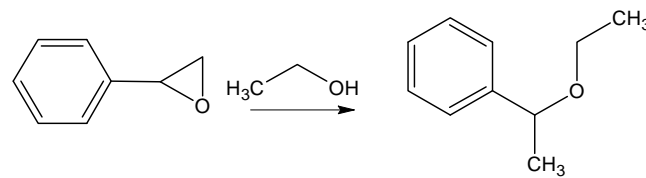
Se han realizado estudios catalíticos en reacciones catalizadas por centros ácidos como procedimiento de caracterización de algunos de los catalizadores preparados, de forma que se puedan diferenciar fuerza y naturaleza de los centros ácidos (Brønsted o Lewis) [44].

En este trabajo se han escogido dos reacciones modelo:

- La isomerización de óxido de estireno para la obtención de β -fenilacetaldehido (Esquema 14).
- La apertura del anillo del óxido de estireno para la obtención de 2-etoxy-2-feniletanol (Esquema 15)



Esquema 14. Isomerización de óxido de estireno.



Esquema 15. Apertura del anillo de óxido de estireno.

La reacción de isomerización de óxido de estireno para la obtención de β -fenilacetaldehido ha sido escogida debido al gran interés de este aldehído a escala industrial en química fina para la producción de fragancias, fármacos, insecticidas, fungicidas y herbicidas [45]. Esta reacción está catalizada por centros ácidos (principalmente centros ácidos de Brønsted). En cambio, la reacción de apertura del anillo de óxido de estireno está principalmente catalizada tanto por centros ácidos de Brønsted como de Lewis. [46].

Equipo utilizado:

El sistema utilizado para llevar a cabo las reacciones de isomerización de óxido de estireno y la apertura del anillo de óxido de estireno en fase líquida consta de un matraz de fondo redondo de 250 ml, un refrigerante y una placa agitadora, tal como se representa en la figura 4.

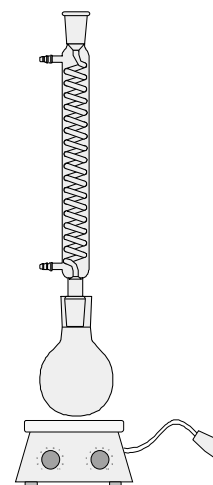


Figura 4. Montaje utilizado para la reacción de isomerización y de apertura del anillo de óxido de estireno.

El análisis de los productos de reacción se ha realizado mediante cromatografía de gases, utilizando un cromatógrafo modelo Shimadzu GC-2010, equipado con un detector de ionización de llama (FID), y una columna del tipo capilar de 30 metros de longitud, con el nombre comercial “DB-1” que contiene como fase mayoritaria fenilmetilsilicona.

Parte experimental

Condiciones experimentales:

La reacción de isomerización del óxido de estireno se ha realizado en fase líquida, a presión atmosférica y a temperatura ambiente. Para las pruebas catalíticas se han utilizado 0.8 g de catalizador (NaM, M9, M12, M13 y M14) 20 ml de tolueno y 4 mmol de óxido de estireno.

La reacción de apertura del anillo del óxido de estireno se ha llevado a cabo en las mismas condiciones que la anterior con la única diferencia que el medio de reacción ha sido 20 ml de etanol en lugar de tolueno.

3.3 Montaje del sistema de reacción e identificación analítica para la reacción de hidrogenación del óxido de estireno

La hidrogenación de óxido estireno para la obtención selectiva de 2-feniletanol se ha llevado a cabo en fase líquida en un sistema como el de la figura 5.

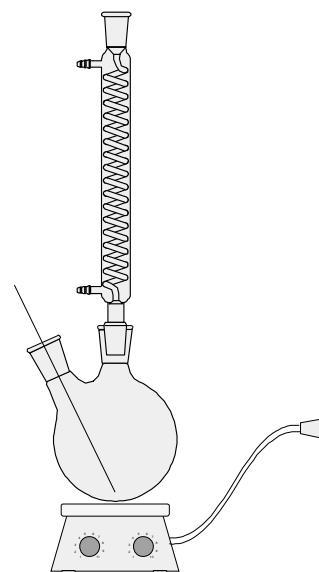


Figura 5. Montaje utilizado para llevar a cabo la reacción de hidrogenación de óxido de estireno en fase líquida.

El sistema utilizado consiste en un matraz de dos bocas de 250 ml, un refrigerante, un borboteador por dónde se hace pasar el gas hidrógeno, un imán y una manta calefactora con agitación.

En todas las pruebas catalíticas se ha utilizado 20 ml de etanol absoluto (Panreac, 99.5 %) y 4 mmol de óxido de estireno (Aldrich, 97 %) con un flujo de hidrógeno puro de 2 ml/s y una agitación de 700 rpm. La cantidad de catalizador depende del tipo de catalizador testado.

El rango de temperatura utilizado va desde temperatura ambiente a 323 K.

Parte experimental

Los productos de reacción se han analizado mediante cromatografía de gases, utilizando un cromatógrafo modelo Shimadzu GC-2010, equipado con un detector de ionización de llama (FID), y una columna del tipo capilar de 30 metros de longitud, con el nombre comercial “DB-1” que contiene como fase mayoritaria fenilmethylsilicona.

La detección se lleva a cabo a una temperatura de inyector y detector de 598 K y desde 343 K hasta 473 K con una rampa de 5 K/min.

Para poder identificar los productos de reacción de la hidrogenación del óxido de estireno se han utilizado muestras patrones, en la que se compara los tiempos de retención en columna con los tiempos de retención de los productos de reacción, y rectas de calibrado para cuantificación de productos y reactivos. Para ello se han preparado muestras patrones de distintas concentraciones con cada uno de los productos de reacción y reactivos (2-feniletanol y óxido de estireno), usando etanol como disolvente y ciclohexanol como patrón interno.

4. RESULTS AND DISCUSSION

4.1 Ni and Ni-MgO catalytic systems

4.1.1 Introduction

The properties of nickel oxide, as precursor of Ni catalysts, have been widely studied [47-49]. Systems containing Ni are known to be active catalysts in hydrogenation reactions due to the ability of metallic nickel to chemisorb dissociatively molecular hydrogen [50,51]. The Raney-Ni catalyst, first synthesized at thirties [52], is one of the most used hydrogenation catalysts at industrial level due to its high metallic area, and its great versatility to be used at low hydrogen pressures as well as under more vigorous conditions.

Taking into account that the properties of metallic catalysts are related to their catalytic activity, we have found many studies focused in the obtention of nickel oxides with different properties by using different preparative methods. Thus, nickel oxides with different degrees of crystallinity, particle sizes [53], morphologies [54] and specific surface areas have been prepared [55,56]. One of the most used NiO preparation methods is the decomposition of nickel nitrate hexahydrate [54,57,58]. These works report that when using thermal treatment with an efficient reduction of the residual water pressure on the sample, only decomposition products such as the dehydration nickel nitrates (tetrahydrate, dihydrate and the anhydrous samples) are obtained in the first steps. In contrast, the presence of water over the sample produces simultaneously dehydration and hydrolytic reactions causing the formation of basic nickel nitrates such as $2\text{Ni}(\text{NO}_3)_2\text{Ni(OH)}_2$ and $\text{Ni}(\text{NO}_3)_2\text{Ni(OH)}_2$. The physisorption study of the samples obtained at several temperatures and residual pressure conditions suggests the presence of intermediate compounds with different characteristics, which give place to NiO samples with different surface properties. Thus, the NiO obtained from nickel nitrate anhydrous has much higher area (about $50 \text{ m}^2/\text{g}$)

than the NiO formed by decomposition in stationary air (about 1 m²/g) using a basic nitrate as a precursor [57].

In previous studies made in our research group, we observed that a careful decomposition of nickel nitrate hexahydrate until the formation of Ni₃(NO₃)₂(OH)₄ as a single phase, and subsequently calcination of this intermediate to form NiO, led to very homogeneous octahedral NiO particles [54].

MgO is a well-known basic solid [59]. Different Mg-O pairs exist at the surface of MgO, where Mg²⁺ and O²⁻ ions have different coordination numbers depending on their location (terrace, corner or edge). The stronger basic sites are generally considered to be oxide ions of low coordination [60]. Another characteristic of MgO is its great tendency to hydration.

Thus, NiO-MgO materials constitute a very interesting system since, after reduction, a Ni metallic catalyst with basic properties is obtained. This catalyst has been used in several reactions such as steam reforming of light hydrocarbons [61], hydrogenation of nitriles [62,63], isomerization of double bonds [64] and hydrogenation of ketones [65,66].

NiO-MgO systems have a tendency to form NiO-MgO solid solutions due to facile diffusion of Ni ions into the MgO support. Many studies have related the reducibility of the NiO-MgO systems with the catalytic performance of the corresponding Ni catalysts [67-69]. Other studies show the striking differences in the reactivity between the NiO formed on the MgO surface and the Ni ions dispersed into the MgO lattice [70]. It has been reported that the interaction of Ni ions with MgO has a positive effect on the resistance to coking, [71] whereas the strong interaction resulting from the high dispersion of Ni ions often lowers the reactivity of catalysts since the strong interaction depresses the formation of the active reduced Ni sites [72]. Therefore, the catalytic performance and reducibility of NiO-MgO systems are very influenced by the preparation conditions [73,74,75].

As commented in the introduction, bulk nickel, palladium and platinum catalysts have shown to be good catalysts for the catalytic hydrogenation of

styrene oxide to 2-phenylethanol [34,36]. Their activity and selectivity were considerably improved with the addition of basic solutions to the reaction medium (88% of selectivity to 2-phenylethanol for a 95% of conversion for a Raney-Ni catalyst) [34]. From these results, Mitsui et al. proposed that this basic reaction medium decreases the interaction between the oxygen of styrene oxide and the catalytic surface minimizing the ethylbenzene formation, and favouring the obtention of 2-phenylethanol (Esquema 7, pg 12).

Taking into account the good results found by using a Raney-Ni catalyst [34,36], we want to study the influence of the surface properties of differently prepared bulk nickel catalysts on the reaction, and also verify the effect of adding basicity to the reaction medium by introducing a solid with basic properties, as magnesia, in the nickel catalyst. The aim of this work is the preparation, characterization and study the catalytic activity for the styrene oxide hydrogenation of three bulk nickel catalysts with different morphologies, and several Ni-MgO systems. In these Ni-MgO systems, we modified the following parameters: a) the basic solid used (commercial magnesia (MgO) and rehydrated magnesia ($MgOr$)), b) the metallic nickel amount, and c) the distribution of basic and nickel sites by using two preparative methods. The catalytic results will be compared with a commercial Raney-Ni catalyst tested at the same reaction conditions. Moreover, the catalytic behaviour of the Ni-MgO systems will be correlated with CO_2 -TPD studies.

4.1.2 Experimental

Catalysts preparation

Table 1 shows the preparation conditions of the different catalytic precursors. The structural differences of the bulk nickel catalysts were obtained by varying the preparation procedure of the NiO precursor through different decomposition ways of $Ni(NO_3)_2 \cdot 6H_2O$.

Table 1. Preparation conditions of the catalytic precursors.

Catalytic precursor	Calcination temperature (K)	Direct precursor of NiO	NiO:MgO weight ratio
NiOA	553	$\text{Ni}(\text{NO}_3)_2$	-
NiOB	593	$\text{Ni}(\text{NO}_3)_2$	-
NiOC	593	$\text{Ni}_3(\text{NO}_3)_2(\text{OH})_4$	-
NiOMgO	593	$\text{Ni}(\text{NO}_3)_2$	1:1
4NiOMgO	593	$\text{Ni}(\text{NO}_3)_2$	4:1
NiOMgOr	593	$\text{Ni}(\text{NO}_3)_2$	1:1
4NiOMgOr	593	$\text{Ni}(\text{NO}_3)_2$	4:1

Commercial $\text{Ni}(\text{NO}_3)_2 \cdot 6\text{H}_2\text{O}$ (Panreac, 99%) was thermally decomposed, flowing Ar through the sample, at 453 K (about 6h) until $\text{Ni}(\text{NO}_3)_2$ was obtained as single phase. This was later calcined at 553 K for 6h to obtain the sample NiOA or at 593 K for 6h to obtain the sample NiOB. When the decomposition of $\text{Ni}(\text{NO}_3)_2 \cdot 6\text{H}_2\text{O}$ was made at 393 K in an air static system, to maintain a certain water steam pressure on the sample, the product obtained after 14 days as single phase was the basic salt $\text{Ni}_3(\text{NO}_3)_2(\text{OH})_4$. This salt was then calcined, flowing Ar through the sample, at 593 K for 6h to obtain the catalytic precursor NiOC.

NiO/MgO and NiO/MgO systems were obtained with different weight ratios (1:1 and 4:1) from physical mixtures of the NiOB samples (previously prepared) with commercial magnesia (Aldrich, 99%) (MgO), or rehydrated magnesia (MgOr), respectively, by stirring the mixture in cyclohexane for 1 hour at room temperature. Rehydrated magnesia (MgOr) was prepared by refluxing commercial MgO in distilled water for 1 h. Then the solid was filtered and dried at 393 K overnight. The organic solvent was then evaporated. These catalytic precursors were named as NiOMgO, 4NiOMgO, NiOMgOr and 4NiOMgOr.

The reduction of the catalytic precursors to obtain the corresponding catalysts, NiA, NiB, NiC, NiMgO, 4NiMgO, NiMgOr and 4NiMgOr was made with pure H₂ at 523 K for 4 h. Other two catalysts, with Ni/MgO ratios of 1:1 and 4:1 (catalysts NiMgOa, 4NiMgOa), were prepared from physical mixtures of commercial MgO with metallic NiB by stirring in degassed cyclohexane at room temperature for 1 hour and later evaporation of the solvent.

The Raney-nickel catalyst used was a commercial nickel sponge suspension in water (Fluka, 99%) and was dried under pure H₂ flow at 453 K for 1 h (referred to as Raney-Ni).

Air-free sampling

The catalysts were always handled under air-free conditions after the reduction step. The catalysts were transferred in degassed cyclohexane and under a hydrogen atmosphere at room temperature. The cyclohexane surface-impregnated samples were further isolated from the air with sticky tape for XRD monitoring, where a glove box was used for mounting.

Characterization of the samples

The catalytic precursors and the catalysts were characterized by Infrared Spectroscopy, X-Ray Diffraction (XRD), BET areas, Temperature-programmed reduction (TPR), Scanning electron microscopy (SEM), Temperature-programmed desorption-mass spectrometry experiments (CO₂-TPD) and Hydrogen Chemisorption. The experimental conditions used have been indicated in the Experimental Section (3.2).

Catalytic activity determination

The catalytic hydrogenation of styrene oxide was made in the liquid phase, using for all tests 0.5 g of active phase, 20 mL of absolute ethanol (Panreac, 99.5%) and 4 mmol of styrene oxide (Aldrich, 97%) with a hydrogen flow of 2 ml/s and agitation of 700 rpm. The reaction was performed at room temperature, and at 323 K. Sample was taken each 1, 3 and 6 h. The reaction

products were analyzed by gas chromatography, using a chromatograph Shimadzu GC-2010 with 30 m of capillary column “DB-1” and a FID detector. They were quantified by adding internal standard and by using a calibrated line. We also tested the catalytic lifetime of the best catalyst by reusing the catalyst five times at the same catalytic conditions.

4.1.3 Results and discussion

Characterization of the catalytic precursors and catalysts

The rehydrated sample (MgOr) was characterized by infrared spectroscopy in order to determine the presence of hydroxyl groups. Fig.6 shows the IR spectrum for this sample where an intense band appeared at 3698 cm⁻¹, corresponding to hydroxyl groups, indicates the rehydration of magnesia. XRD pattern of MgOr (not shown here) confirms the complete transformation of periclase to brucite ($Mg(OH)_2$) after the rehydration process.

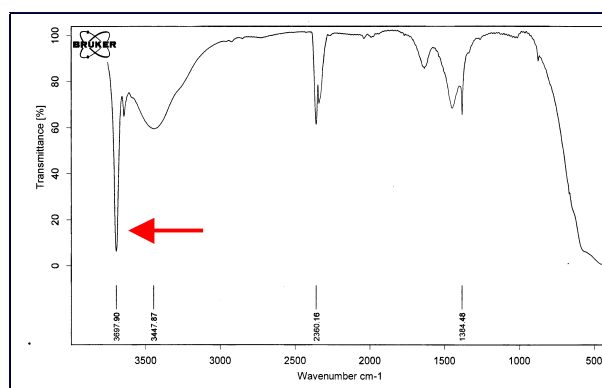


Figure 6. Infrared spectrum of rehydrated magnesia.

Table 2 shows several characterization data for the catalytic precursors. Powder diffraction patterns of the bulk NiO precursors exhibit five sharp peaks, which correspond to the crystalline NiO phase, whereas the NiO-MgO and NiO-MgOr systems show the expected NiO and MgO phases, and NiO and $Mg(OH)_2$ phases, respectively. The presence of two phases indicates that

there is not solid solution in none of these catalytic precursors and, therefore, NiO-MgO and NiO-Mg(OH)₂ interactions are low [75].

Table 2. Characterization of the catalytic precursors.

Catalytic precursors	Crystalline phases (XRD)	BET area (m ² /g)	NiO crystallite size (nm) ^a	Initial reduction temperature ^c (K)
NiOA	NiO	64	12.9	581
NiOB	NiO	43	23.3	619
NiOC	NiO	55	31.8	611
NiOMgO	NiO, MgO	93	23.2 ^b	644
4NiOMgO	NiO, MgO	67	23.5 ^b	627
NiOMgOr	NiO, Mg(OH) ₂	56	23.3 ^b	636
4NiOMgOr	NiO, Mg(OH) ₂	48	23.3 ^b	621

^a Using the Scherrer equation.^b Calculated for the NiO phase.^c Initial reduction temperature obtained from TPR experiments

Regarding the NiO precursors, sample NiOA has the highest BET area (64 m²/g) and the smallest crystallite size (12.9 nm), as expected. Sample NiOB has lower surface area (43 m²/g) and larger crystallite size (23.3 nm) than NiOA. This can be related to a greater sintering of the particles of this sample, which was calcined at higher temperature (593 K). This justifies a higher diffraction domain and its lower surface area. On the other hand, NiOC has an intermediate BET area (55 m²/g) whereas its crystallite size is higher (31.8 nm) than those of the other samples. Taking into account that NiOC was calcined at 593 K (as NiOB), these values can be explained by the different characteristics of its corresponding precursor (Table 1), which gives place to a less crystalline NiO phase with a higher diffraction domain.

The BET area values observed for the MgO and MgOr samples are 130 and 73 m²/g, respectively. Ni-MgO and Ni-MgOr precursors have BET area values proportional to the amount of added magnesia. Thus, the sample with higher magnesia content (NiOMgO) has the highest surface area (Table 2). The precursors with MgOr show lower surface areas than the precursors with commercial MgO (Table 2). These results were expected due to the lower surface area of the MgOr sample. Taking into account that the average crystallite size for the NiOB sample is 23.3 nm and for the commercial MgO

and sample MgOr are 16.9 nm and 19.4 nm, respectively, we observe that the NiOB average crystallite sizes obtained for the Ni-MgO and Ni-MgOr precursors did not practically change during the mixture process (Table 2).

In order to test the reducibility of the nickel oxides and to obtain more information about the NiO-MgO interaction, several temperature-programmed reduction studies were performed. From each plot, the initial reduction temperature (just when the reduction of NiO starts) was determined. The results are shown in Table 2.

The initial reduction temperature observed for the different NiO samples can be related to their surface area values. A higher surface area involves a lower initial reduction temperature. Thus, NiOA, with the highest surface area, starts to reduce before than the other NiO samples (NiOB and NiOC) (Table 2). NiO-MgO and NiO-MgOr systems show higher initial reduction temperature than its NiO precursor (NiOB) being the samples with commercial magnesia those that have higher initial reduction temperature values (Table 2). These results let us to think that there is a certain interaction between NiO and MgO, and between NiO and Mg(OH)₂, respectively. This interaction is slightly higher for the catalytic precursors with commercial magnesia. Thus, the system with higher amount of commercial magnesia (NiMgO) presents the highest initial reduction temperature (Table 2).

Scanning electron microscopy was used to monitor the morphology of the particles for the different catalytic precursors (Fig.7). The presence of particles which remind the octahedral morphology was observed for all of the NiO precursors (Figs.7a, 7b and 7c) but it is important to remark the lack of homogeneity in the particle sizes of the precursors NiOA (Fig.7a) and NiOB (Fig.7b). Sample NiOA has particle sizes between 1000 and 4000 Å whereas sample NiOB exhibits particle sizes in the range 1000-8000 Å. On the other hand, sample NiOC (Fig.7c) shows more defined octahedral particles with homogeneous size (1500 Å). This can be related to the use of Ni₃(NO₃)₂(OH)₄ as direct precursor of NiOC, as observed in previous work [53].

All the precursors prepared NiOB with commercial magnesia or with rehydrated magnesia show some particles with a certain octahedral morphology that should correspond to NiOB (Fig.7d, 7e). Additionally, the samples with MgOr exhibit particles with lamellar morphology corresponding to the brucite phase (Fig. 7e).

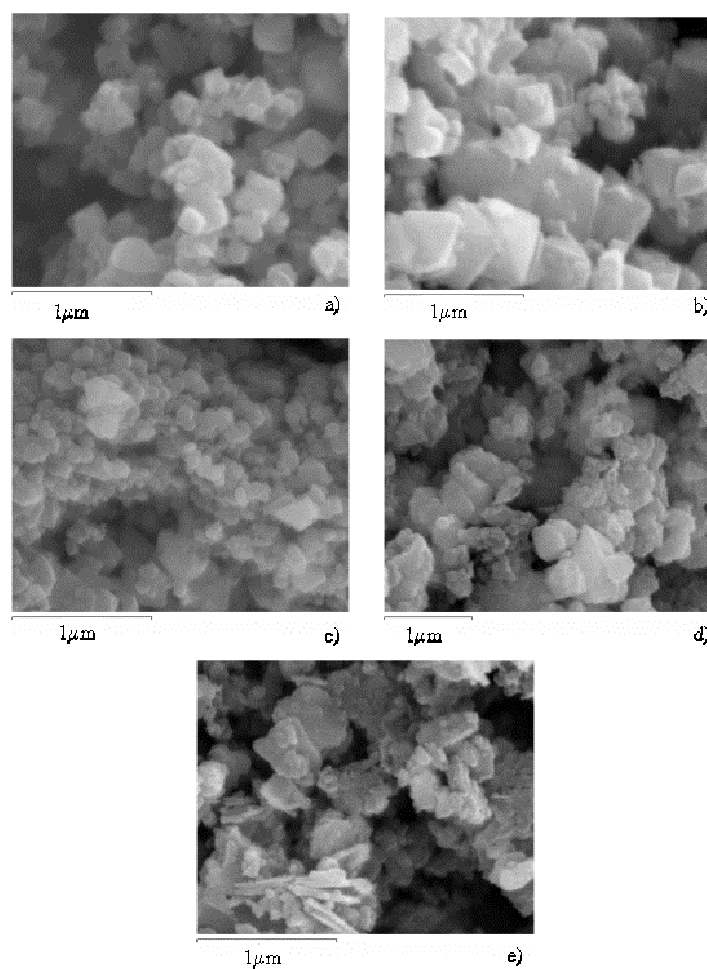


Figure 7. Scanning electron micrographs taken from the surface of the catalytic precursors: a) NiOA, b) NiOB, c) NiOC, d) NiOMgO, e) NiOMgOr.

Table 3 shows some characterization data of the prepared catalysts. Once reduced, as observed by XRD, all NiO is converted to crystalline metallic

nickel for all catalysts together with the corresponding MgO or Mg(OH)₂ phase for the Ni-MgO and Ni-MgOr catalysts, respectively. Catalyst NiB has the highest metallic area. The best reducibility of the catalytic precursors NiOA and NiOC, as deduced from TPR data, seems to favour a greater sintering of their nickel particles formed under the same reduction conditions than NiB.

Table 3. Characterization of the catalysts.

Catalyst	Crystalline phases (XRD)	% Ni	Metallic area (m ² /g sample)
NiA	Ni	100	0.5
NiB	Ni	100	1.7
NiC	Ni	100	0.6
NiMgO	Ni, MgO	44	0.9
4NiMgO	Ni, MgO	76	0.6
NiMgOr	Ni, Mg(OH) ₂	44	0.4
4NiMgOr	Ni, Mg(OH) ₂	76	0.2
NiMgOa	Ni, MgO	44	0.9
4NiMgOa	Ni, MgO	76	1.2

For the catalysts with MgOr (NiMgOr and 4NiMgOr) and for the catalyst 4NiMgO, we observe lower metallic areas than for catalyst NiB and for the catalysts prepared by mixing NiB with MgO (NiMgOa, 4NiMgOa). This can be related to the water formed during the reduction process that should give to some agglomeration of the periclase or brucite particles due to the hygroscopic properties of these basic compounds [64,75]. This involves, indirectly, a sintering of the metallic particles. For the samples with MgOr, their lower metallic area could be explained by a higher agglomeration due to the additional water formed by dehydroxylation of the surface hydroxyl groups. For the catalyst NiMgO, lower agglomeration and, consequently, higher metallic area can be expected, due to the more efficient water removing in this system, which presents lower reducibility (Table 2). Not

significant variations in the morphology of the NiO particles after reduction were observed by SEM.

The commercial Raney-Ni was characterized by H₂ chemisorption and SEM techniques. This catalyst has the highest metallic area (30 m²/g) and, in contrast to the other catalysts, presents very amorphous nickel particles.

Basicity study of the catalytic precursors and catalysts by CO₂-TPD

In order to characterize the basic properties of the catalytic precursors with magnesia, NiOB, and their corresponding catalysts, the strength distribution of their basic sites were determined by TPD-MS of preadsorbed carbon dioxide.

Fig.8 shows the CO₂-TPD profiles of commercial MgO, sample NiOB and the catalytic precursors 4NiOMgO and NiOMgO.

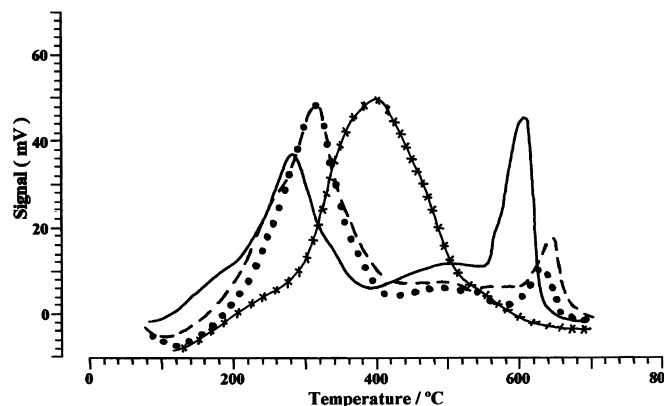


Figure 8. CO₂-TPDs of the samples: MgO(—), NiO (xxxx), 4NiOMgO (••••) and NiOMgO (---).

The TPD profile of commercial MgO mainly shows two intense desorption peaks at 280°C and at 600°C whereas the TPD profile of the NiO sample only shows one desorption peak around 420°C. For the 4NiOMgO and NiOMgO precursors obtained by physical mixing of the NiOB sample and

commercial MgO in the appropriate amounts, we can observe two desorption peaks with different intensity and position respect to the peaks of the TPDs of commercial MgO and sample NiOB. This could be explained taking into account the NiOB/MgO ratio of the catalytic precursors and the existence of some interaction between NiOB and MgO.

Fig. 9 shows the CO₂-TPD profiles of rehydrated MgO (MgOr), the catalytic precursors NiOMgOr and 4NiOMgOr, and also of the NiOB sample for comparison.

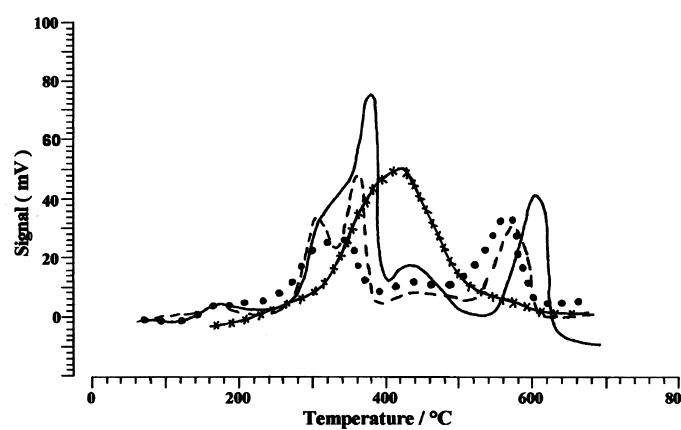


Figure 9. CO₂-TPDs of the samples: MgOr (—), NiO (xxxx), 4NiOMgOr (••••) and NiOMgOr (----).

The TPD profile of sample MgOr exhibits four desorption peaks: a medium-intense peak around 300°C, which is a shoulder of the highest-intense peak appeared at 390°C, a very low intense peak at 440°C, and a peak with medium intensity at 600°C. The catalytic precursors 4NiOMgOr and NiOMgOr show some changes in the position and intensity of the desorption peaks respect to the MgOr and NiOB TPDs. Again, the different NiOB/MgOr ratio and the presence of some NiOB/Mg(OH)₂ interaction could explain these results.

Fig. 10a shows the CO₂-TPD profile of catalyst NiMgO. The peaks in this thermogram have been assigned by comparison with the thermogram of

commercial MgO (Fig.8) and the thermogram obtained for the Ni sample without MgO (Fig 10b).

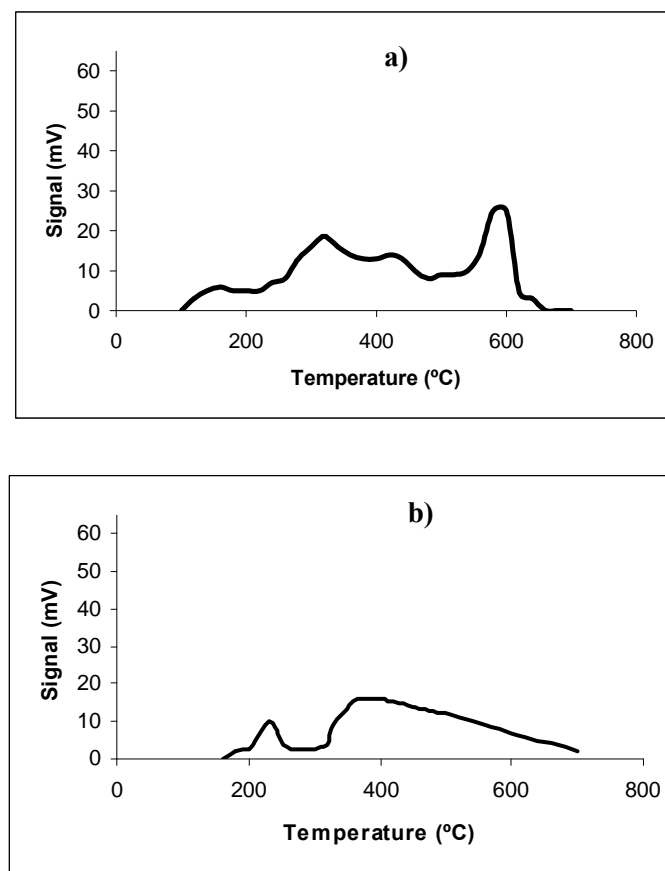


Figure 10. a) CO₂-TPD of the catalyst NiMgO; b) CO₂-TPD of the NiB catalyst.

In the TPD profile of the NiMgO catalyst, we can mainly see two desorption peaks: one with low intensity at 330°C, which can be assigned by intensity and position to metallic nickel (see Fig.10b), and a peak with medium intensity at 600°C which can be related to the stronger basic sites of magnesia (see Fig.8). When compared with the CO₂-TPD profile of MgO, we observe that the intense peak at 280°C, corresponding to the weakest basic sites of commercial magnesia, now does not appear. This fact, together with the presence of the desorption peak characteristic of metallic nickel let us to

think that the metallic nickel particles formed by the NiOB reduction should cover the weakest basic sites of MgO in catalyst NiMgO, explaining the disappearance of this peak. These results suggest the existence of some interaction between the nickel and the weakest basic sites of magnesia. As it has been reported by other authors, CO₂ interacts with nickel being this interaction weaker when the nickel sites increase their electronic density in the presence of other oxide species [76]. This could explain the shift of the CO₂ desorption peak assigned to Ni sites at lower temperatures in the TPD of NiMgO (330°C) respect to the same peak observed in the TPD of the NiB sample (370°C). Lastly, the peak desorbed at 600 °C (Fig.10a) has similar intensity and similar desorption temperature to that of commercial magnesia (Fig.8) taking into account the different MgO amount present in the two samples. This means that NiB particles do not interact practically with the stronger basic sites of magnesia.

Fig. 11 shows the CO₂-TPD profile of catalyst NiMgOr.

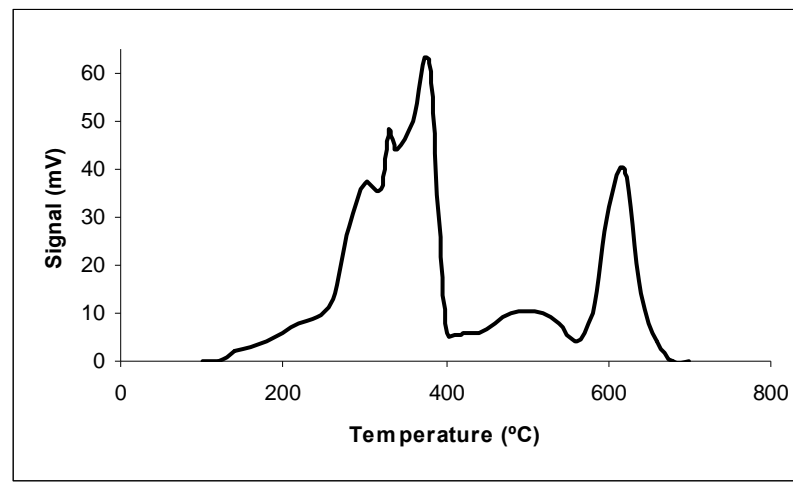


Figure 11. CO₂-TPD of the catalyst NiMgOr.

For the catalysts with rehydrated magnesia, the CO₂-TPD profiles are very similar to that of the rehydrated magnesia (Fig.9). However, a new peak appears around 340 °C (between the peaks at 300°C and 390°C observed for

MgOr). This could be related to nickel sites interacting with basic sites or to basic sites of Mg(OH)₂ which are covering some nickel particles. Both situations involve a certain interaction between the Ni and the brucite particles.

Lastly, the CO₂-TPD profile of NiMgOa catalyst presents three desorption peaks at 280°C, 370°C, and 620°C (Fig. 12).

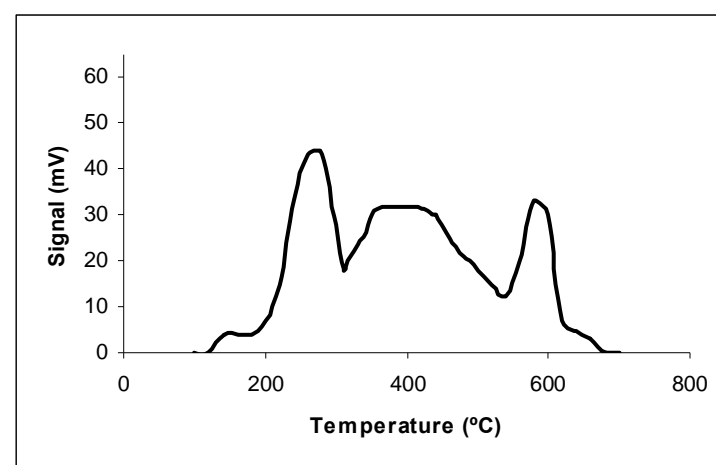


Figure 12. CO₂-TPD of the catalyst NiMgOa.

The peaks that desorb around 280°C and 600°C are proportional in intensity (taking into account the magnesia amount) to those of commercial magnesia (Fig.8) whereas the peak around 370°C can be associated to metallic nickel (Fig.10b), as commented above. Consequently, the interaction Ni-MgO practically does not exist. All these results will be correlated later with the catalytic activity data.

Catalytic activity

Fig. 13 shows the catalytic activity of the three bulk nickel catalysts at room temperature, and at 323 K for the hydrogenation of styrene oxide.

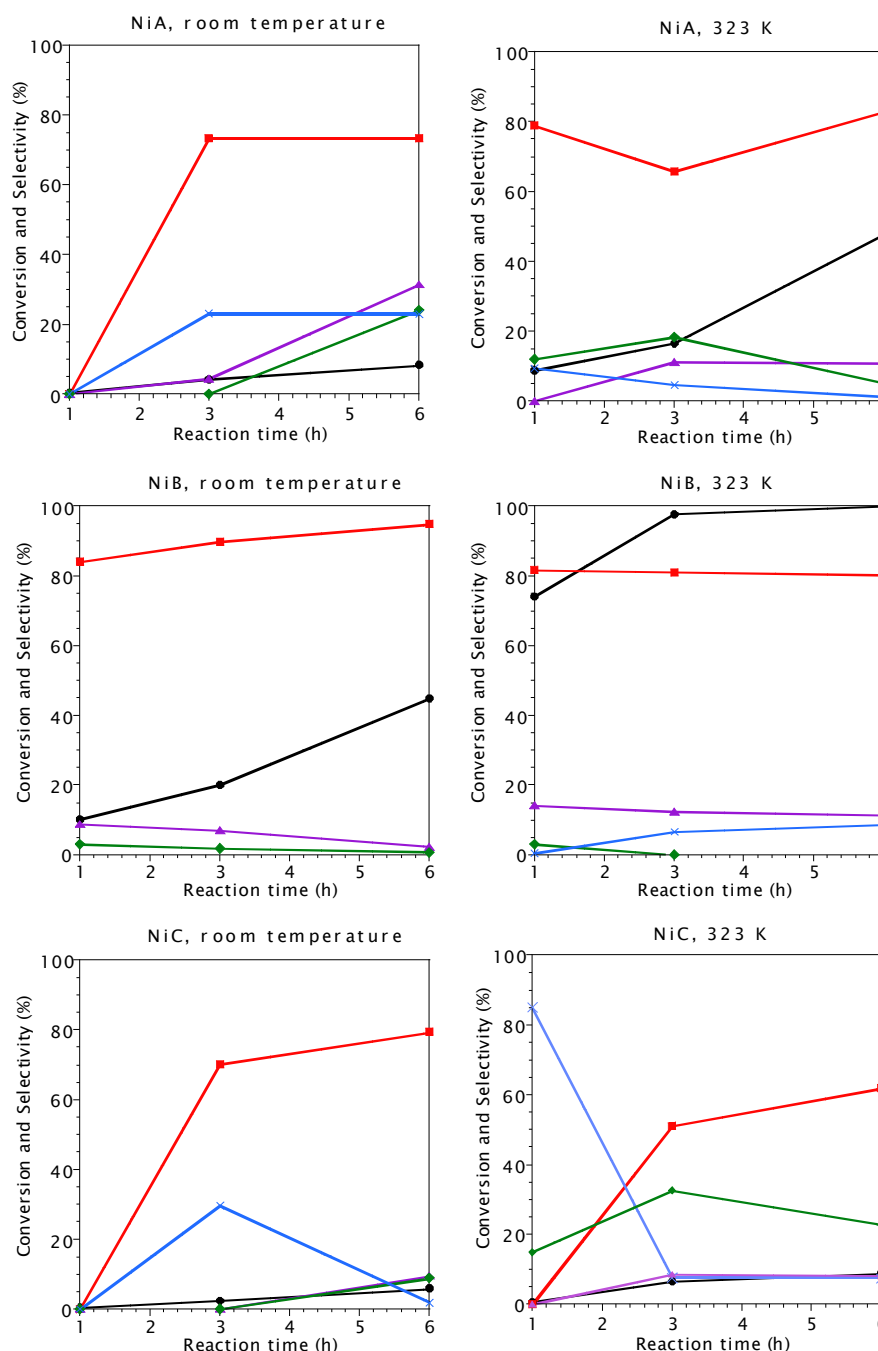


Figure 13. Catalytic activity of the catalysts NiA, NiB, NiC at room temperature and at 323K. Symbols: ● Conversion (%), ■ Selectivity to 2-phenylethanol (%), ✕ Selectivity to Condensation Products (%), ▲ Selectivity to Ethylbenzene (%), ◆ Selectivity to Styrene (%).

These catalysts present low conversion and high selectivity to 2-phenylethanol at room temperature with a maximum of 95 % of selectivity to 2-phenylethanol for a 45 % of conversion for catalyst NiB at 6 h of reaction. The other products, formed in similar amounts, are ethylbenzene, styrene and condensation products. For all catalysts, an increase of conversion, and selectivity to 2-phenylethanol at expenses of the other reaction products, is observed with the reaction time.

By increasing the reaction temperature (323 K), an important increase of conversion maintaining high selectivity to 2-phenylethanol (around 80%) is obtained for catalysts NiA and NiB, whereas for catalyst NiC the conversion is similar than that observed at room temperature decreasing the selectivity to 2-phenylethanol (\approx 60%). Regarding the other reaction products, a slight increase of ethylbenzene is observed for catalyst NiA and, especially, for NiB (around 10% at 6 h) whereas NiC leads to important amounts of styrene (about 20% at 6 h), and condensation products (particularly at the beginning of reaction, 80% at 1 h). Again, catalyst NiB shows the best catalytic results with selectivity to 2-phenylethanol about 80 % for a total conversion at 6 h of reaction.

The modification of the products distribution observed for the styrene oxide hydrogenation when increasing the reaction temperature should be related to a reaction rate of styrene formation lower than the reaction rate of 2-phenylethanol obtaining. It is important to remark that 1-phenylethanol was not detected for any catalyst under these reaction conditions. This is in agreement with the results reported by other authors when using bulk nickel catalysts of type Raney-Ni [34,36].

NiB is the most active catalyst at the two reaction temperatures tested. This can be due to its higher metallic area ($1.7\text{ m}^2/\text{g}$) (Table 3). In contrast, catalysts NiA and NiC, with similar metallic areas (0.5 and $0.6\text{ m}^2/\text{g}$, respectively), show a very different catalytic behaviour. NiC is the less active catalyst with the same low conversion value (10%) at the two reaction temperatures. The detection of higher amounts of styrene than its

corresponding hydrogenated product, ethylbenzene, justifies the low activity of this catalyst. Interestingly, this catalyst showed more defined small octahedral particles than the other bulk nickel catalysts (Fig.7). We think that these octahedral morphologies could favour the formation of more amounts of high-weight condensation products during the first hours of reaction, which can block partially the active centres of the catalyst, decreasing its activity.

Figure 14 shows the results of catalytic activity of one commercial Raney-Ni catalyst at room temperature, and at 323 K for the hydrogenation of styrene oxide. These catalytic studies were made in order to compare them with the results obtained by our catalysts at the same reaction conditions.

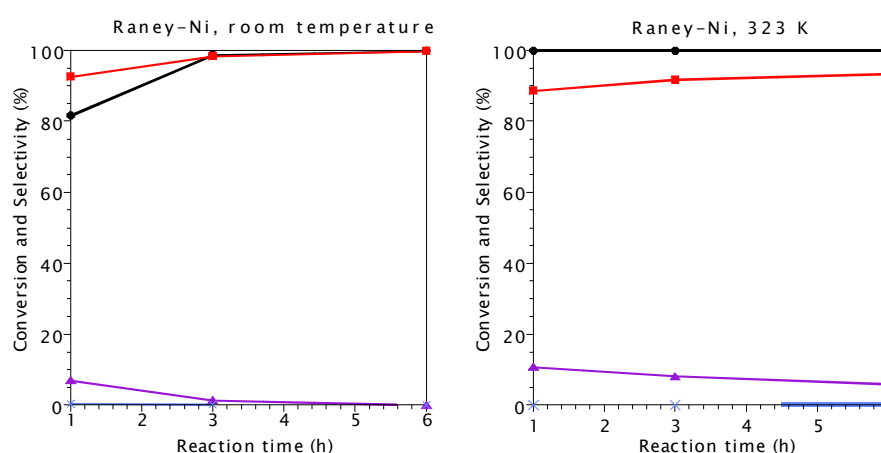


Figure 14. Catalytic activity of commercial Ni-Raney catalysts at room temperature and at 323K. Symbols: • Conversion (%), ■ Selectivity to 2-phenylethanol (%), ✕ Selectivity to Condensation Products (%), ▲ Selectivity to Ethylbenzene (%), ◆ Selectivity to Styrene (%).

This commercial Raney-Ni catalyst presents much higher conversion values and higher selectivity to 2-phenylethanol than the prepared bulk nickel catalysts although the differences are higher respect to NiA and NiC than respect to NiB. Also, ethylbenzene was detected in small amounts. This higher conversion can be related to its much higher metallic area ($30 \text{ m}^2/\text{g}$), whereas the selectivity values should be related to its electronic characteristics that are

very different respect to the other prepared crystalline bulk nickel catalysts. This allows us to adjudge to the characteristics of the metallic centres an important role in the catalytic behaviour of the studied reaction.

Figure 15 shows the results of catalytic activity of Ni-MgO catalysts at room temperature, and at 323 K for the hydrogenation of styrene oxide.

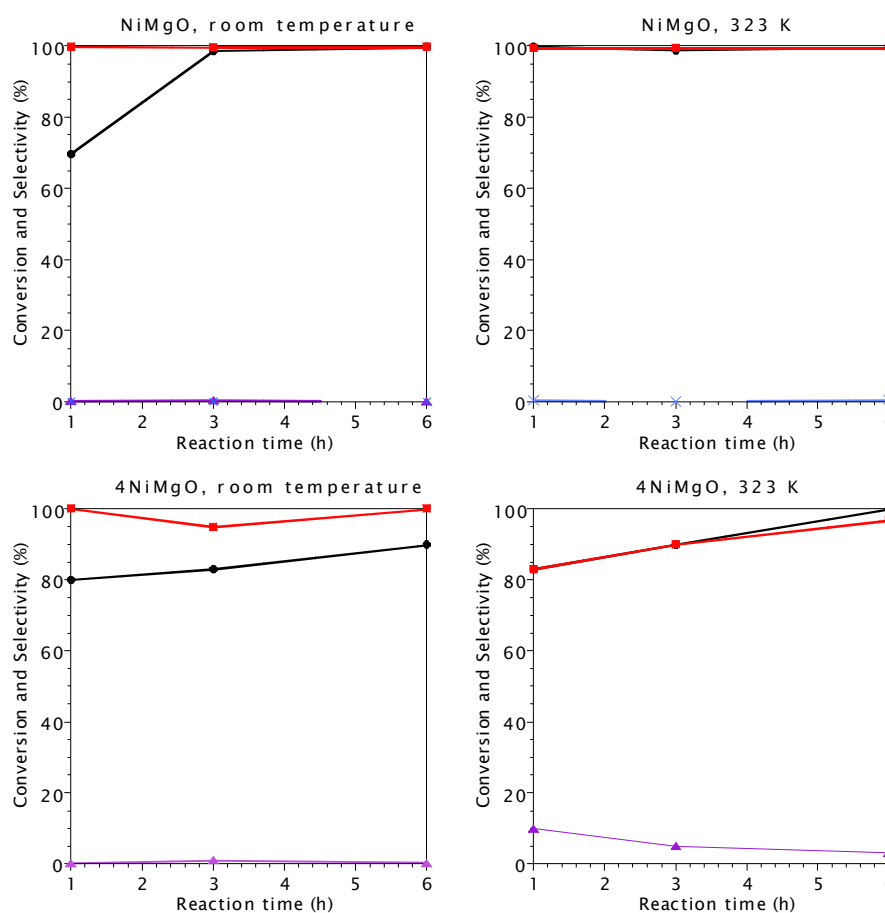


Figure 15. Catalytic activity of the catalysts 4NiMgO and NiMgO at room temperature and at 323K. Symbols: ● Conversion (%), ■ Selectivity to 2-phenylethanol (%), ✕ Selectivity to Condensation Products (%), ▲ Selectivity to Ethylbenzene (%), ♦ Selectivity to Styrene (%).

These catalysts present high conversion and high selectivity values to 2-phenylethanol from the first hour of reaction with a maximum of 100% of selectivity to 2-phenylethanol for a total conversion when using catalyst NiMgO at 323 K at any reaction time.

As we can see, the conversion increases when increasing the reaction time, the reaction temperature and the magnesia content. It is important to note that only ethylbenzene in small amounts was observed as by-product, and only for the catalyst with less magnesia content, 4NiMgO. This confirms the importance of the contribution of basicity on the reaction mechanism, and shows magnesia as a good material to obtain the desired basic sites. These results are in agreement with the mechanism proposed by Mitsui et al. for this reaction in basic solution medium (Esquema 7, pg.12) [34]. Additionally, this basicity seems to play a fundamental paper to control the formation of condensation products, which could be responsible for the deactivation of the catalyst, as commented above for catalyst NiC. Thus, both effects of magnesia explain the higher conversion and selectivity to 2-phenylethanol values achieved when using NiMgO catalyst, with higher magnesia content, respect to 4NiMgO.

Another fact to comment is that despite having the same precursor, NiOB, catalyst NiB shows lower conversion, especially at room temperature (Fig.13), than the Ni-MgO catalysts. This again confirms the effect of magnesia which avoids the formation of condensation products on the metallic surface giving higher activity to the mixed catalysts.

Figure 16 shows the catalytic activity of the catalysts 4NiMgOr and NiMgOr at room temperature.

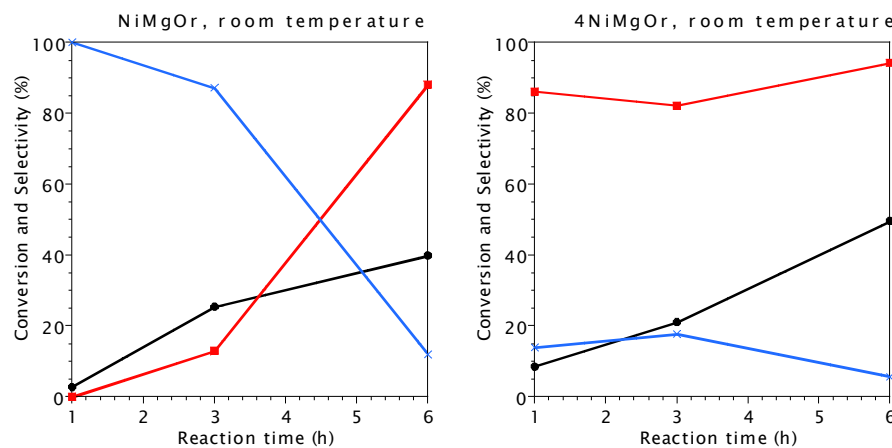


Figure 16. Catalytic activity of the catalysts 4NiMgOr and NiMgOr at room temperature.
Symbols: • Conversion (%), ■ Selectivity to 2-phenylethanol (%), ✕ Selectivity to Condensation Products (%), ▲ Selectivity to Ethylbenzene (%), ◆ Selectivity to Styrene (%).

By using NiMgOr and 4NiMgOr catalysts, much lower conversion and lower selectivity to 2-phenylethanol values at expenses of higher amounts of condensation products were observed.

Finally, catalysts NiMgOa and 4NiMgOa show low conversion and very low or null selectivity to 2-phenylethanol (Figure 17).

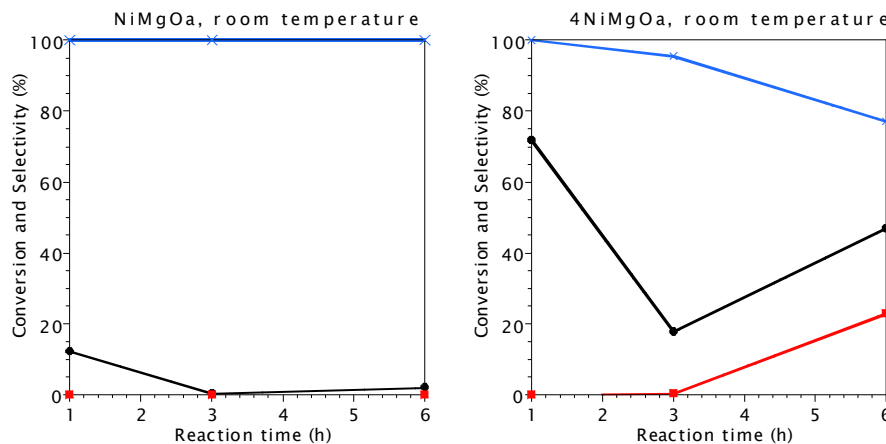


Figure 17. Catalytic activity of the catalysts 4NiMgOr and NiMgOr at room temperature.
Symbols: Symbols: • Conversion (%), ■ Selectivity to 2-phenylethanol (%), ✕ Selectivity to Condensation Products (%), ▲ Selectivity to Ethylbenzene (%), ◆ Selectivity to Styrene (%).

We detected very high amounts of condensation products in these catalysts (77 % for 4NiMgOa and 100 % for NiMgO).

The metallic area of these catalysts cannot explain these catalytic results, since the highest metallic area ($1.2 \text{ m}^2/\text{g}$) (Table 3) corresponds to the catalyst 4NiMgOa with low conversion and very low selectivity to 2-phenylethanol. Interestingly, the catalytic behavior of these catalysts with magnesia could be related to the different CO_2 -TPD profiles observed for these catalysts. Thus, the catalyst with higher MgO content (NiMgO), whose CO_2 -TPD showed metallic nickel partially covering the weakest basic sites of magnesia (Fig.10a) is more active and selective to 2-phenylethanol than the rest of catalysts. On the other hand, the CO_2 -TPDs of catalysts NiMgOr and NiMgOa showed an important amount of available basic sites that favour the formation of higher amounts of condensation products, which are responsible for the catalyst deactivation [13]. In these Ni-MgOr and Ni-MgOa systems the interaction between metallic and basic particles are very low or null. Therefore, we can conclude that the metallic nickel under the influence of the weakest basic sites of commercial magnesia should be related to the selective formation of 2-phenylethanol. This minimizes the formation of other reaction products such as ethylbenzene or condensation products, which were not detected in these catalysts.

Interestingly, the catalyst with higher magnesia content, NiMgO, shows similar conversion values but higher selectivity to 2-phenylethanol (Fig. 15) than the Raney-Ni catalyst (Fig.14). This reveals, again, the effect of magnesia which favours the selective formation of 2-phenylethanol.

The catalytic lifetime of the best catalyst (NiMgO) was also tested (Fig.18). After reusing the catalyst once, the same conversion and selectivity values were obtained. When the catalyst is used again we observe a slight conversion decrease from 100% to 83%, whereas the selectivity to 2-phenylethanol remains around 95 %. These catalytic activity values are maintained when the catalyst is reused three more times. These slight variations could be explained by the formation of small amounts of

condensation products, which block some metallic sites. Therefore, there is a clear influence of basicity in the catalytic behaviour of these Ni-MgO systems.

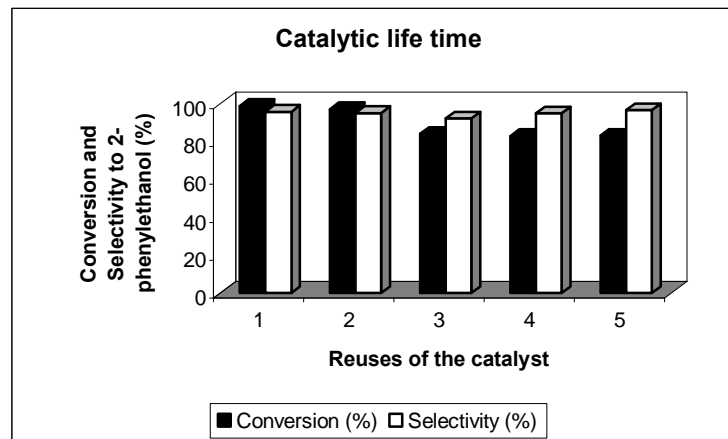


Figure 18. Catalytic life time of the best catalyst NiMgO.

4.1.4 Conclusions

The bulk nickel catalysts prepared present high selectivity to 2-phenylethanol (60-95%) despite their different conversion values. These catalysts give to the formation of condensation products which block the active centres of the catalyst, decreasing its activity. This behaviour appears more marked for catalyst NiC (the less active) which, interestingly, is the catalyst that showed more homogeneous and defined octahedral particles. When increasing the temperature of reaction, an increase of the conversion as well a certain decrease of the selectivity to 2-phenylethanol is observed at expenses of styrene and ethylbenzene formation. The most active of the bulk nickel catalysts prepared is catalyst NiB. This can be related to its higher metallic area.

On the other hand, the basic sites available in the Ni-MgO catalysts determine the distribution of the reaction products for the hydrogenation of styrene oxide. Catalysts with commercial MgO (NiMgO and 4NiMgO) present conversion and selectivity to 2-phenylethanol values that increase when the content of magnesia increases arriving to 100% for catalyst NiMgO at the two temperatures of reaction tested. The CO₂-TPD profile of the best catalyst, NiMgO, showed the disappearance of the peak corresponding to the weaker basic sites of commercial magnesia. This means that the metallic nickel, obtained after reduction, cover these basic sites and, therefore, there is some influence between the nickel particles and the basic sites, which become less available. The existence of a certain interaction between the nickel and the weakest basic sites of magnesia in these Ni-MgO catalysts favour the quickly formation of 2-phenylethanol, and consequently, minimizes other side reactions like the formation of condensation products. This explains the higher conversion and selectivity to 2-phenylethanol values of these Ni-MgO catalysts despite having lower metallic area than NiB and Raney-Ni catalysts.

In contrast, the CO₂-TPD profiles obtained for catalysts NiMgOr and NiMgOa showed that they have higher amounts of basic sites available. This can explain the higher amounts of condensation products, detected for catalysts NiMgOr, 4NiMgOr, NiMgOa and 4NiMgOa, which are responsible for their lower activity.

The catalyst prepared with the highest amount of commercial magnesia (NiMgO) maintains high conversion and selectivity to 2-phenylethanol values after reusing several times.

4.2 Catalytic systems based on Hydrotalcite-like compounds

4.2.1 Introduction

Hydrotalcite-like compounds, a class of layered materials having the general formula $[M(II)]_{1-x} M(III)_x (OH)_2][A^{n-}]_m H_2O$, have been receiving increasing attention in the last years owing to their potential applications as basic catalysts, supports, ion-exchangers and precursors for composite materials [77-79]. Structurally, layered double hydroxides (LDHs) have brucite-like ($Mg(OH)_2$) sheets where isomorphous substitution of Mg^{2+} by a trivalent cation, like Al^{3+} , occurs (Fig. 19). The resulting positive charge excess of the layered network is compensated by anions, which occupy the interlayer space along with water molecules. Their basicity is mainly related to the amount and nature of divalent cations present.

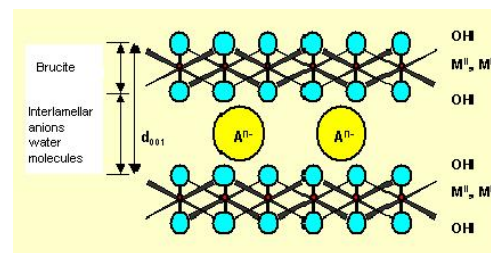


Figure 19. Hidrotalcite structure.

Controlled thermal decomposition of hydrotalcites gives to high-area mixed oxides that have numerous catalytic applications such as the removal of SO_x and NO_x , aldol condensations, phenol alkylations, epoxidation of olefines, and partial oxidation, hydrodehalogenation or hydrogenation reactions [80-89]. The acidic-basic properties of calcined hydrotalcites can be tailored by changing the calcination temperature, the nature and amount of structural cations and compensating anions, as well as, the method of synthesis of the LDHs [77,90]. Besides, these mixed oxides show a memory effect, a property by which they can recover the original lamellar structure if they come in contact with water vapour or are immersed in liquid water. These

rehydrated materials have been applied to a number of base-catalyzed reactions on account of their Brønsted basic character [81,91,92].

Unfortunately, hydrotalcites are not often found in nature so they have to be synthesized. Hydrotalcites are conventionally prepared by coprecipitation, wherein metal nitrates and precipitants are added slowly and simultaneously at a fixed pH under stirring. The main disadvantage of this method is the time required to crystallize the hydrotalcite. Thus, the precipitated gel has to be aged for a long time (about one day) [93,94]. New synthetic routes have been explored, for instance the sol-gel method, but expensive reactants are required and the resulting solid is not fully crystalline [95].

Microwave irradiation has been widely used for the synthesis of inorganic solids and in organic synthetic reactions [96,97]. From middle of 90s, the formation of well-crystallized and pure hydrotalcite-like phases, when aging the coprecipitated gels under microwaves, have been reported with a considerably decrease of the aging time. On the whole, these hydrotalcites aged under microwaves present smaller particles sizes and higher surface areas than conventional samples [98-102]. The most part of studies published concerns the influence of the microwave irradiation power on the aging of binary hydrotalcite gels [103-105], basically Mg/Al, and the study of the basic properties of the resulting mixed oxides [104]. Recently, the effect of microwave power on Zn/Mg/Al gels and the influence of the irradiation temperature of aged Mg/Al gels on the surface properties of calcined samples have been reported [106,107].

Interestingly, Tichit et al. reported the presence of surface-defective sites with an increase of both basic and acid sites in the resulting Mg/Al mixed oxides when the hydrotalcite was aged by microwave irradiation [108]. Also, a decrease of aluminium in the hydrotalcite structure accompanied by the formation of hydroxylated aluminium species in the extraframework has been detected in some cases. This could be related to some erosion of the hydrotalcite layers because of the microwaves interaction [108-110].

The basicity of the hydrotalcites and the mixed oxides obtained after their calcination can be studied by temperature-programmed desorption (TPD) using an acid probe molecule, such as CO₂. This technique also can allow us to study the surface modifications associated to the acid-basic properties of these materials.

Firstly, in this chapter, we present a systematic study on several hydrotalcites of Ni/Mg/Al prepared from coprecipitated gels with the same composition using a laboratory microwave oven, equipped with a temperature controller, to age the gel at various temperatures and times in order to study the influence of treatment conditions on the basic and surface properties of the resulting hydrotalcites and their calcination compounds. Besides, we synthesized these Ni/Mg/Al hydrotalcites aged by the traditional refluxing method and by autoclaving for comparison. All samples were characterized by a wide number of techniques.

Taking into account the good results found by using basic Ni-MgO catalysts, as commented in the previous chapter, we believe that Ni/Mg/Al hydrotalcites can be good candidates to be used as catalytic precursors for the hydrogenation of styrene oxide in order to obtain selectively 2-phenylethanol since, after calcination-reduction, they can lead to well-dispersed metallic nickel interacting with basic sites. Hydrotalcites were prepared using low amounts of Mg and Al in order to avoid high basicity that could be responsible for undesirable reactions [36]. Several catalysts based on hydrotalcite-like compounds have been tested in the hydrogenation of styrene oxide in the liquid phase in order to study the influence of the hydrotalcites aging step on their surface properties and, consequently, on the catalytic behaviour of the resulting catalysts.

4.2.2 Experimental

Catalysts preparation

The starting gel was synthesized by the traditional coprecipitation method at room temperature at constant pH ($\text{pH} = 8 \pm 0.1$), using an aqueous solution containing in appropriate amounts $\text{Ni}(\text{NO}_3)_2 \cdot 6\text{H}_2\text{O}$, $\text{Mg}(\text{NO}_3)_2 \cdot 6\text{H}_2\text{O}$ and $\text{Al}(\text{NO}_3)_3 \cdot 9\text{H}_2\text{O}$, and a 1M NaOH titrating solution which were simultaneously added to an aqueous solution of $\text{Na}_2\text{CO}_3 \cdot 10\text{H}_2\text{O}$ 0.05M. The ratio $\text{M}^{2+}/\text{Al}^{3+}$ was 4:1 and the ratio $\text{Ni}^{2+}/\text{Mg}^{2+}$ was 6:1. Dropwise addition was performed under vigorous magnetic stirring. After complete precipitation, the gel was aged at different conditions resulting in 27 samples to be compared.

One sample was obtained by refluxing the gel under stirring at 343 K for 1080 min (R_{1080}). Four samples were obtained by refluxing the gel under microwave irradiation at 343 K for 60, 120, 240 and 480 min, respectively (RMW_{60} , RMW_{120} , RMW_{240} , RMW_{480}). Another four samples were aged in an autoclave in an oven at 403 and 423 K for 120 and 360 min, respectively (403A_{120} , 403A_{360} , 423A_{120} , 423A_{360}). The last series of samples were aged in an autoclave into a microwave oven (Milestone ETHOS-TOUCH CONTROL) at 403 K, 423 K and 453 K for 1, 5, 15, 30, 60 and 120 min for each temperature (403MW_1 , 403MW_5 , 403MW_{15} , 403MW_{30} , 403MW_{60} , 403MW_{120} , 423MW_1 , 423MW_5 , 423MW_{15} , 423MW_{30} , 423MW_{60} , 423MW_{120} , 453MW_1 , 453MW_5 , 453MW_{15} , 453MW_{30} , 453MW_{60} , 453MW_{120}). Finally, all samples were filtered and washed several times with deionised water and the solids were dried in an oven at 393 K overnight.

Five of these samples (403MW_{15} , 453MW_{120} , RMW_{120} , R_{1080} and 403A_{360}) were calcined flowing nitrogen through the sample (2 ml/s) at 623 K for 3 h to obtain the samples named as R_{1080}C , $403\text{A}_{360}\text{C}$, RMW_{120}C , $403\text{MW}_{15}\text{C}$ and $453\text{MW}_{120}\text{C}$. These catalytic precursors were reduced flowing hydrogen through the sample (2 ml/s) at 623 K for 6 h to obtain the corresponding catalysts named as R_{1080}R , $403\text{A}_{360}\text{R}$, RMW_{120}R , $403\text{MW}_{15}\text{R}$ and $453\text{MW}_{120}\text{R}$.

Air-free sampling

The catalysts were always handled under air-free conditions after the reduction step. The catalysts were transferred in degassed cyclohexane and under a hydrogen atmosphere at room temperature. The cyclohexane surface-impregnated samples were further isolated from the air with sticky tape for XRD monitoring, where a glove box was used for mounting.

Characterization of the samples

The catalytic precursors and the catalysts were characterized by Infrared Spectroscopy, X-Ray Diffraction (XRD), Nitrogen physisorption, Scanning electron microscopy (SEM), Transmission electron microscopy (TEM), Temperature-programmed desorption-mass spectrometry experiments (CO_2 -TPD and H_2 -TPD), Atomic absorption, Thermogravimetric analyses (TGA) and Hydrogen Chemisorption. The experimental conditions used have been indicated in the Experimental Section (3.2).

Catalytic activity determination

The catalytic hydrogenation of styrene oxide was made in the liquid phase, using for all tests 0.5 g of active phase, 20 mL of absolute ethanol (Panreac, 99.5%) and 4 mmol of styrene oxide (Aldrich, 97%) with a hydrogen flow of 2 ml/s and agitation of 700 rpm. The reaction was performed at room temperature. Sample was taken each 15 minutes. The reaction products were analyzed by gas chromatography, using a chromatograph Shimadzu GC-2010 with 30 m of capillary column "DB-1" and a FID detector. They were quantified by adding an internal standard and by using a calibrated line. We also tested the catalytic lifetime of these catalysts by reusing them ten times at the same reaction conditions.

4.2.3 Results and discussion

Characterization of the hydrotalcites

➤ X-Ray diffraction (XRD)

Figs. 20-22 show the XRD patterns obtained for all samples whereas tables 4 and 5 exhibit the FWHM and cell parameters values.

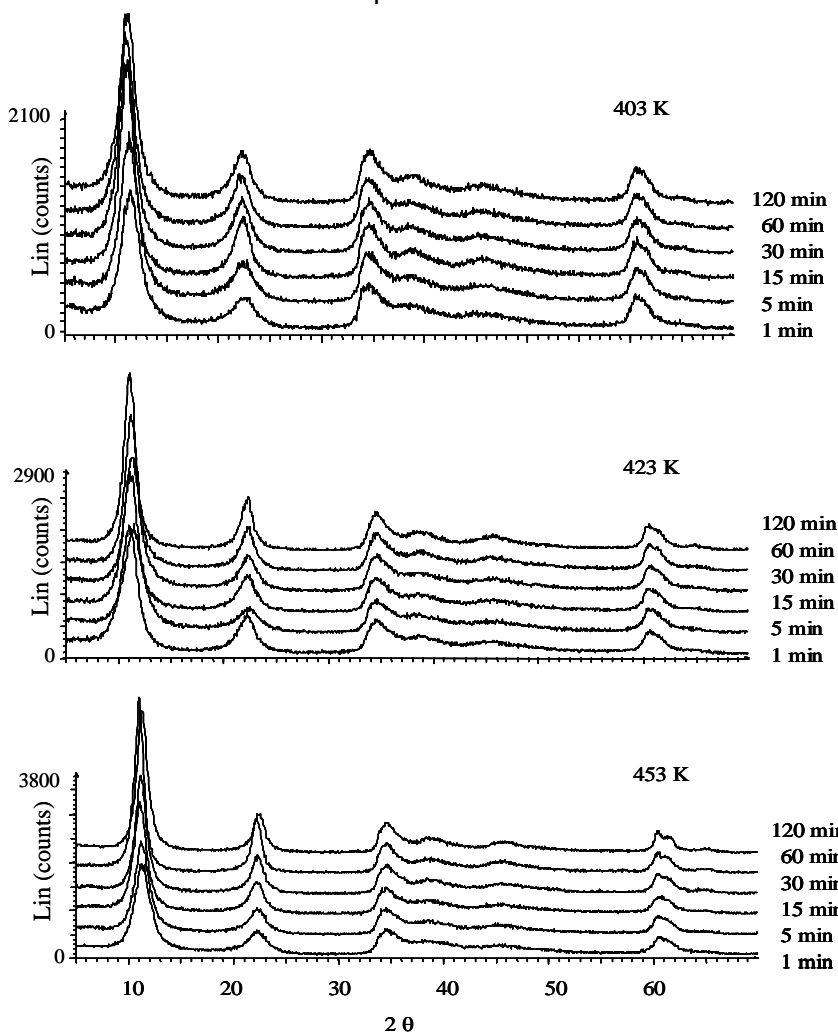


Figure 20. XRD patterns of the hydrotalcites aged in an autoclave under microwaves.

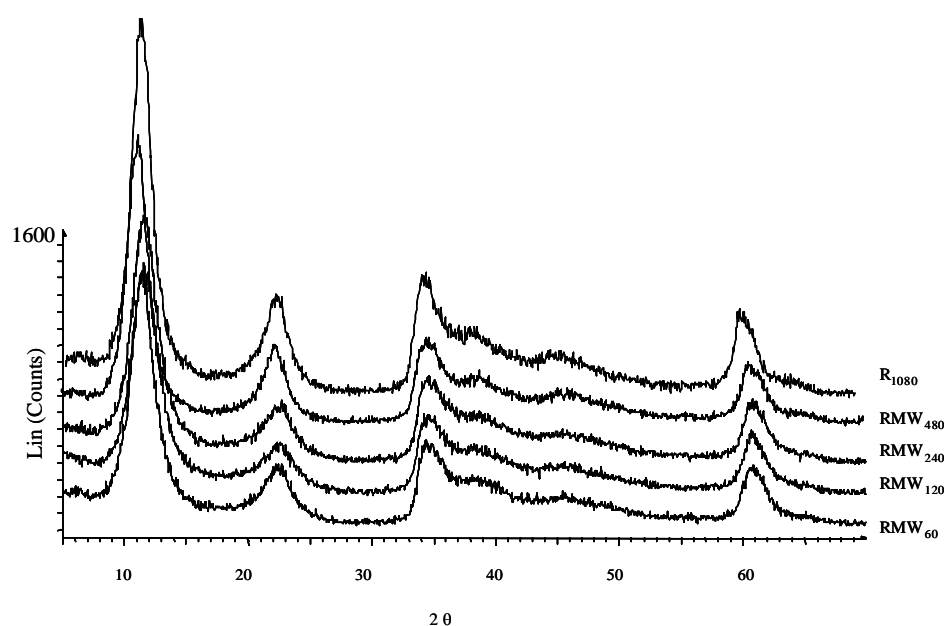


Figure 21. XRD patterns of the hydrotalcites aged by conventional refluxing and by refluxing under microwave irradiation.

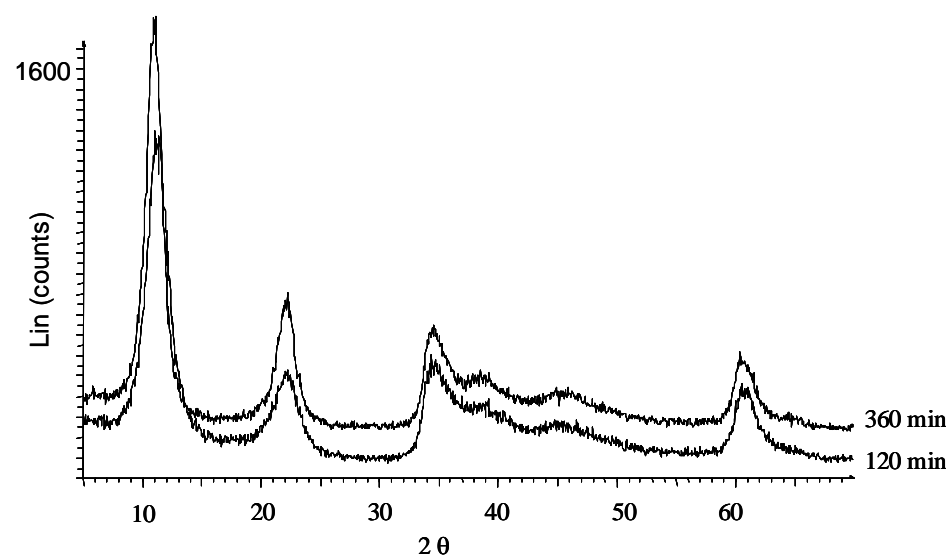


Figure 22. XRD patterns of the hydrotalcites aged by heating in a conventional oven at 403 K.

Results and Discussion

Catalytic systems based on Hydrotalcite-like compounds

Table 4. Characterization results obtained by XRD and nitrogen physisorption for the samples aged under microwave irradiation.

	FWHM ^a (degrees)	c (nm)	a (nm)	Surface Area (m ² /g)
403MW₁	2.06	2.336	0.306	32.0
403MW₅	2.00	2.362	0.305	20.3
403MW₁₅	1.82	2.398	0.305	12.6
403MW₃₀	1.80	2.399	0.305	3.7
403MW₆₀	1.77	2.408	0.306	4.4
403MW₁₂₀	1.76	2.383	0.306	2.9
423MW₁	2.05	2.415	0.306	26.9
423MW₅	1.84	2.339	0.306	14.5
423MW₁₅	1.66	2.398	0.306	11.8
423MW₃₀	1.63	2.361	0.306	2.6
423MW₆₀	1.43	2.383	0.306	< 2.5
423MW₁₂₀	1.23	2.411	0.306	< 2.5
453MW₁	1.74	2.367	0.306	< 2.5
453MW₅	1.56	2.376	0.306	< 2.5
453MW₁₅	1.38	2.401	0.306	< 2.5
453MW₃₀	1.23	2.389	0.306	8.0
453MW₆₀	1.00	2.415	0.306	11.9
453MW₁₂₀	0.94	2.407	0.306	87.2
RMW₆₀	2.05	2.301	0.305	2.5
RMW₁₂₀	2.04	2.345	0.305	3.3
RMW₂₄₀	2.02	2.302	0.305	3.4
RMW₄₈₀	1.80	2.370	0.305	3.2

^a FWHM values have been measured for peak (003).

Table 5. Characterization results obtained by XRD and nitrogen physisorption for the samples aged by conventional methods.

	FWHM ^a (degrees)	c (nm)	a (nm)	surface area (m ² /g)
403A₁₂₀	2.01	2.379	0.305	< 2.5
403A₃₆₀	1.79	2.333	0.306	< 2.5
423A₁₂₀	1.76	2.381	0.306	2.9
423A₃₆₀	1.45	2.386	0.306	< 2.5
R₁₀₈₀	1.87	2.359	0.306	32.3

^a FWHM values have been measured for peak (003).

Hydrotalcite-like compounds have characteristic XRD patterns with sharp and intense peaks for the (003), (006), (110) and (113) planes, as well as broad symmetric peaks for the (009), (015) and (016) planes. The full width at half maximum (FWHM) of the basal reflection plane (003) is usually taken to evaluate their crystallinity in the stacking direction.

In the starting precipitated gel, without aging, as well as in the 27 samples aged at different conditions (Figs. 20-22) only one phase, corresponding to hydrotalcite, was detected. On the whole, the crystallinity of the hydrotalcites is low although they show different crystallinity degrees. Once measured the FWHM values, we can see that the starting precipitated gel without aging has higher FWHM value (2.06), and therefore, lower crystallinity than the samples aged by any method (Tables 4 and 5).

For the hydrotalcites aged in an autoclave by microwaves, the FWHM values decrease when increasing the aging time and the aging temperature (Table 4) indicating an increase of the crystallinity. Therefore, both factors, higher temperatures and longer times of aging, favour crystallization in the stacking direction. Thus, the hydrotalcite aged at 453 K for 120 min is the most crystalline. The better resolution of the peaks at higher 2θ values, specifically those which correspond to the (110) and (113) planes, also confirms a higher interlayer ordering in this sample (Fig. 20). For the hydrotalcites aged by refluxing under microwaves, the FWHM values also decrease when increasing the aging time but less significantly than for the samples aged by autoclaving under microwaves (Table 4). It is well known that the crystallization of hydrotalcites is a consequence of the growing of the seeds formed during the coprecipitation process [110]. Therefore, the variation of the FWHM values with time allows us to interpret when the seeds formed during coprecipitation begin growing favouring the crystallization. Taking as a reference the FWHM value of the coprecipitated gel without aging (2.06), for the hydrotalcites aged in an autoclave by microwaves at 403 K, 15 min are necessary to detect a significant growing of the seeds whereas for the hydrotalcites aged at 423 K and at 453 K only 5 min and 1 min are needed,

respectively (Table 4). In contrast, the hydrotalcites aged by refluxing under microwaves need more than 240 min to obtain a noticeable crystallization of the seeds (Table 4). Furthermore, these hydrotalcites are less crystalline than those obtained by autoclaving under microwaves.

By comparing the hydrotalcites prepared by refluxing under microwaves and by conventional method (Fig. 21), we observe that sample R₁₀₈₀, prepared by refluxing without microwaves at 343 K for 1080 min, has similar crystallinity in the stacking direction (FWHM = 1.87) (Table 5) than the hydrotalcite RMW₄₈₀, aged by refluxing under microwaves at the same temperature for 480 min (FWHM = 1.84) (Table 4). Therefore, we obtained hydrotalcites with higher crystallinity in the half of time when using microwaves.

This effect was also observed by comparing the hydrotalcites aged in an autoclave with and without microwaves (Figs. 20 and 22). The crystallinity of the hydrotalcites aged in a conventional autoclave at 403 and 423 K for 360 min and 120 min, respectively (samples 403A₃₆₀ and 423A₁₂₀) is similar to that of the hydrotalcites obtained in an autoclave by microwave irradiation at the same temperatures at 30 min and less than 15 min, respectively (samples 403MW₃₀ and 423MW₁₅) (Tables 4 and 5). Besides, the seeds begin growing approximately twelve times faster in the hydrotalcites aged in an autoclave by microwaves at 403 K and at 423 K than those prepared in a conventional oven.

The cell parameters (*a* and *c*), calculated from the (110) and (003) interplanar distances, respectively, were determined in order to obtain information about modifications in the sheets and in their stacking for all the hydrotalcites prepared (Tables 4 and 5). The cell parameter *a*, which is mainly related to the cation composition, practically does not change (*a*= 0.305-0.306). Taking into account that nickel is the main component of these hydrotalcites, the very low differences observed in the *a* values could indicate that the nickel composition of the samples does not practically vary. For the cell parameter *c*, which is proportional to the interplanar distance, any defined

tendency cannot be observed. The variations observed could be due to the different distribution of the species in the interlamellar space.

➤ Nitrogen physisorption

The specific surface areas measured for all the hydrotalcites aged with and without microwaves are summarized in tables 4 and 5, respectively.

The BET area of the coprecipitated gel without aging is 38.6 m²/g. Having in mind this value, the surface area decreases when increasing the microwave irradiation time for the samples aged in an autoclave at 403 K and 423 K. This can be related to the increase of the crystallinity observed by XRD (Fig. 20, Table 4). On the other hand, the hydrotalcites aged in an autoclave under microwaves at 453 K have low surface areas the first 15 min (< 2.5 m²/g). However, after this time, a considerably increase of the surface area was observed (87.2 m²/g at 120 min). These results are very surprising since XRD results showed an increase of the crystallinity with the increase of the aging time, as expected (Fig. 20, Table 4). This area increase suggests the existence of some microwave effect on the surface of the sample that has been already commented by other authors [108].

The samples aged in an autoclave without microwaves at 403 K and 423 K (403A₁₂₀, 403A₃₆₀, 423A₁₂₀, 423A₃₆₀) have not practically surface areas (Table 5).

Respect to the hydrotalcites aged by refluxing, the sample prepared by conventional refluxing (R₁₀₈₀) has higher surface area than those refluxed under microwaves (Tables 4 and 5). Taking into account that similar FWHM values were obtained for all the refluxed samples, the higher surface area of sample R₁₀₈₀ could be explained by the remaining mesoporosity which was also observed in the starting coprecipitated gel, as commented below.

Figs. 23 and 24 show the N₂ adsorption-desorption isotherms and the pore size distribution graphics of some representative hydrotalcites. Although all the hydrotalcites prepared show a nitrogen adsorption isotherm of type IV,

the hysteresis loops differ depending on the aging conditions. However, we can establish three main groups of samples.

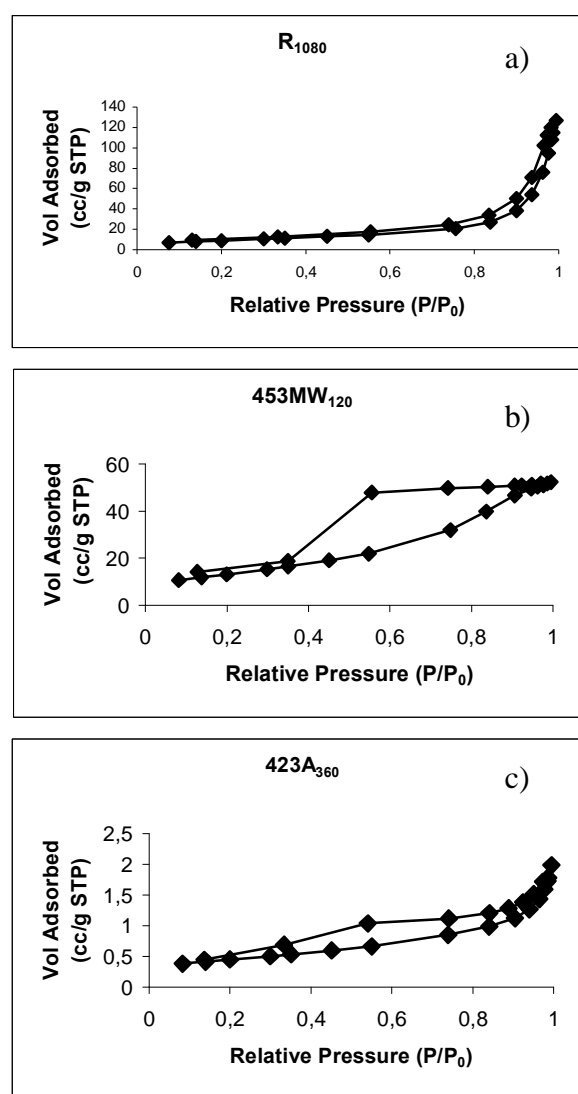


Figure 23. N_2 sorption / desorption isotherms at 77 K for the samples: a) R_{1080} , b) $453MW_{120}$ and c) $423A_{360}$.

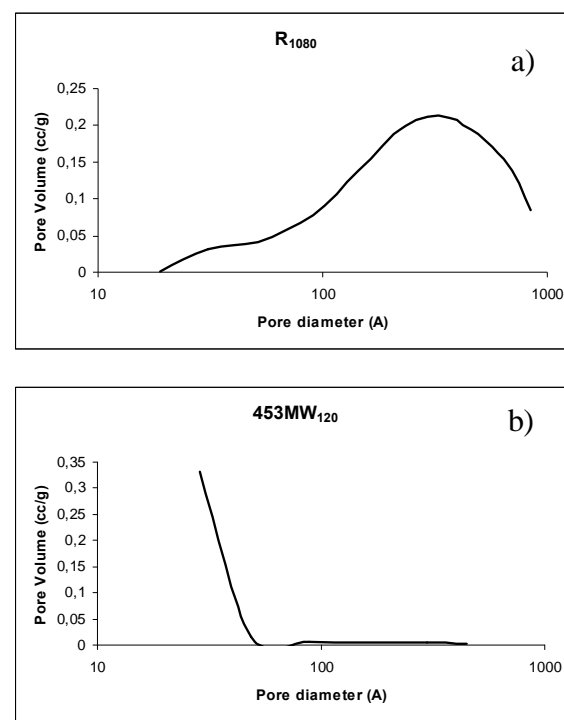


Figure 24. Pore size distribution from the N_2 desorption isotherms at 77 K of the samples: a) R_{1080} and b) $453MW_{120}$.

Figure 23a depicts the nitrogen adsorption-desorption isotherm for the sample aged by conventional refluxing (R_{1080}). This isotherm is very similar to those of the samples aged by refluxing under microwave irradiation (RMW_{60} , RMW_{120} , RMW_{240} , RMW_{480}) and those of the samples aged in an autoclave under microwaves at 403 K and 423 K ($403MW_1$, $403MW_5$, $403MW_{15}$, $403MW_{30}$, $403MW_{60}$, $403MW_{120}$, $423MW_1$, $423MW_5$, $423MW_{15}$, $423MW_{30}$, $423MW_{60}$, $423MW_{120}$). The adsorption and desorption ways are quite similar for these mesoporous samples. The pore size distribution graphic for sample R_{1080} (Fig. 24a) shows a main peak around 350 Å that also appears for all the samples of this group. This is in agreement with the typical mesoporosity described for the hydrotalcites obtained by conventional refluxing [79]. However, this porosity decreases with the time of aging for these microwaved samples as confirmed by the surface area decrease observed (Tables 4 and 5).

On the other hand, the samples aged at 453 K by microwaves from more than 15 min constitute the second group of samples. The N₂ isotherm for the hydrotalcite aged by microwaves at 453 K for 120 min (Fig. 23b) is very similar to those of the samples prepared at this temperature for 30 and 60 min (453MW₃₀, 453MW₆₀). In this case, the adsorption and desorption ways are quite different. This could be associated to an increase of the mesoporosity of low pore diameter observed in the pore size distribution graphics where only one peak under 30 Å appears for these samples (Fig. 24b). This is confirmed by the higher surface area (Table 4) and the increase of pore volume observed especially at longer times of aging (Fig. 24b). These new surface properties could be related to some disaggregations of the hydrotalcite layers due to some local overheating during microwave treatment at the conditions used for these samples. This gives to the formation of surface-defective sites which are responsible for the new porosity and the area increase although we cannot completely discard the presence of small amounts of insoluble amorphous species that can also contribute to the area increase.

The samples aged in an oven at 403 K and 423 K for 120 min and 360 min (403A₁₂₀, 403A₃₆₀, 423A₁₂₀, 423A₃₆₀) together with the samples aged under microwave irradiation at 453 K for 1, 5 and 15 min (453MW₁, 453MW₅, 453MW₁₅) form the third group of samples. They show a nitrogen adsorption-desorption isotherm similar to that of the sample 453MW₁₂₀ (Fig. 23b) but in this case, the difference between the adsorption and desorption ways is lower (Fig. 23c) than for the sample 453MW₁₂₀. The pore size distribution graphics of this group of samples exhibit in general two peaks, one around 350 Å and another around 30 Å. The contribution of the peak at 30 Å increases with the time of aging. The low porous volumes and the low surface area values obtained for these samples (Tables 4 and 5) mean that the initial mesoporosity decreases but practically no additional porosity appears.

➤ Elemental chemical analysis

In this study, the atomic absorption of 9 representative samples was performed in order to determine the chemical formulae, and mainly to detect the possible material loss as a consequence of the microwave treatment. The carbonate content has been obtained from decomposition studies using a calibrated detector whereas the amount of nitrate has been calculated as the difference between the total anions content, determined from the M(II)/M(III) ratio, and the carbonate values. The interlayer water was calculated from TG curves. The results are shown in table 6.

Table 6. Chemical analysis for the most representative samples.

Sample	Ni/Al	Mg/Al	Ni/Mg	Chemical formula ^a
R ₁₀₈₀	3.40	0.60	5.67	[Ni _{0.68} Mg _{0.12} Al _{0.20} (OH) ₂][(CO ₃ ²⁻) _{0.08} (NO ₃) _{0.04}]1.10 H ₂ O
RMW ₄₈₀	3.89	0.67	5.83	[Ni _{0.70} Mg _{0.12} Al _{0.18} (OH) ₂][(CO ₃ ²⁻) _{0.08} (NO ₃) _{0.02}]0.84 H ₂ O
403MW ₁₂₀	3.89	0.67	5.83	[Ni _{0.70} Mg _{0.12} Al _{0.18} (OH) ₂][(CO ₃ ²⁻) _{0.08} (NO ₃) _{0.02}]0.87 H ₂ O
423MW ₁₂₀	4.18	0.71	5.91	[Ni _{0.71} Mg _{0.12} Al _{0.17} (OH) ₂][(CO ₃ ²⁻) _{0.06} (NO ₃) _{0.05}]0.88 H ₂ O
453MW _s	4.18	0.71	5.91	[Ni _{0.71} Mg _{0.12} Al _{0.17} (OH) ₂][(CO ₃ ²⁻) _{0.07} (NO ₃) _{0.03}]0.90 H ₂ O
453MW ₃₀	4.50	0.75	6.00	[Ni _{0.72} Mg _{0.12} Al _{0.16} (OH) ₂][(CO ₃ ²⁻) _{0.06} (NO ₃) _{0.04}]0.81 H ₂ O
453MW ₁₂₀	6.90	1.18	5.84	[Ni _{0.76} Mg _{0.13} Al _{0.11} (OH) ₂][(CO ₃ ²⁻) _{0.04} (NO ₃) _{0.03}]0.74 H ₂ O
403A ₃₆₀	3.63	0.63	5.75	[Ni _{0.69} Mg _{0.12} Al _{0.19} (OH) ₂][(CO ₃ ²⁻) _{0.06} (NO ₃) _{0.07}]0.86 H ₂ O
423A ₃₆₀	3.63	0.63	5.75	[Ni _{0.69} Mg _{0.12} Al _{0.19} (OH) ₂][(CO ₃ ²⁻) _{0.06} (NO ₃) _{0.07}]0.86 H ₂ O

^a The possible presence of minoritary amorphous phases has not been considered in the calculation of the chemical formulae.

From these results we can confirm that the hydrotalcite R₁₀₈₀, obtained by traditional refluxing, practically maintains the theoretical cations ratio. On the other hand, there is an important increase in the Ni/Al and Mg/Al molar ratios whereas the Ni/Mg ratio is similar for the sample 453MW₁₂₀. Regarding the stoichoimetry obtained for this sample, it is possible to think that the formation of additional phases could take place, although we have not found any evidence by XRD. From the parameter mol Al/g HT obtained for both samples we can calculate % of aluminium loss expressed as g Al /100 g HT

(%). Thus, the sample 453MW_{120} has around 45% less of aluminium than sample R_{1080} . The cation ratios obtained could be explained because of a progressive degradation process on the sheets due to the microwaves action. Therefore, some local overheating during the microwaves treatment generates disaggregations of aluminium species in an important amount for this sample. These disaggregated aluminium species should be mainly eliminated during the washing of the gel. For the rest of the samples aged under microwaves, there is a decrease of the aluminium content but in less extension than for sample 453MW_{120} (Table 6). From these results we can conclude that the increase in the aging temperature and in the aging time under microwaves involves a progressive dealumination of the hydrotalcite layers. In contrast, the samples aged in a conventional oven do not show a significant dealumination even after 360 min. These results are in agreement with the nitrogen physisorption studies presented above.

➤ **CO_2 -TPD/FT-IR studies**

In order to obtain information about the basicity of the hydrotalcites synthesized we used the CO_2 -TPD technique. The CO_2 -desorption profiles are similar for all samples. However, it is possible to distinguish two groups of samples with several differences. Figure 25 shows the results of the CO_2 -TPD experiments of two samples that are representative of each group.

The CO_2 -TPD profile of the hydrotalcite aged by conventional refluxing (R_{1080}) (Fig. 25a) is very similar to those of the samples 403MW_1 , 403MW_5 , 403MW_{15} , 403MW_{30} , 403MW_{60} , 403MW_{120} , 423MW_1 , 423MW_5 , 423MW_{15} , 423MW_{30} , 423MW_{60} , 423MW_{120} , 453MW_1 , 453MW_5 , 453MW_{15} , RMW_{60} , RMW_{120} , RMW_{240} , RMW_{480} , R_{1080} , $403A_{120}$, $403A_{360}$, $423A_{120}$ and $423A_{360}$. Fig. 25b shows the CO_2 -TPD profile of the sample 453MW_{120} that is representative of those of the hydrotalcites aged by microwaves at higher temperatures (453 K) and longer times (from 30 min).

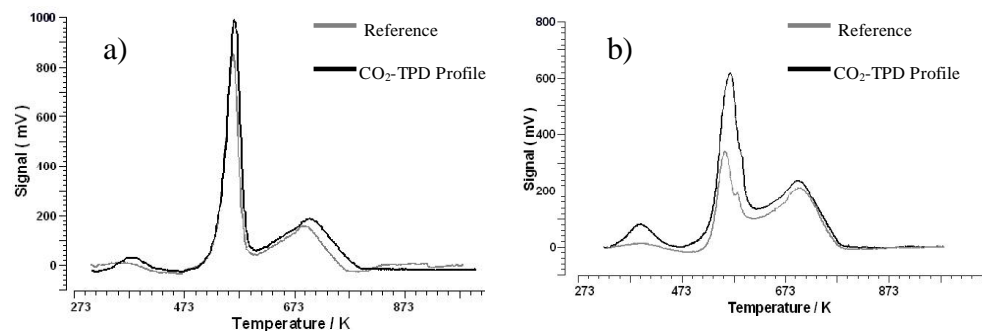


Figure 25. CO_2 -TPD profiles for the samples: a) R_{1080} and b) 453MW_{120} .

It is important to have in mind that hydrotalcites decompose with temperature and, therefore, for each sample, besides the adsorption-desorption CO_2 experiment, a thermogram was recorded without CO_2 treatment. Fig.25 also shows these decomposition thermograms for the hydrotalcites R_{1080} (Fig.25a) and 453MW_{120} (Fig.25b) as references. The basicity of the samples has been evaluated from the difference between the CO_2 desorption profile and the decomposition profile (reference).

Besides CO_2 , other decomposition species were detected by TCD. All thermograms show three peaks. One intense and narrow at 573 K, which is related to the decomposition of carbonate observed in the reference profiles, that in the CO_2 desorption profiles is also related to CO_2 bound to basic sites. Another broader peak at 696 K is related to the formation of NO_x (identified by a mass-spectrometer) as a result of the decomposition of the nitrate at higher temperatures. Besides, a peak with low intensity appears at 398 K due to the adsorbed atmospheric CO_2 on the external surface in the reference profiles that in the CO_2 desorption profiles could also be due to some CO_2 bound to weaker basic sites.

By comparing the two reference profiles (Fig.25a and 25b), we can observe that the peak at 573 K has lower intensity in the sample 453MW_{120} . This agrees with the loss of aluminium observed by atomic absorption for this sample. Thus, the laminas are less positively loaded. This could explain the lower amount of carbonated species observed for this sample.

All hydrotalcites show basic characteristics since we can see differences in intensity between the CO₂ desorption profile and its corresponding reference. This can be associated to the amount of CO₂ that interacts with the different basic centres of the sample. In the thermograms of the hydrotalcites aged by refluxing or by autoclaving with or without microwaves at 403 K and 423 K (e.g. Fig. 25a) we can only see a slight increase of the intensity of the peaks at 398 K and 573 K respect to those of the reference. Therefore, we can say that these samples have low amount of accessible basic sites. This behaviour was also observed for the hydrotalcites aged under microwaves at 453 K at shorter aging time (< 30 min). On the other hand, the samples aged under microwaves at 453 K but at higher aging time present higher amounts of basic sites since there is a higher difference in intensity between the CO₂ desorption profile and the reference profile (e.g. Fig.25b). Interestingly, the peak at 573 K has a shoulder at higher temperatures in the two profiles whose intensity increases, together with the intensity of the peak, after CO₂ treatment (Fig.25b). This was not observed for the rest of samples (Fig.25a). Besides, the total amount of CO₂ (subtracting the CO₂ from the reference profile) was calculated as 134.7 µmolCO₂/g HT for sample R₁₀₈₀ and 452.7 µmolCO₂/g HT for sample 453MW₁₂₀. Therefore, the higher basicity observed, especially for the sample 453MW₁₂₀, is a consequence of the dealumination that takes place during the microwaves irradiation. This is in agreement with the higher surface area of this sample.

In order to obtain more information about the nature of the basic sites, a FT-IR study was performed for the samples R₁₀₈₀ and 453MW₁₂₀, as synthesized, and also after CO₂ adsorption, at the conditions commented in the Experimental section (Apertat 3.2.4). Figure 26 shows the IR spectra taken for these hydrotalcites in the range 1100-1800 cm⁻¹ where the carbonate (1350-1385 cm⁻¹) and bicarbonate (\approx 1625 cm⁻¹) bands appear [79].

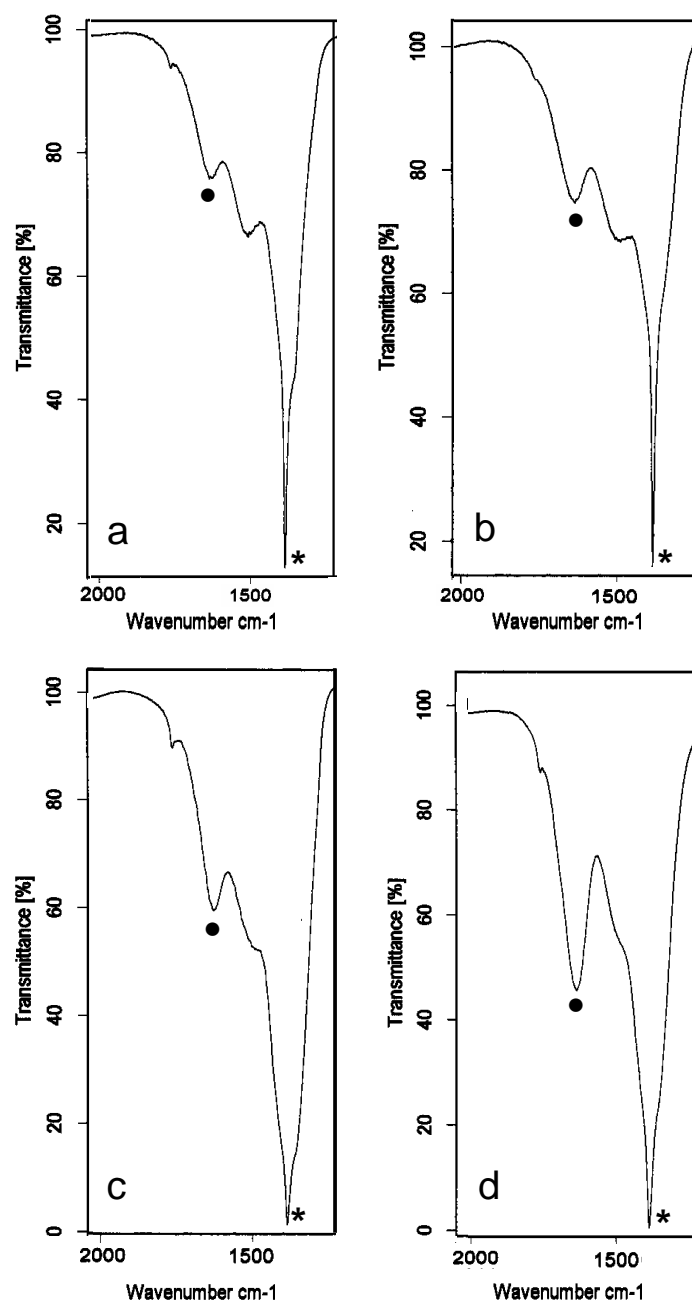


Figure 26. FT-IR of the samples: a) R_{1080} as synthesized, b) R_{1080} after CO_2 adsorption, c) 453MW_{120} as synthesized, and d) 453MW_{120} after CO_2 adsorption. Symbols: (●)bicarbonate band, and (*)carbonate band.

A different behaviour was observed when comparing the two samples. Thus, the spectrum of sample R₁₀₈₀ has a similar profile before and after CO₂ adsorption (Fig. 26a and 26b) whereas after CO₂ treatment of the hydrotalcite aged by microwaves (453MW₁₂₀) we observe a clear increase of the bicarbonate band (Fig. 26c and 26d). From these results, we can conclude that these new basic sites, associated to dealumination, are mainly OH⁻ that are detected as HCO₃⁻ species when interact with the CO₂ molecules.

➤ **Scanning electron microscopy (SEM) and transmission electron microscopy (TEM).**

Samples R₁₀₈₀ and 453MW₁₂₀ aged without and with microwaves, respectively, were chosen as representative hydrotalcites to be studied by SEM in order to visualize possible differences in their morphologies (Fig. 27).

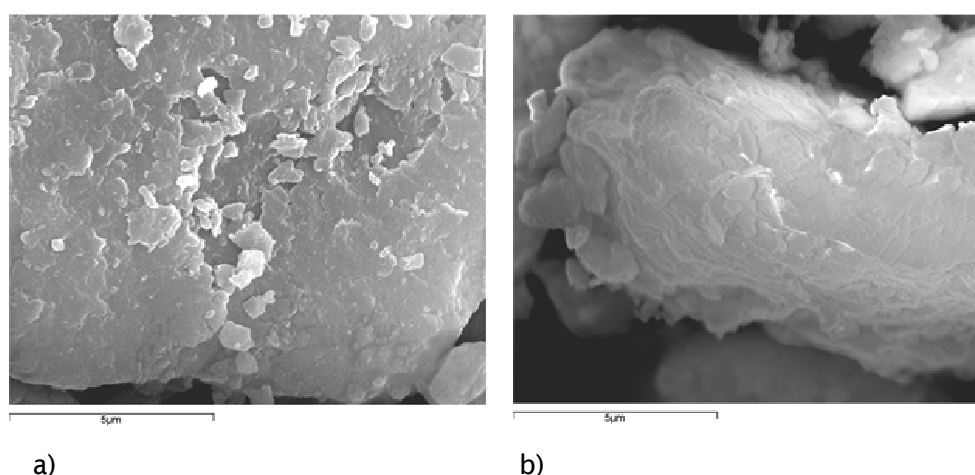


Figure 27. SEM micrographs for the samples: a) R₁₀₈₀ (x10000) and b) 453MW₁₂₀ (x10000).

For the two samples, we observe the typical hydrotalcite particles formed by superposition of sheets. However, some differences arise. The hydrotalcite aged by microwaves at higher temperature and longer time (453MW₁₂₀) has

sheets orientated in the same direction that are more defined (Fig. 27b) than those of the hydrotalcite obtained by conventional refluxing (Fig 27a).

These differences were confirmed by TEM. Fig. 28 shows the TEM micrograph taken for the sample 453MW₁₂₀ where the well definition and orientation of the sheets can be observed. This is in agreement with the XRD results.

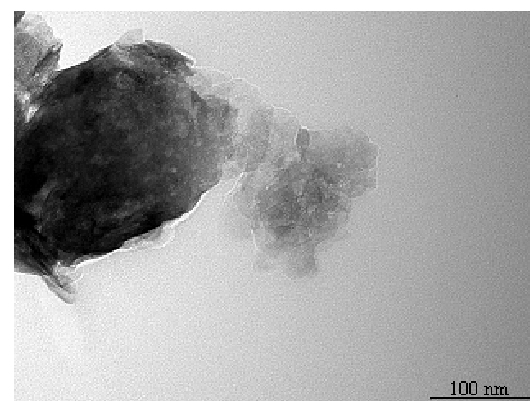


Figure 28. TEM image for the sample 453MW₁₂₀.

Characterization of the most representative calcined hydrotalcites

In order to obtain information about the calcined hydrotalcites we select five hydrotalcites which are representative all of those synthesised. The hydrotalcites are: R₁₀₈₀, 403MW₁₅, 403A₃₆₀, RMW₁₂₀ and 453MW₁₂₀.

XRD patterns of calcined hydrotalcites only show one crystalline phase that corresponds to NiO (Figure 29). The most crystalline NiO is that obtained from the calcination of the hydrotalcite aged in an autoclave by conventional heating (403A₃₆₀ C), as confirmed by regarding its crystallite size (Table 7), whereas the less crystalline is the catalytic precursor R₁₀₈₀ C, whose hydrotalcite was aged by conventional refluxing. For the catalytic precursors obtained from the microwaved hydrotalcites, the most crystalline is the sample 453MW₁₂₀ C whereas samples RMW₁₂₀ C and 403MW₁₅ C, whose starting hydrotalcites were aged in softer conditions, show lower NiO crystallite size values (Table 7).

Results and Discussion

Catalytic systems based on Hydrotalcite-like compounds

Other amorphous or minority phases like MgO and Al₂O₃ were not possible to detect by this technique.

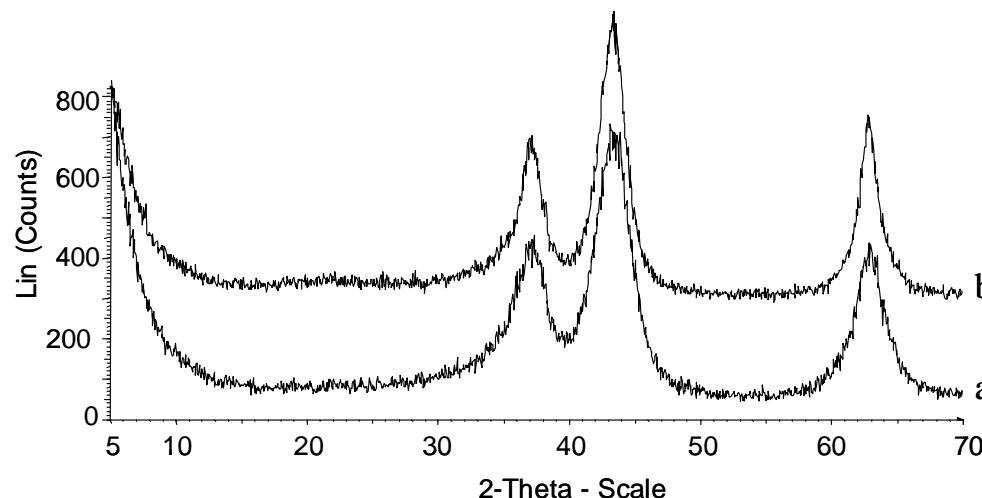


Figure 29. XRD patterns for the calcined hydrotalcites: a) R₁₀₈₀C and b) 453MW₁₂₀C.

Table 7. Characterization of calcined hydrotalcites.

Sample	R ₁₀₈₀ C	403A ₃₆₀ C	RMW ₁₂₀ C	403MW ₁₅ C	453MW ₁₂₀ C
Crystalline phases (XRD)	NiO	NiO	NiO	NiO	NiO
Crystallite size (nm) ^a	28	45	30	31	39
NiO/Al ₂ O ₃ ^b	6.8	7.3	7.3	7.8	13.8
MgO/Al ₂ O ₃ ^b	1.2	1.3	1.3	1.3	2.4
NiO/MgO ^b	5.7	5.7	5.7	5.8	5.8
BET area (m ² /g)	243	182	222	214	169
T _d (K) ^c	713	701	697	701	709
μmol CO ₂ /m ² ^d	2.3	3.4	3.1	3.2	2.8

^a Calculated from XRD results by using the Debye-Scherrer equation.

^b Results obtained from atomic absorption.

^c Maximum of the CO₂ desorption temperature peak.

^d Obtained from the results of CO₂-TPD and nitrogen physisorption techniques.

From atomic absorption results, we observe that the cation ratios between Ni, Mg and Al of the calcined samples (Table 7) were found to practically correspond to those presented by their respective starting hydrotalcites (Table 6). Thus the catalytic precursor R_{1080} C practically maintains the theoretical composition ratio values. Samples $403A_{360}$ C, RMW_{120} C and $403MW_{15}$ C present similar composition ratio values with slightly lower amount of alumina than the sample R_{1080} C. On the other hand, an important amount of aluminium loss, which was already detected in its starting hydrotalcite, was observed for the catalytic precursor $453MW_{120}$ C (the highest $\text{NiO}/\text{Al}_2\text{O}_3$ and $\text{MgO}/\text{Al}_2\text{O}_3$ ratios respect to the rest of samples) due to the most drastic conditions used under microwaves during the aging of its hydrotalcite precursor, as commented above. The NiO/MgO ratio practically remains constant for all samples (Table 7).

Table 7 also shows the BET area values of the calcined hydrotalcites. The decomposition process, which takes place during calcination, produces an increase in the BET area values up to 169-243 m^2/g respect to the aged hydrotalcites due to the fast release (craterisation) of H_2O , NO_x and CO_2 gases from the solid during calcination [77]. These area values can be explained taking into account the crystallinity of NiO, from XRD results, and the percentage of amorphous phases present in each sample that we know from atomic absorption results. Thus, sample R_{1080} C presents the highest BET area since this is the sample with lowest crystalline NiO (smaller crystallite size) and with the highest content of amorphous Al_2O_3 (Table 7). In contrast, sample $403A_{360}$ C, has the most crystalline NiO (higher crystallite size) although it has higher BET area than $453MW_{120}$ C. This is due to the lowest amount of amorphous Al_2O_3 detected in this sample that, consequently, contributes with lower BET area.

CO_2 TPD profiles are similar for all calcined hydrotalcites (Fig.30). They mainly show one desorption peak whose maximum of CO_2 desorption appears at similar temperature for all samples (around 700 K) (Table 7). By comparing with the CO_2 TPD profiles of the hydrotalcites (Figs.25a and 25b), we observe that, after calcination, the peak due to NO_x disappears, as expected, whereas the peak observed in the hydrotalcites around 573 K (which was assigned to the CO_2 bound to basic sites) practically disappears and shifts to higher desorption temperatures. Also, the thermograms of the calcined hydrotalcites show a very low-intense peak around 373 K which can be mainly related to the adsorbed atmospheric CO_2 on the external surface, as observed before in the hydrotalcite samples.

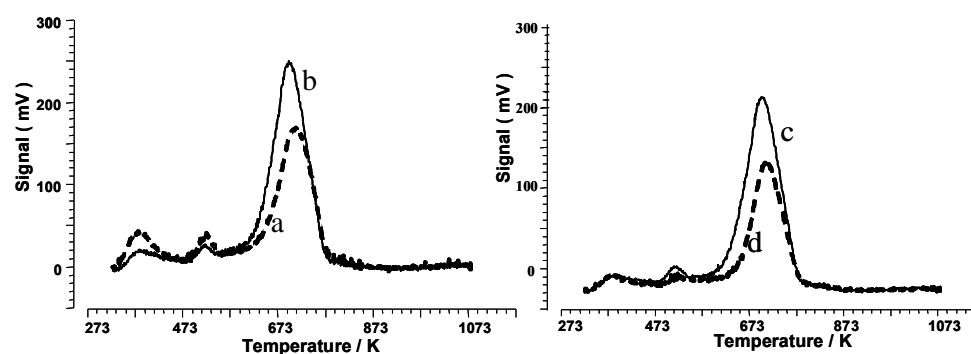


Figure 30. CO_2 -TPD profiles for the calcined hydrotalcites: a) R_{1080}C , b) RMW_{120}C , c) $403\text{MW}_{15}\text{C}$ and d) $453\text{MW}_{120}\text{C}$.

Therefore, after calcination, the strength of basicity increases considerably as deduced by comparing the variation in the maxima of the desorption temperatures for each sample. This can be explained by regarding the nature of the basic sites. In the hydrotalcites, the basicity is related to the OH^- groups whereas in the calcined hydrotalcites, the basicity can be assigned to the surface O^{2-} anions [107, 111].

The calcined hydrotalcites obtained from the hydrotalcites aged under microwaves have a greater amount of basic sites by m^2 than the calcined sample obtained from the hydrotalcite aged by conventional reflux (R_{1080}C)

(Table 7). This is in agreement with the results reported by Corma et al. for Mg/Al oxides obtained from hydrotalcites aged under microwaves in soft conditions [107]. However, the mixed oxides obtained from the hydrotalcites prepared under microwaves in softer conditions (RMW_{120} and 403MW_{15}) present a slightly higher amount of basic sites by m^2 than that obtained from the hydrotalcite aged under microwaves at more drastic conditions (453MW_{120}) (Table 7). The amorphous alumina obtained from the calcination of the hydrotalcites aged under microwaves should have some surface characteristics that could be responsible for the basicity increase. Sample $403\text{A}_{360}\text{C}$ has the highest value of basic sites by m^2 . The higher NiO crystallinity and the alumina amount can explain this result.

SEM technique was used to compare the morphology of the calcined hydrotalcites R_{1080}C and $453\text{MW}_{120}\text{C}$ with their hydrotalcite precursors, which were aged by conventional refluxing, and under microwaves in drastic conditions, respectively (Fig. 31). We choose these calcined hydrotalcites since their precursors are aged at very different conditions. After calcination, the two samples show particles with morphologies that remind the lamellar structure of the starting hydrotalcites. This is due to the soft calcination conditions used. Interestingly, the gases released during calcination seem to produce a different effect in the morphology of the two samples. For the sample aged by conventional refluxing, after calcination, there is an increase in the number of smaller particles due to the breaking of the hydrotalcite particles during the release of gases (Figs. 31a and 31c). In contrast, the particles of the sample $453\text{MW}_{120}\text{C}$ show an eroded appearance (Fig. 31d) when compared with those of its corresponding hydrotalcite (Fig. 27b) but practically no breaking of the particles was observed. In this case, we think that the surface-defective sites detected for the starting hydrotalcite, due to the microwaves effect, makes easy the release of gases during calcination, and consequently, a less breaking of the particles is observed. The differences in basicity detected for these samples could be related to the differences observed on their morphology.

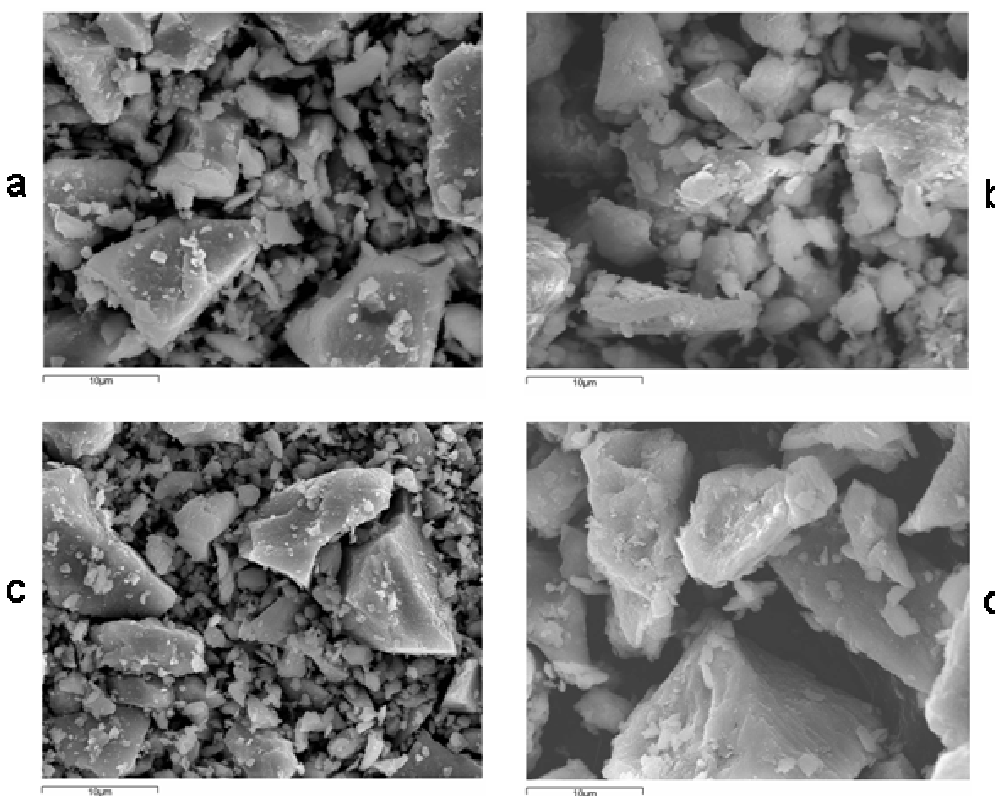


Figure 31. SEM micrographs for the samples: a) R₁₀₈₀ (x3000), b) 453MW₁₂₀ (x3000), c) R_{1080C} (x3000) and d) 453MW_{120C} (x3000).

Characterization of the catalysts

Table 8 shows some characterization data of the catalysts. After reduction of the calcined hydrotalcites, only one phase, identified as metallic nickel, was observed by XRD for all samples. Other amorphous or minority phases, like MgO and Al₂O₃, were not possible to detect again by this technique.

Table 8. Characterization of the catalysts.

Catalyst	Crystalline phases (XRD)	Metallic area (m ² /g sample)
R ₁₀₈₀ R	Ni	26
403A ₃₆₀ R	Ni	25
RMW ₁₂₀ R	Ni	46
403MW ₁₅ R	Ni	47
453MW ₁₂₀ R	Ni	34

Regarding the metallic area values, the catalysts obtained from the hydrotalcites aged under microwaves (RMW₁₂₀R, 403MW₁₅R and 453MW₁₂₀R) showed higher metallic areas than those obtained from the hydrotalcites aged in a conventional oven (403A₃₆₀R) or by conventional refluxing (R₁₀₈₀R). The crystallinity of the NiO and the BET areas of the calcined hydrotalcites can explain the metallic areas obtained for their corresponding catalysts. The higher surface area of sample R₁₀₈₀C and the lowest crystallinity of its starting NiO favour the reduction process, and consequently more sintering occurs when compared with the rest of samples at the same reduction time, explaining the lower metallic area observed for catalyst R₁₀₈₀R. Catalyst 403A₃₆₀R has similar metallic area than catalyst R₁₀₈₀R (Table 8) although its catalytic precursor, 403A₃₆₀C, showed a more crystalline NiO and less surface area than the catalytic precursor R₁₀₈₀C (Table 7). This indicates that less sintering of the nickel particles takes place for catalyst 403A₃₆₀R, because of the lower reducibility of its catalytic precursor.

On the other hand, catalysts RMW₁₂₀R and 403MW₁₅R exhibit the highest metallic area values. Interestingly, their catalytic precursors have slightly lower surface areas and similar NiO crystallinity than the catalytic precursor R₁₀₈₀C (Table 7). Therefore, it seems clear that the use of microwaves during the hydrotalcite aging should favour higher metal dispersion in the final catalysts. Lastly, catalyst 453MW₁₂₀R has an intermediate value of metallic area (34 m²/g) that is lower than those obtained for the other catalysts whose hydrotalcite precursors were aged under microwaves and higher than those

whose starting hydrotalcites were aged by conventional heating. Taking into account that this sample presents the lowest alumina content, due to the dealumination process as a consequence of the microwaves action, higher sintering of the nickel particles can be expected. From these results, we can conclude that there is a clear effect of using microwaves during hydrotalcite aging in the surface properties of the corresponding catalysts.

To obtain more information about differences in the active surface of the catalysts, the temperature-programmed desorption of hydrogen were performed for all of them. The mechanisms of adsorption-desorption of hydrogen can become extremely complex [112-117], especially over supported catalysts, because phenomena related to the interaction between the active phase and the support can interfere. The number and approximate population of the various adsorbed species depend on many factors: how the catalyst was prepared, the kind of support used and the experimental conditions of the measurement such as the weight of the sample examined, the flow rate of the carrier gas, the use of ultra-high vacuum (UHV) or the shape of the reactor system which affect conditions for removal of desorbed hydrogen.

Fig.32 shows some representative H₂-TPD profiles whereas table 9 depicts the desorption temperature at the maximum of the peaks observed for all catalysts.

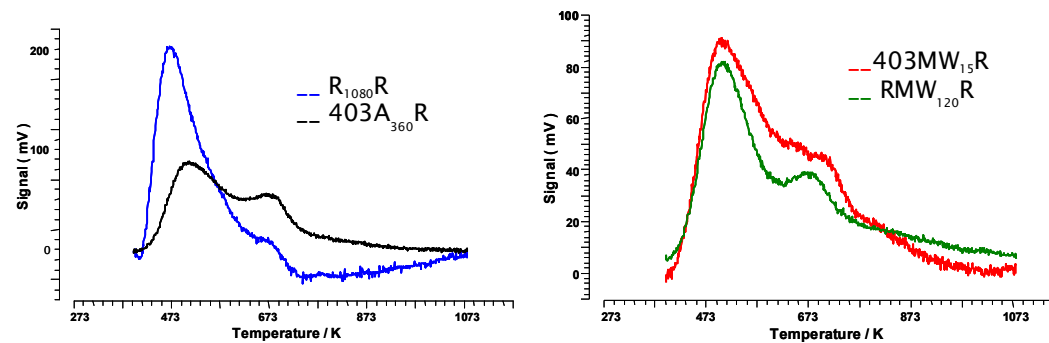


Figure 32. H₂-TPD profiles of some catalysts.

Table 9. H₂-TPD data for all catalysts.

Catalyst	T _D (K) Peak 1	T _D (K) Peak 2
R ₁₀₈₀ R	473	-
403A ₃₆₀ R	513	673
RMW ₁₂₀ R	510	683
403MW ₁₅ R	500	703
453MW ₁₂₀ R	483	685

T_D (K) Maximum temperature of the desorption peak.

All H₂-TPD profiles exhibit one narrow peak with a maximum between 480 K and 515 K but with different intensities (peak 1). Catalyst R₁₀₈₀R has the most intense peak 1 (Fig. 32). Moreover, we observe another peak around 680 K (peak 2) for all catalysts except for catalyst R₁₀₈₀R (Fig.32). The H₂-TPD profile of catalyst 453MW₁₂₀R is similar to that of catalyst 403A₃₆₀R with slight higher intensity of the two peaks.

On supported-nickel catalysts [87,115,118,119], the low temperature domain of desorption, below 600 K, has been associated to different adsorption states of the hydrogen. Several authors have ascribed the high temperature peaks (above 600 K) to reverse spill-over which can take place during high-temperature (above 773 K) treatments of the catalysts [112,116]. These arguments cannot be applied for our catalysts because we used milder experimental conditions (623 K). In our case, a more probable explanation is that this high-temperature peak might be associated to other adsorption states of the hydrogen (presumably related to a different morphology, electronic properties and/or size of metal particles). We had previously observed such desorption peaks for bulk nickel and other supported nickel catalysts [87,118,119].

The different states of hydrogen observed for the catalysts will be correlated later to the activity and selectivity for the hydrogenation of styrene oxide.

Catalytic activity

Fig. 33 exhibits the catalytic activity results for all catalysts. As we can see, all catalysts show total conversion and very high selectivity to 2-phenylethanol (around 95%) at 1 hour of reaction. On the whole, we detected ethylbenzene in very low amounts (around 3 %) for all catalysts except for catalyst 403MW₁₅R that is 9% (Fig.33).

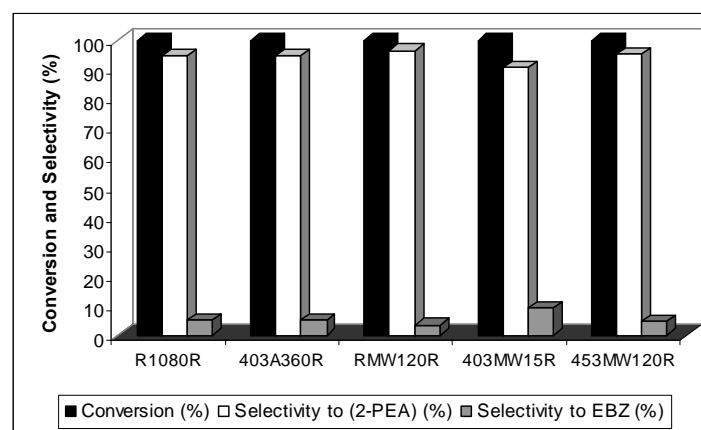


Figure 33. Catalytic activity of the catalysts after 1 hour of reaction (2-PEA = 2-phenylethanol and EBZ = ethylbenzene).

These catalytic systems based on hydrotalcites are more active than the Ni and Ni-MgO catalysts, previously tested, which were obtained from the reduction of NiO and NiO/MgO mixtures, respectively. In a previous chapter, we concluded that the presence of small nickel particles with a certain degree of interaction with the basic sites together with low contents of available basic sites favours the activity and selectivity to 2-phenylethanol, in Ni-MgO catalysts. Thus, the higher metallic area and a more homogeneous distribution of low amounts of basic sites, when hydrotalcite precursors are used, explain their catalytic results since in these catalysts higher amounts of small nickel particles with a certain degree of interaction with the basic sites can be expected. Additionally, the use of these catalytic systems, with low amounts of oxide species, minimizes the condensation reactions, responsible for the catalyst deactivation, which were not detected in any case.

In order to explain the higher selectivity to ethylbenzene (9%) observed for catalyst $403\text{MW}_{15}\text{R}$, we have compared the H_2 -TPD profiles of catalysts $403\text{MW}_{15}\text{R}$ and RMW_{120}R (Fig. 32b), which have similar metallic areas (around $46 \text{ m}^2/\text{g}$). The H_2 -TPDs of these catalysts show two peaks; the first one, appears at similar desorption temperature (around 500 K), whereas the second peak shifts to higher desorption temperature in catalyst $403\text{MW}_{15}\text{R}$ (Table 9). This can explain the presence of certain amounts of more active sites in this catalyst that could be related to its higher ethylbenzene selectivity. This is in agreement with Mitsui et al. who reported that the formation of ethylbenzene is related to the presence of more active sites [34].

More catalytic studies were performed to detect differences in the behaviour of the catalysts used. We studied the catalytic lifetime of all catalysts after reusing them ten times. The results show total conversion for catalysts R_{1080}R , RMW_{120}R and $403\text{MW}_{15}\text{R}$ whereas for catalysts $403\text{A}_{360}\text{R}$ and $453\text{MW}_{120}\text{R}$ only 78 % of conversion was obtained (Fig.34). On the whole, the selectivity to 2-phenylethanol is maintained around 92 % except for catalyst $403\text{MW}_{15}\text{R}$ that gives to 83 % of selectivity to 2-phenylethanol.

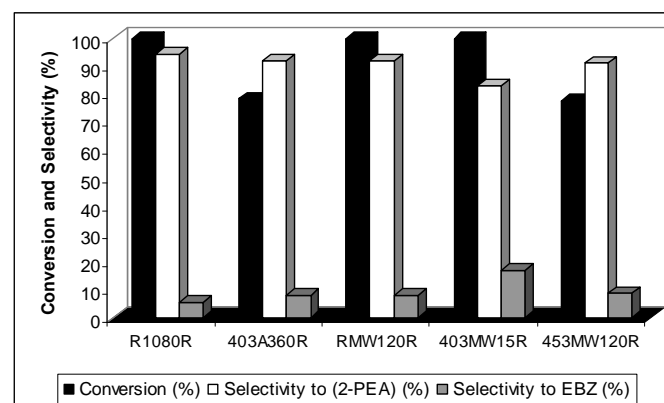


Figure 34. Catalytic lifetime of the catalysts after reusing ten times (2-PEA = 2-phenylethanol and EBZ = ethylbenzene).

The higher deactivation of catalysts $403\text{A}_{360}\text{R}$ and $453\text{MW}_{120}\text{R}$ could be understood by regarding the activity results obtained for all catalysts at

shorter reaction times. Fig. 35 shows that these two catalysts have lower conversion at shorter reaction times than the rest of catalysts although their selectivity to 2-phenylethanol is similar (85-90%).

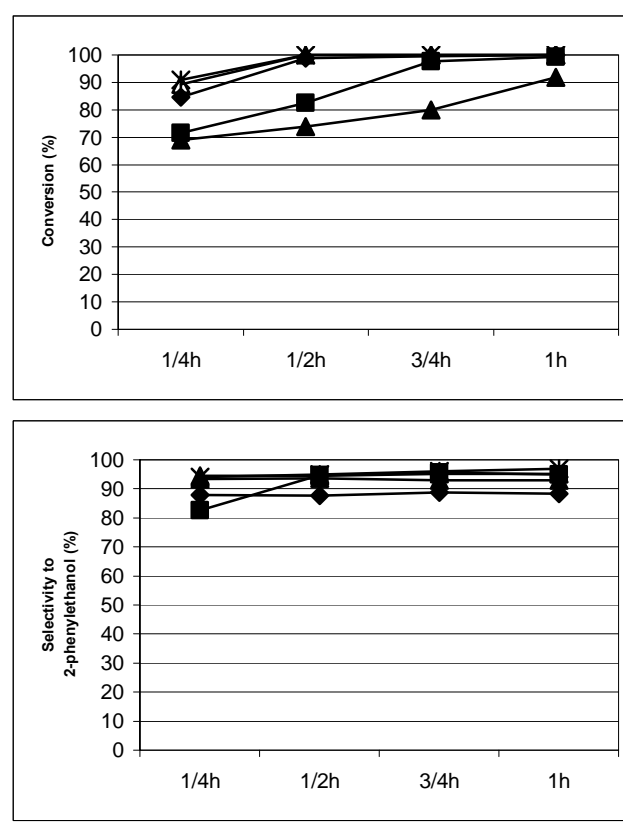


Figure 35. Catalytic activity at short reaction times for all catalysts $R_{1080}R$ (*), $403A_{360}R$ (■), $RMW_{120}R$ (△), $403MW_{15}R$ (◆) and $453MW_{120}R$ (▲).

Comparing the H_2 -TPDs of two catalysts ($R_{1080}R$ and $403A_{360}R$) which have similar metallic area (around $25\text{ m}^2/\text{g}$, Table 2) but different activity at shorter reaction times (Fig.35), we observe that catalyst $R_{1080}R$ has a much more intense peak 1 than catalyst $403A_{360}R$ (Fig.32). Taking into account that catalyst $R_{1080}R$ is more active than catalyst $403A_{360}R$ (Fig.35), we can conclude that the hydrogen desorbed at lower temperature can be mainly related to the activity and selectivity to the desired product, 2-phenylethanol. Thus, the

presence of lower amounts of this hydrogen desorbed at lower temperature for catalysts $403A_{360}R$ and $453MW_{120}R$ can explain their lower activity and, consequently, easier deactivation.

4.2.4 Conclusions

We have confirmed that the use of microwaves during aging gives to the obtaining of hydrotalcites with higher crystallinity in shorter times than the hydrotalcites aged by conventional refluxing. Moreover, the increase of the aging temperature and the aging time favours an increase of the hydrotalcite crystallinity. Interestingly, the hydrotalcites aged in an autoclave under microwaves at the highest temperature (453 K) and at longer times (from 30 min) present new mesoporosity, higher surface area, higher basicity and higher stacking in the interlayer order than the hydrotalcites aged under microwaves in softer conditions or by traditional refluxing. These new surface properties could be related to some disaggregations of the hydrotalcite layers due to some local overheating during microwaves treatment at the conditions used for these samples. This gives to the formation of surface defective sites which are responsible for these different surface and basic characteristics.

The mixed oxides obtained by calcination of the hydrotalcites aged under microwaves in softer conditions (refluxing at 343 K for 120 min or autoclaving at 403 K for 15 min) have higher basicity by m^2 than that obtained from the hydrotalcite aged in more drastic conditions ($453MW_{120}$). This can be associated to the presence of different surface characteristics in the amorphous alumina obtained during calcination due to the effect of microwaves on their hydrotalcite precursors. The lower amount of this amorphous alumina in sample $435MW_{120}C$ justifies its lower basicity by m^2 . This is corroborated by SEM since this sample presents a more eroded appearance.

The catalysts obtained from the hydrotalcites aged under microwaves showed higher metallic areas, and therefore best metal dispersion, than those

Results and Discussion

Catalytic systems based on Hydrotalcite-like compounds

obtained from the hydrotalcites aged by conventional heating. However, the hydrotalcite aged under microwaves at hard conditions (higher temperature and time) leads to a catalyst with lower metallic area than the other microwaved samples. The lowest alumina content of this catalyst, which is due to the dealumination occurred as a consequence of the microwaves action during the hydrotalcite aging step, can explain a higher sintering of their nickel particles.

All catalysts showed total conversion and very high selectivity to 2-phenylethanol (around 95 %) after 1 h of reaction. The higher metallic area (25-47 m²/g) and the more homogeneous distribution of low amounts of basic sites of these catalysts based on hydrotalcites when compared with other basic catalysts, as Ni-MgO systems, can explain these catalytic results. The higher amount of ethylbenzene (9 %) observed for catalyst 403MW₁₅R has been related to the presence of certain amounts of more active sites, as observed by H₂-TPD. After reusing ten times, all catalysts maintain high conversion and high selectivity values to 2-phenylethanol. However, catalysts 403A₃₆₀R and 453MW₁₂₀R exhibit higher deactivation than the rest of catalysts. These two catalysts also showed lower activity at shorter reaction times (< 45 min). This catalytic behaviour can be explained by the lower amount of hydrogen desorbed at lower temperatures, detected by H₂-TPD for these catalysts. Therefore, this low-temperature desorbed hydrogen can be related to the activity and selectivity to 2-phenylethanol.

4.3 Ni-Mordenite catalytic systems

4.3.1 Introduction

Mordenite is a high-silica zeolite ($\text{Si}/\text{Al} > 5$) characterized by its strong acidity together with size and shape selectivity. This zeolite is used in several catalytic industrial processes, including cracking and isomerization of hydrocarbons [120]. Mordenite is comprised of two 2-D straight channel types: i) larger channels, also called main channels, accessible through twelve member oxygen rings with an opening of $7.0 \times 6.5 \text{ \AA}$, and ii) smaller channels, often referred to as compressed channels which include eight member oxygen rings with $2.6 \times 5.7 \text{ \AA}$ (Fig. 36). The 3-D diffusion only is possible for small molecules and the mono-dimensional diffusion is for larger molecules due to a shift among the connected channels. Each aluminum atom introduces a negative charge, counterbalanced by extraframework cations that can be located in different parts of the zeolite channels having different roles in adsorption and catalytic processes [121].

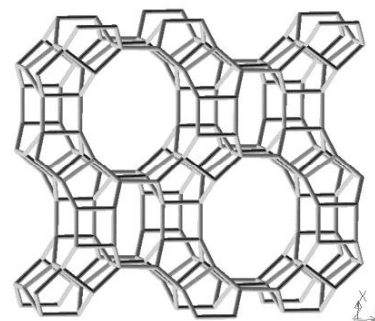


Figure 36. Structure of Mordenite

Zeolites can be modified by replacing some or all of their exchangeable cations with those of transition metals. The most used procedures to introduce cations into zeolites are impregnation and ion-exchange. The impregnation method gives to high cation concentration but it is hard to obtain regular cation dispersion [122]. Ion-exchange in zeolites is

mainly performed in the liquid phase obtaining a high initial dispersion, but for some of transition metals like Cu, Co or Ni the exchange process becomes difficult and incomplete due to an increase in the effective size of the cations in aqueous solution by hydration and/or hydrolysis [123]. In order to facilitate the diffusion of these bulky cations, an intermediate calcination step can be made between several exchange processes [124]. Solid-state ion exchange could be used as an alternative method to improve the cation exchange [125]. In this method, a mechanical mixture of the zeolite and the cation precursor is heated at relatively high temperatures and long times.

There is of increasing interest to incorporate Ni in zeolites due to the many applications that this transition metal has as catalyst in hydrogenation/dehydrogenation, hydrogenolysis [126], hydrodewaxing [127], hydrocracking and hydroisomerization reactions [128]. However, the conventional ion-exchange method in the liquid phase only gives to 40-50% of exchanged nickel, depending on the zeolite and the exchange conditions, due to the increase in the effective size of the nickel cations in aqueous solutions, as commented above [129,130].

Nowadays, microwave irradiation is being applied for chemical synthesis [96]. The use of microwaves considerably decreases the preparation times and modifies the properties of the synthesized samples when compared to those obtained by conventional heating. In the field of zeolites, microwaves have been mostly used to their dry or synthesis [131-133], and more recently, to the cation-exchange of Na^+ by La^{3+} , Co^{2+} , Cu^{2+} and Zn^{2+} in NaX and Na-ZSM-5 zeolites [134-137]. Other studies reported modifications in Brønsted and Lewis acid centres in the X zeolite by ion-exchange of Na^+ by K^+ under microwaves heating [138]. We have not found in the literature any reference about the use of microwaves for the nickel ion-exchange of zeolites in the liquid phase. There is only one study about the solid state ion-exchange of nickel in zeolite Y under microwaves arriving to 70 % of nickel exchanged [139].

The isomerisation of styrene oxide to β -phenylacetaldehyde is an important reaction due to the great interest of this aldehyde at industrial scale in fine chemistry for the production of fragrances, pharmaceuticals, insecticides, fungicides and herbicides [45]. This reaction is mainly catalysed by Brønsted acid sites. In a previous work, we observed that Na-Mordenite has very low activity in the isomerization of styrene oxide whereas with H-Mordenite we obtained high selectivity to β -phenylacetaldehyde. We also observed that the epoxide ring of styrene oxide opens mainly catalysed by both Brønsted and Lewis acid sites [46].

In this chapter, we report a wide study of the ion-exchange of Na^+ by Ni^{2+} in a commercial mordenite under microwave irradiation in the liquid phase with the aim to achieve higher Ni^{2+} exchange degrees that can give to systems with high Ni dispersion. Some parameters, such as the salt solution concentration and volume, and the time and temperature of the exchange were modified. Besides, two samples were exchanged by conventional method for comparison. We characterized the exchanged samples by common techniques in order to study the effect of microwaves irradiation on the introduction of Ni^{2+} in the mordenite structure and on its acid properties. Four of the nickel exchanged mordenites were tested as catalysts in two reactions catalysed by different acid sites: the isomerization of styrene oxide to obtain β -phenylacetaldehyde, which is mainly catalysed by Brønsted acid sites, and the styrene oxide ring-opening to give 2-ethoxy-2-phenylethanol, which is catalysed by both Brønsted and Lewis acid sites.

Moreover, the most representative samples obtained by liquid exchange, together with several samples prepared in solid state were calcined and then, reduced to obtain Ni-Mordenite catalysts. These catalysts have been tested in the hydrogenation of styrene oxide. They present acid properties and nickel distributed in the microporous support. In this new study we want to compare the catalytic behaviour of these Ni-Mordenite catalysts with the behaviour of the basic catalytic systems previously commented (Section 4.1). The competition between the hydrogenation, and the side reactions catalysed

by acid sites together with other factors associated to the microporous support will be studied.

4.3.2 Experimental

Preparation of Ni-Mordenite samples

The starting material was a commercial Na-Mordenite CBV 10A Lot No. 1822-50, designated as NaM, which was supplied by Zeolist as hydrated powder with a $\text{SiO}_2/\text{Al}_2\text{O}_3$ mole ratio of 6.5 and Na_2O wt % of 6.6.

- **Synthesis of HMordenite:** We prepared H-Mordenite (HM) in order to use it, later, for the synthesis of a catalyst with nickel. HM is prepared by the ion-exchange method using 1 g of NaM with 33 ml of NH_4Cl (Panreac, 99 %) 2.2 M stirred for 6 h at room temperature. Then, the sample was washed with distilled water and dried at 393 K overnight. The resulting sample was calcined at 673 K for 12 h to remove NH_3 of the sample.

Table 10 summarizes the preparation conditions for all the Ni-Mordenite samples. Commercial $\text{Ni}(\text{NO}_3)_2 \cdot 6\text{H}_2\text{O}$ (Panreac, 99%) was used for these preparations.

- **Preparation of Ni-exchanged samples by microwaves:** We took 0.5 g of NaM for each preparation. The ion-exchanged samples prepared under microwaves were performed in an autoclave in a microwave oven (Milestone ETHOS-TOUCH CONTROL equipped with a temperature controller). The six first samples were prepared by putting NaM with 50 ml of $\text{Ni}(\text{NO}_3)_2 \cdot 6\text{H}_2\text{O}$ 0.14M at different temperatures and times under microwaves. M1, M2 and M3 were obtained at 333 K for 15, 30 and 45 minutes, respectively, whereas M4, M5 and M6 were prepared at 353, 373 and 393 K, respectively,

for 15 minutes. Two more samples (M7 and M8) were also prepared under microwaves but by using 25 ml of $\text{Ni}(\text{NO}_3)_2 \cdot 6\text{H}_2\text{O}$ 0.14 M. M7 was obtained at 333 K for 15 minutes and M8, at 393K for 15 minutes. Another block of experiments were carried out under microwaves with 50 ml of $\text{Ni}(\text{NO}_3)_2 \cdot 6\text{H}_2\text{O}$ 1 M: M9 and M10 were prepared at 333 and 393 K, respectively, for 15 minutes.

Table 10. Preparation conditions of the Ni-Mordenite samples.

Nomenclature of the samples	Amount of $\text{Ni}(\text{NO}_3)_2 \cdot 6\text{H}_2\text{O}$	Exchange Time	Exchange Temperature (K)
Samples exchanged in a microwave oven			
M1	50 ml 0.14M	15 minutes	333
M2	50 ml 0.14M	30 minutes	333
M3	50 ml 0.14M	45 minutes	333
M4	50 ml 0.14M	15 minutes	353
M5	50 ml 0.14M	15 minutes	373
M6	50 ml 0.14M	15 minutes	393
M7	25 ml 0.14M	15 minutes	333
M8	25 ml 0.14M	15 minutes	393
M9	50 ml 1M	15 minutes	333
M10	50 ml 1M	15 minutes	393
Samples exchanged by conventional method			
M11	50 ml 1M	24 hours	333
M12	50 ml 1M	24 hours	298
Samples exchanged twice in a microwave oven with a thermal treatment between the exchanges			
M13	50 ml 1M	15 minutes each exchange thermal treatment in an oven at 673 K	333
M14	50 ml 1M	15 minutes each exchange thermal treatment in a microwave oven at 453 K	333
Samples prepared in solid state			
NaM-NiO	2.5 g	-	-
HM-NiO	2.5 g	-	-
NiNaM33	2.5 g	24 hours	473
NiNaM6	0.33 g	24 hours	473

- **Preparation of Ni-exchanged samples by conventional method:** To compare with the microwaved samples, two samples (M11 and M12) were exchanged by traditional ion-exchange method without microwaves by using 50 ml of $\text{Ni}(\text{NO}_3)_2 \cdot 6\text{H}_2\text{O}$ 1 M. M11 was prepared at 333 K for 24 hours whereas M12 was obtained at 298 K for 24 hours.

- **Preparation of samples by two exchange processes in a microwave oven with a thermal treatment between them:** Samples M13 and M14 were exchanged twice at the same conditions than sample M9 making an intermediate thermal treatment between the two exchanges. Thus, M13 was heated in an oven at 673 K for 12 hours between the two exchange processes. This temperature was chosen taking into account the values found in the literature to improve exchange in transition metals [140]. M14 was heated between the two exchanges, in the microwave oven at 453 K for 6 hours.
- **Preparation of samples in solid state:** NiNaM33 was prepared by mixing in solid state 2.5 g of $\text{Ni}(\text{NO}_3)_2 \cdot 6\text{H}_2\text{O}$ (to achieve 0.5 g of active phase after reduction step, which corresponds to 33% of Ni) with 0.5 g of NaM. The resulting mixture was placed in an oven at 343 K (melting state for $\text{Ni}(\text{NO}_3)_2 \cdot 6\text{H}_2\text{O}$) for 12 hours. Then, the sample was heated in a furnace at 473 K for 24 h, in order to favour the migration of the Ni^{2+} inside the NaM. Sample NiNaM6 was prepared in the same way that sample NiNaM33 but by mixing in solid state 0.33 g of $\text{Ni}(\text{NO}_3)_2 \cdot 6\text{H}_2\text{O}$ (stoichiometric amount to obtain total exchange, which corresponds to 6.4% of Ni) with 0.5 g of NaM. Finally, samples NaM-NiO and HM-NiO were prepared by stirring in cyclohexane 0.4 g of NiOB (prepared as previously commented in section 4.1) with 0.4 g of NaM or HM, respectively, in order to compare with NiNaM33 and NiNaM6.

Samples M9, M12, M13, M14, NiNaM33 and NiNaM6, were calcined at 673 K for 12 hours.

Samples M9, M12, M13, M14, NaM-NiO, HM-NiO, NiNaM33 and NiNaM6 were heated under $\text{H}_2(\text{g})$ to be reduced in order to test their activity for the hydrogenation of styrene oxide. M9, M12, M13 and M14 were heated under

$H_2(g)$ at 623 and 773K for 12 hours. NaM-NiO and HM-NiO were reduced at 523 K for 4 hours and NiNaM33 and NiNaM6 were reduced at 623 K for 6 hours and 12 hours, respectively. The resulting catalysts were named as M9R, M12R, M13R, M14R, NaM-Ni, HM-Ni, NiNaM33R and NiNaM6R.

Air-free sampling

The catalysts were always handled under air-free conditions after the reduction step. The catalysts were transferred in degassed cyclohexane and under hydrogen atmosphere at room temperature. The cyclohexane surface-impregnated samples were further isolated from the air with sticky tape for XRD monitoring, where a glove box was used for mounting.

Characterization of the samples

The catalytic precursors and the catalysts were characterized by X-Ray Diffraction (XRD), Nitrogen physisorption, Infrared Spectroscopy, Temperature-programmed desorption-mass spectrometry experiments (NH_3 -TPD), X-Ray Microanalysis, Atomic Absorption, using model reactions to study the acid properties and Hydrogen Chemisorption. The experimental conditions used have been indicated in the Experimental Section (3.2).

Catalytic activity in the hydrogenation of styrene oxide

The catalytic hydrogenation of styrene oxide was made in the liquid phase, with NaM, HM, M9R, M12R, M13R, M14R, NaM-Ni, HM-Ni, NiNaM33R and NiNaM6R as a catalysts. We used 1 g of each catalyst, 20 ml of absolute ethanol (Panreac, 99.5%) and 4 mmol of styrene oxide (Aldrich, 97 %) with a hydrogen flow of 2 ml/s and agitation of 700 rpm. The reaction was performed at room temperature. Sample was taken each 1, 3 and 6 hour. The reaction products were analysed by gas chromatography, using a gas chromatograph Shimadzu GC-2010 instrument equipped with a 30 m capillary column DB-1 coated with phenylmethylsilicon and a FID detector.

4.3.3 Results and discussion

Characterization of the samples

➤ Atomic absorption

Figs 37, 38 and 39 show the percentage of Na^+ exchanged by Ni^{2+} obtained by atomic absorption for the M1-M14 samples.

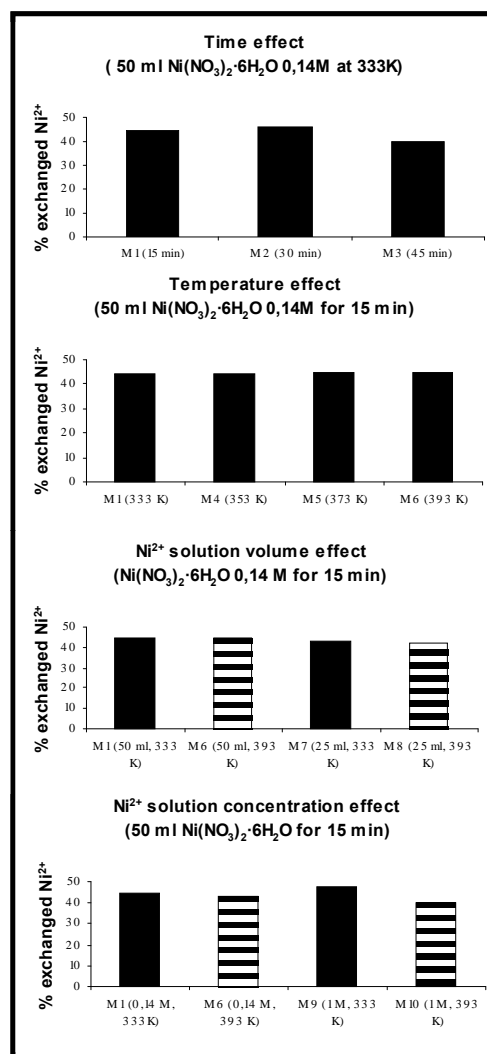


Figure 37. Exchange degree of Ni^{2+} for the samples exchanged under microwaves.

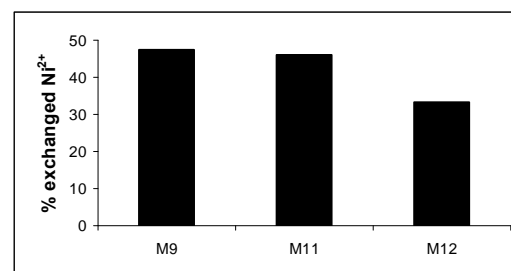


Figure 38. Exchange degree of Ni²⁺ for the samples exchanged with conventional method and by microwaves.

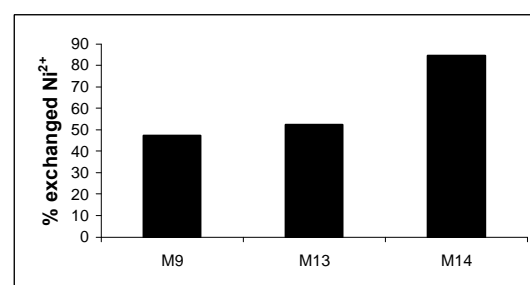


Figure 39. Exchange degree of Ni²⁺ for the samples exchanged by improving conditions.

a) *Exchange under microwaves*

We carried out several experiments using a microwave oven modifying different exchange variables like the temperature and time of irradiation, and the concentration and the volume of the Ni(NO₃)₂·6H₂O solution in order to optimise them and achieve a high exchange degree.

We studied the effect of the exchange time at the same temperature (333 K) with the three first samples (M1, M2 and M3). The atomic absorption results show that practically there is not modification in the exchange values; even there is a slight decrease in the exchanged Ni²⁺ from 30 minutes to 45 minutes (Fig. 37). Thus, the optimum time condition is 15 minutes.

From M1, M4, M5 and M6 samples we can observe the influence of the exchange temperature (333, 353, 373 and 393 K). The results for these samples indicate that practically there is not influence of the temperature on

the exchange process at these conditions since the % of exchanged Ni^{2+} is practically the same ($M1 = 44.4\%$ and $M6 = 44.8\%$) (Fig.37). So, we can choose 333 K between all the tested temperatures.

If we compare M7 with M1 and M8 with M6 (samples prepared at the same temperature but with different volume of nickel solution), we can see that the percentage of exchanged nickel is slightly higher in the samples exchanged with 50 ml of nickel solution (M1 and M6), but the values are not too much different (Fig. 37).

The last two experiments (M9 and M10) were made to investigate the influence of the nickel solution concentration with the temperature. We compared M9 with M1 and M10 with M6. An increase of the nickel solution concentration leads to an increase of the exchanged nickel at 333 K from 44.4 % to 47.4 %. In contrast, at 393 K an increase of the nickel solution concentration leads to a decrease of the exchanged nickel (from 44.8 % for M6 to 40.1 % for M10) (Fig.37).

From these results, we observe that the best exchange conditions under microwaves were found when using 50 ml $\text{Ni}(\text{NO}_3)_2 \cdot 6\text{H}_2\text{O}$ 1M at 333 K for 15 minutes. However, the exchange degree obtained is lower than 50 % in all cases.

b) Exchange by conventional method

In order to compare the exchanged values obtained by using microwaves with the conventional exchange method we carried out two experiments. Samples M11 and M12 were prepared by using 50 ml of $\text{Ni}(\text{NO}_3)_2 \cdot 6\text{H}_2\text{O}$ 1M for 24 hours at 333 and 298 K, respectively. The results are shown in Fig. 38. For the sample obtained at 298 K (M12) we observed the lowest Ni^{2+} exchanged value (33 %) respect to all the prepared samples whereas at 333 K (M11), the exchanged Ni^{2+} (46 %) is similar to that obtained for sample M9 (Fig 38).

The exchanged Ni^{2+} values obtained under microwaves and by conventional heating are similar, around 47 %, but, interestingly, we obtained this value 95 times faster using a microwave oven. Suzuki et al. estimated that half of the acid sites in H-Mordenite can be exchanged by nickel ions. They concluded that these exchangeable sites are situated in the main channels whereas the rest are located in side pockets, which are hardly exchangeable by the hydrated nickel ions [141].

c) *Exchange improvement*

In order to improve the exchanged Ni^{2+} values we carried out other experiments. Firstly, we washed with distilled water the NaM previously to the exchange process to discard problems in Ni^{2+} diffusion by the presence of species that could block the porous. Other NaM sample was submitted to two exchange processes. Each exchange was carried out with 50 ml $\text{Ni}(\text{NO}_3)_2 \cdot 6\text{H}_2\text{O}$ 1M at 333 K for 15 minutes in a microwave oven and the sample was washed with distilled water and dried between the two exchange processes. The results of these two experiments did not show better exchange values.

Finally, two new experiments were performed in order to try to increase the migration of the Ni^{2+} located in the main channels, after one exchange, to the other positions less accessible of mordenite. This consists to submit the exchanged Ni^{2+} sample to a thermal treatment, to favour the cation migration, followed by a second exchange to increase the % of exchanged Ni^{2+} . For this proposal, samples M13 and M14 were prepared from commercial mordenite by exchange twice at 333 K for 15 minutes in a microwave oven (at the same exchange conditions than sample M9) with an intermediate thermal treatment between the two exchanges at 673 K in a conventional oven for 12 hours for sample M13, and an intermediate thermal treatment at 453 K in a microwave oven for 6 hours for sample M14 (Table 10). Fig. 39 shows the % of exchanged Ni^{2+} for these samples compared with sample M9. For the two new samples, we observe an increase of the Ni^{2+} content respect to M9. M13 only

shows a slight increase in the Ni²⁺ content (52 %). In fact, a grey colour due to the formation of NiO was observed for this sample after the conventional thermal step. The low increase in the Ni²⁺ content indicates that probably no diffusion of the cations occurs due to the NiO formation. On the other hand, the sample treated in a microwave oven before the second exchange (M14) has almost double content of Ni²⁺ (84 %) than the rest of prepared samples (Figs.37, 38, 39). This Ni²⁺ exchanged value is higher than those found in the literature [129,130,139]. In this case, the microwaves irradiation could favour the migration of the Ni²⁺ of the main channels to other less accessible sites of the mordenite. Some other studies pointed out that the microwave irradiation might enhance the diffusion respect to the conventional heating at the same temperature, for example, in the diffusion of various cations in Pyrex glasses [142], and ethylene oxide in polyvinyl chloride [143]. Besides, in this sample M14 more intense green colour was observed after the second exchange, confirming the higher presence of Ni²⁺.

It is important to note that, for all the exchanged samples, we have not observed modifications of the mordenite structure or the presence of other crystalline phases by XRD. Also, IR spectra did not show dealumination of the zeolite after exchange. The calcination of the exchanged mordenites at 623 K gives to a darker grey colour but no additional crystalline phases were detected by XRD.

d) Samples prepared in solid state

The samples prepared in solid state (NiNaM33, NiNaM6, NaM-NiO and HM-NiO) were not submitted to washing treatment, so all the nickel remains in the sample. Thus, the nickel content in these samples is 44 % for NaM-NiO and HM-NiO, 33.4 % for NiNaM33 and 6.4 % for NiNaM6.

➤ **Physisorption of nitrogen**

All samples showed an isotherm of type I that corresponds to microporous materials. Table 11 depicts the nitrogen physisorption results of some representative exchanged mordenites respect to those of commercial Na-Mordenite (NaM). The BET area of the commercial Na-Mordenite is 380 m²/g whereas its micropore area, obtained by the t-plot method, is 338 m²/g. On the whole, the exchanged samples have similar BET area and similar micropore area values than commercial mordenite.

Table 11. Nitrogen physisorption results for the most representative samples.

Samples	BET Area (m ² /g)	Micropore Area (m ² /g)
NaM	380	338
M1	376	334
M9	370	323
M10	353	309
M11	378	333
M12	376	338
M13	386	342
M14	307	263
NaM-NiO	109	77
HM-NiO	103	72
NiNaM33	111	76
NiNaM6	196	151

However, sample M14, prepared by two exchanges under microwaves with an intermediate thermal treatment also under microwaves at 453 K, shows a significant lower BET area (307 m²/g) and lower micropore area (263 m²/g) than sample NaM. This can be explained by the higher amount of exchanged Ni²⁺ obtained for this sample (84 %) that partially blocks the entrance of the pores of the mordenite. The samples prepared in solid state show the highest decrease of the BET and micropore areas. The low surface values of samples prepared by stirring NiOB with NaM or HM (NaM-NiO and HM-NiO) can be explained by the NiO surface values contribution (50 %). In the other two

samples (NiNaM33 and NiNaM6) the amount of NiO blocking the porous of the mordenite structure explain these results. Thus, the sample with lower amount of NiO (NiNaM6) shows higher BET and micropore areas than the rest of samples prepared in solid state.

➤ **X-Ray microanalysis**

X-Ray microanalysis was used to confirm the Ni^{2+} exchange degree by comparing the distribution of the elements such as Al, Si, Na and Ni in one of the microwaved Ni^{2+} exchanged mordenites (M9) and in commercial mordenite. The observation of zones more and less clear in the distribution maps indicates the abundance of the element in the solid. Therefore, darker areas mean lower amount of the element. Figs. 40 and 41 show the results obtained for samples NaM and M9, respectively.

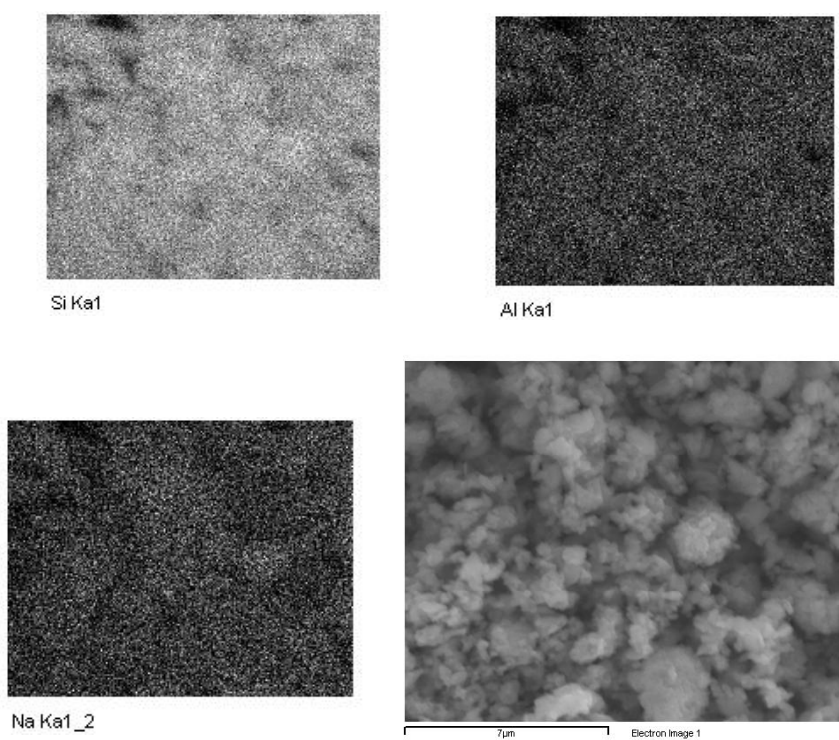


Figure 40. X-Ray microanalysis results for the sample NaM.

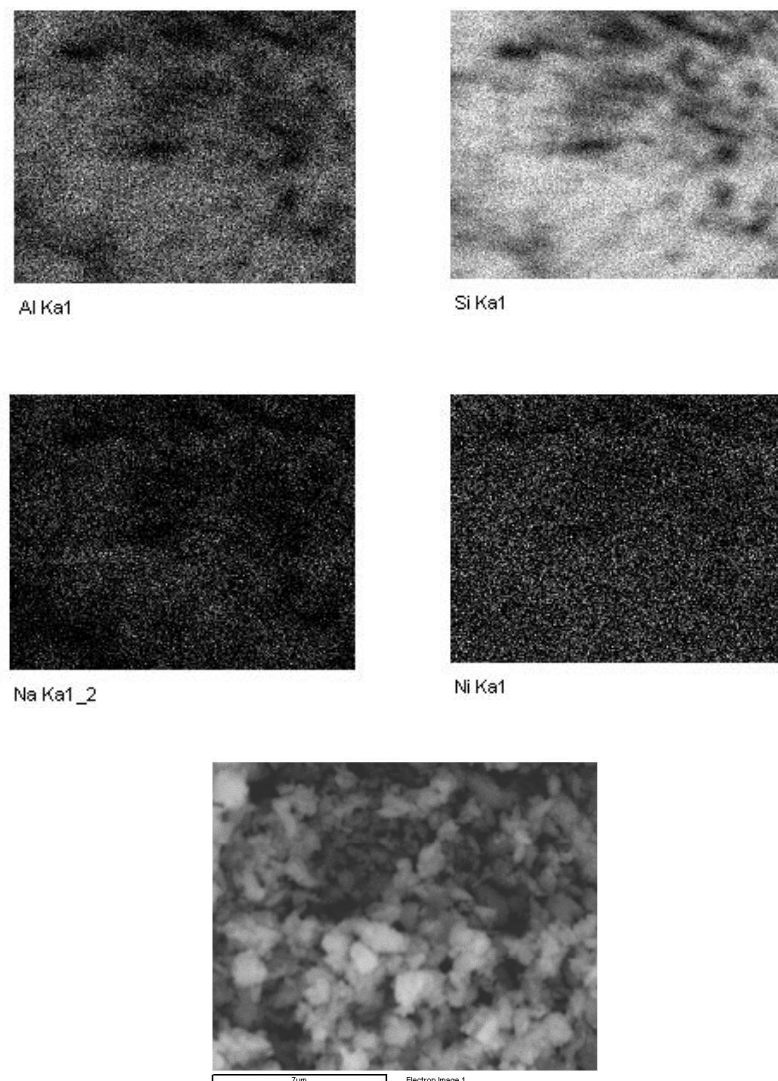


Figure 41. X-Ray microanalysis results for the sample M9.

In the two figures, we can see that the element more abundant is Si and secondly Al, as expected. From these results, we can conclude that the exchange under microwaves takes place since we observe the presence of Ni together with a decrease in the Na amount in sample M9 (Fig.41) when compared with NaM (Fig. 40).

➤ Temperature-programmed desorption-mass spectrometry experiments (TPD)

NH_3 -TPD experiments were carried out in order to evaluate changes in acidity for the most representative exchanged samples (M9, M12, M13 and M14). The maxima of the desorption temperature peaks, with their relative intensities in parenthesis, are shown in table 12.

Table 12. NH_3 -TPD results for some representative exchanged samples.

Samples	$\text{NH}_3 T_D$ (K) ^a			
	Peak 1	Peak 2	Peak 3	Peak 4
NaM	-	475 (l)	-	-
M9	420 (m)	500 (h)	813 (l)	920 (m)
M12	-	513 (h)	813 (l)	933 (m)
M13	407 (h)	475 (h)	813 (vl)	871 (l)
M14	412 (h)	495 (h)	814 (vl)	-

^a T_D : Maxima of NH_3 desorption temperature peaks.

(vl): very low-intense peak; (l): low-intense peak;

(m) medium-intense peak; (h): high-intense peak.

On the whole, we can observe four groups of desorption temperatures for the characterized samples. The first group corresponds to the desorption temperature range 407-420 K, the second group between 475-533 K, the third group corresponds to 813-814 K and the fourth group between 871-933 K. These four groups are named as peaks 1, 2, 3 and 4, respectively (table 12). When the sample exhibits peaks 1 and 2, they are partially overlapping.

The NH_3 -TPD profile of Na-Mordenite only presents one peak with low intensity (peak 2) [46,144]. This peak has been assigned to ammonia weakly held or physically adsorbed on the mordenite [144]. In the rest of samples, new peaks appear at higher temperatures (peaks 3 and 4) and, consequently, different acid sites are present (Table 12). Interestingly, the samples exchanged under microwaves (M9, M13 and M14) show another peak (peak 1) which desorbs at temperatures slightly lower than peak 2. Therefore, this peak should be related to the appearance of new sites on the surface of these

samples due the microwaves action. Microwaves can give to some local overheating and favour punctual structure modifications, especially for samples M13 and M14 since they have been exposed to microwaves for a longer time. In fact, peak 1 appears more intense in these two samples. These results will be correlated later with the catalytic activity data.

➤ **Model reactions to study acid properties**

Four samples with different degree of exchanged Ni²⁺, M9 (47 %), M12 (33 %), M13 (52 %) and M14 (84 %) and commercial Na-Mordenite (NaM), as a reference, were tested as catalysts in two reactions catalysed by different types of acid sites: the isomerization of styrene oxide to give β-phenylacetaldehyde (mainly catalysed by Brønsted acid sites) and the styrene oxide ring-opening to give 2-ethoxy-2-phenylethanol (catalysed by both Brønsted and Lewis acid sites). We used toluene or ethanol as solvent to favour the isomerization of styrene oxide or the styrene oxide ring-opening, respectively.

a) *Isomerization of styrene oxide reaction*

Figure 42 shows the catalytic activity obtained for all samples. NaM has the lowest conversion. Samples M9 and M12 exhibit around total conversion whereas samples M13 and M14 present conversion values around 55-60 %. Moreover, M9 and M12 show the highest yields to β-phenylacetaldehyde (around 90 % and 75 %, respectively) whereas for M13 and M14 samples the yield to β-phenylacetaldehyde is around 40 %. These last two catalysts show important amounts of no identified products that have high molecular weights (named as condensation products).

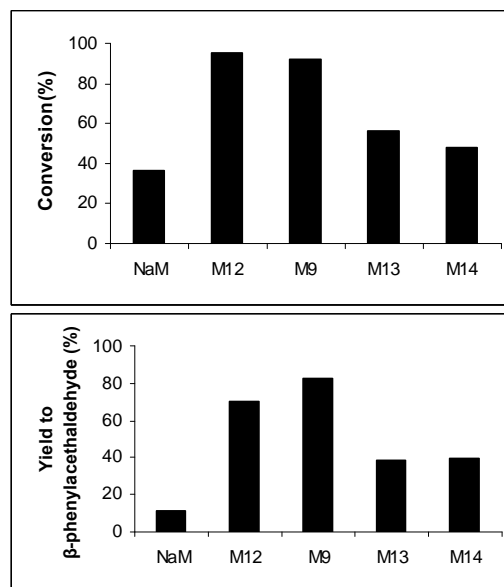


Figure 42. Catalytic activity for the isomerization of styrene oxide to β -phenylacetaldehyde.

The higher yield values to β -phenylacetaldehyde obtained for samples M9 and M12 can be related to the existence of Brønsted acid sites, due to the hydrolysis of Ni^{2+} , but mainly to the presence of stronger Brønsted acid sites, which could be associated to the effect of the proximity of the Ni^{2+} to the acid sites. The higher Ni^{2+} content of sample M9 explains its highest yield to β -phenylacetaldehyde. However, samples M13 and M14 should have lower amount of Brønsted acid sites due to dehydroxilation processes occurred during the intermediate thermal step for both samples. Additionally, in the case of sample M14, with the highest Ni^{2+} content, a lower amount of Brønsted acid sites can be expected due to the presence of some agglomerations of Ni^{2+} partially blocking the entrance of the mordenite pores, as observed from the nitrogen physisorption results.

b) Styrene oxide ring-opening reaction

Figure 43 shows the catalytic activity results obtained for this reaction. Again, sample NaM shows the lowest conversion. On the other hand, the conversion is total for catalysts M9, M12 and M14 being slightly lower when using catalyst M13 (around 90 %). Catalysts M13 and M14 give a higher yield to 2-ethoxy-2-phenylethanol (around 70 %) whereas catalysts M9 and M12 present higher amounts of condensation products and a yield to 2-ethoxy-2-phenylethanol around 40 %.

The presence of stronger Brønsted acid sites in samples M9 and M12 can explain the formation of higher amounts of condensation products. On the other hand, the presence of weaker acid sites (Brønsted and/or Lewis), some of which appeared because of the microwaves action, should explain the higher yields to 2-ethoxy-2-phenylethanol obtained for catalysts M13 and M14.

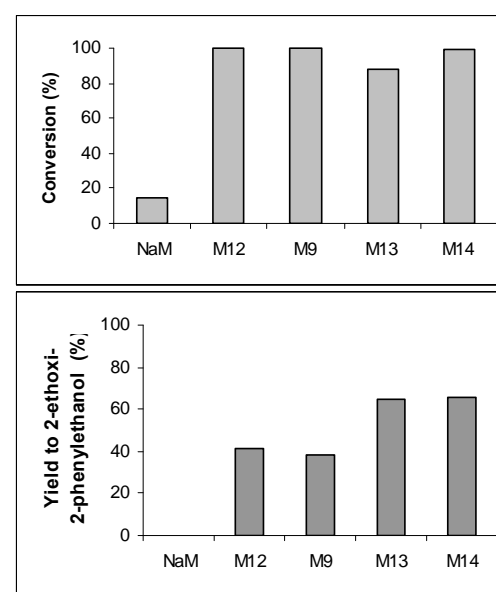


Figure 43. Catalytic activity for the styrene oxide ring-opening to 2-ethoxy-2-phenylethanol.

c) *Correlation between catalytic activity and NH₃-TPD results*

NH₃-TPD results of samples M9 and M12 (the catalysts with the highest yield to β-phenylacetaldehyde in the isomerization of styrene oxide) show two peaks at high desorption temperatures (Table 12, peaks 3 and 4) with higher intensity than the rest of samples (Table 12). It is well known that the isomerization of styrene oxide to β-phenylacetaldehyde is mainly catalysed by Brønsted acid sites [46]. Therefore, taking into account the activity results for this reaction, peaks 3 and 4 can be assigned to Brønsted acid sites. Besides, peak 2 can be also related to Brønsted acid sites as deduced from the comparison with the NH₃-TPD of H-Mordenite which only present one peak at around 513 K [144].

In contrast, catalysts M9, M12, M13 and M14 show high conversion values in the styrene oxide ring-opening reaction, but only M13 and M14 give to high yields to 2-ethoxy-2-phenylethanol (Fig.43) whereas catalysts M9 and M12 give to important amounts of condensation products. The presence of stronger acid sites in catalysts M9 and M12 (Table 12, peak 4) assigned to Brønsted acid sites, as commented above, favours the formation of these condensation products. Interestingly, the catalysts that give to high yields to 2-ethoxy-2-phenylethanol (M13 and M14) present a more intense peak 1 (Table 12). The appearance of this peak with higher intensity in the samples prepared under harder microwaves conditions, allow us to relate it to Lewis or Brønsted acid sites associated to some modifications of the mordenite structure caused by some local overheating because of the microwaves action. Taking into account that the catalytic reactions were performed at room temperature, these weakest acid sites, assigned to peak 1, could have some effect in the catalytic activity results for this reaction. These acid sites together with the weak Brønsted acid sites, assigned to peak 2, also present in these samples can explain the higher yield values to 2-ethoxy-2-phenylethanol obtained for catalysts M13 and M14.

➤ Hydrogen Chemisorption

Several Ni-Mordenite samples were calcined and then heated under H₂ to obtain the corresponding catalysts. These catalysts were characterized by hydrogen chemisorption in order to evaluate their metallic area.

The catalysts obtained from the samples prepared by ion exchange in a microwave oven and by conventional method (M9 and M12), and the samples prepared by two exchanges in a microwave oven with a thermal treatment between them (M13 and M14) do not show metallic areas even when using higher reduction temperatures (673 and 773 K). A possible strong interaction between the nickel cations and the mordenite structure can explain these results. Consequently, reduction does not seem to be achieved for these samples.

On the other hand, catalysts NiNaM33R and NiNaM6R have 5.7 and 1.2 m²/g sample, respectively. The difference in the metallic areas for these samples is proportional to the nickel amount used in their preparation. The obtaining of metallic area in these samples indicate that we have obtained catalysts with metallic sites in competition with acid sites probably located in the internal surface of the support. Catalysts NaM-Ni and HM-Ni, whose precursors were prepared by mixing the phases, show very low metallic areas (< 1 m²/g sample). The low metallic area found for the bulk nickel catalyst (NiB), commented in section 4.1 (1.7 m²/g sample), and the contribution of mordenite amount can explain these results.

Catalytic activity for the hydrogenation of styrene oxide

Ten catalysts with different nickel content were tested in the hydrogenation of styrene oxide. Firstly, we tested samples NaM and HM without metallic phase for comparison. Then, catalysts M9R, M12R, M13R and M14R with 3.2 %, 2.3 %, 3.6 % and 5.8 % of nickel content, respectively, were tried out at the same reaction conditions. Finally, we also tested catalysts NaM-Ni and HM-Ni with 44 % of nickel amount and NiNaM6R and NiNaM33R with 6.4 % and 33.4 % of nickel amount, respectively.

NaM showed low conversion (17 %) even at 6 hours of reaction whereas sample HM exhibited total conversion from 1 hour of reaction but no hydrogenation products were detected (Fig. 44). The main product was 2-ethoxy-2-phenylethanol (around 70 %). It seems that the acid properties of HM favour the styrene oxide ring-opening to give 2-ethoxy-2-phenylethanol. NH₃-TPD results of this sample (HM) shows a thermogram with only one peak at 513 K that has been related to weak Brønsted acid sites [46]. The presence of these acid sites explains the high yield to 2-ethoxy-2-phenylethanol and the practically absence of condensation products. The formation of condensation products has been associated to stronger Brønsted acid sites as commented above in the styrene oxide ring-opening reaction studies.

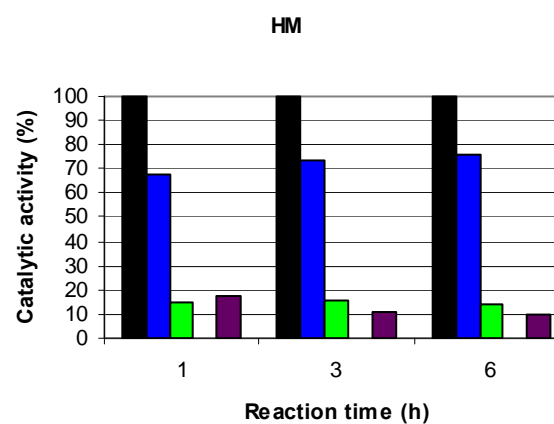


Figure 44. Catalytic activity for the sample HM.
■ Conversion (%), ■ Selectivity to 2-ethoxy-2-phenylethanol (%), ■ Selectivity to β -phenylacetaldehyde (%), ■ Selectivity to 2-phenylethanol (%), ■ Selectivity to condensation products (%).

Figure 45 shows the catalytic activity for the catalysts obtained from the samples prepared by one exchange process (M9R and M12R). The catalytic behaviour of these two catalysts is similar. M9R and M12R show total conversion from 1 hour of reaction but the main products are 2-ethoxy-2-phenylethanol and condensation products. 2-phenylethanol or other hydrogenation products were not detected for any of these catalysts (Fig. 45a and Fig. 45b). Moreover, figure 45c and figure 45d show the yield to 2-ethoxy-

2-phenylethanol which is very similar to that obtained for their precursors, M9 and M12, at 3 hours of reaction (Fig. 43). This result is in agreement with the fact that not metallic areas were detected for these catalysts and, consequently, their catalytic behaviour must be related to the acid properties associated to Ni²⁺. Similar values of catalytic activity were obtained when these catalysts (M9R and M12R) were reduced at higher temperatures (673 K and 773 K).

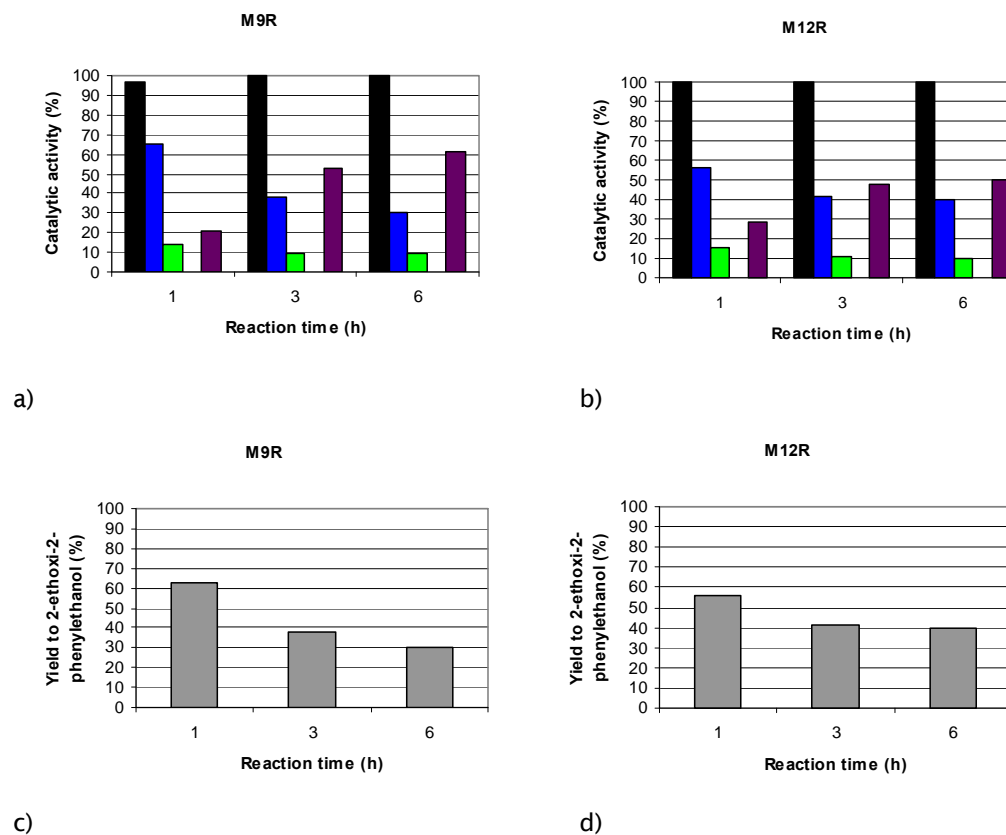


Figure 45. a) Catalytic activity for the catalyst M9R, b) Catalytic activity for the catalyst M12R, c) Yield to 2-ethoxy 2-phenylethanol for the catalyst M9R and d) Yield to 2-ethoxy 2-phenylethanol for the catalyst M12R.

- Conversion (%), ■ Selectivity to 2-ethoxy-2-phenylethanol (%), ■ Selectivity to β -phenylacetraldehyde (%), ■ Selectivity to 2-phenylethanol (%), ■ Selectivity to Condensation products (%), ■ Yield to 2-ethoxy-2-phenylethanol (%).

Figure 46 shows the catalytic results of the catalysts obtained from the samples exchanged twice in a microwave oven with a thermal treatment between them (M13R and M14R).

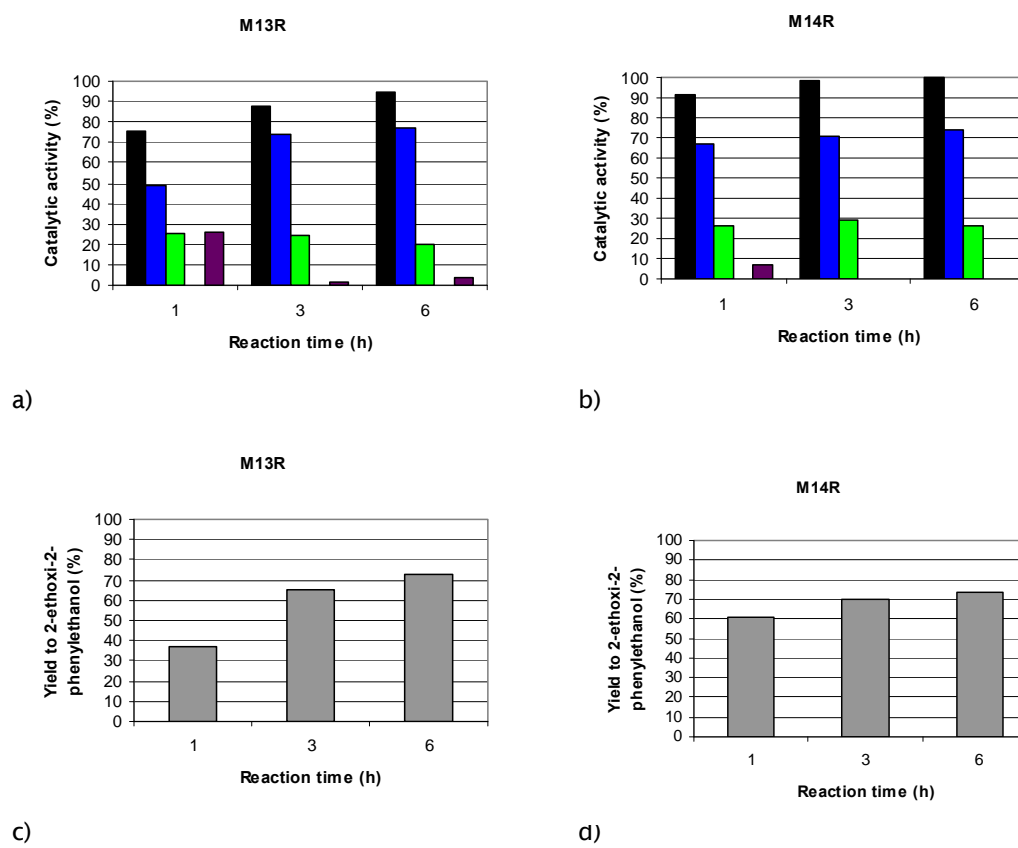


Figure 46. a) Catalytic activity for the catalyst M13R, b) Catalytic activity for the catalyst M14R, c) Yield to 2-ethoxi 2-phenylethanol for the catalyst M13R and d) Yield to 2-ethoxi 2-phenylethanol for the catalyst M14R.

■ Conversion (%), ■ Selectivity to 2-ethoxi-2-phenylethanol (%), ■ Selectivity to β -phenylacetaldehyde (%), ■ Selectivity to 2-phenylethanol (%), ■ Selectivity to Condensation products (%), ■ Yield to 2-ethoxi-2-phenylethanol (%).

M14R shows total conversion at 6 hours of reaction whereas M13R shows 95 % of conversion at the same reaction time. However, the main products are 2-ethoxi-2-phenylethanol and β -phenylacetaldehyde but 2-phenylethanol or other hydrogenation products are not detected for any of these catalysts (Fig 46a and Fig.46b). Moreover, figure 46c and figure 46d

shows the yield to 2-ethoxy-2-phenylethanol which is very similar to that obtained for their precursors M13 and M14 (Fig. 43). Again, this catalytic behaviour can be related to the acid properties associated to Ni²⁺ present in these samples.

Lastly, figure 47 shows the catalytic activity obtained for the catalysts prepared in the solid state.

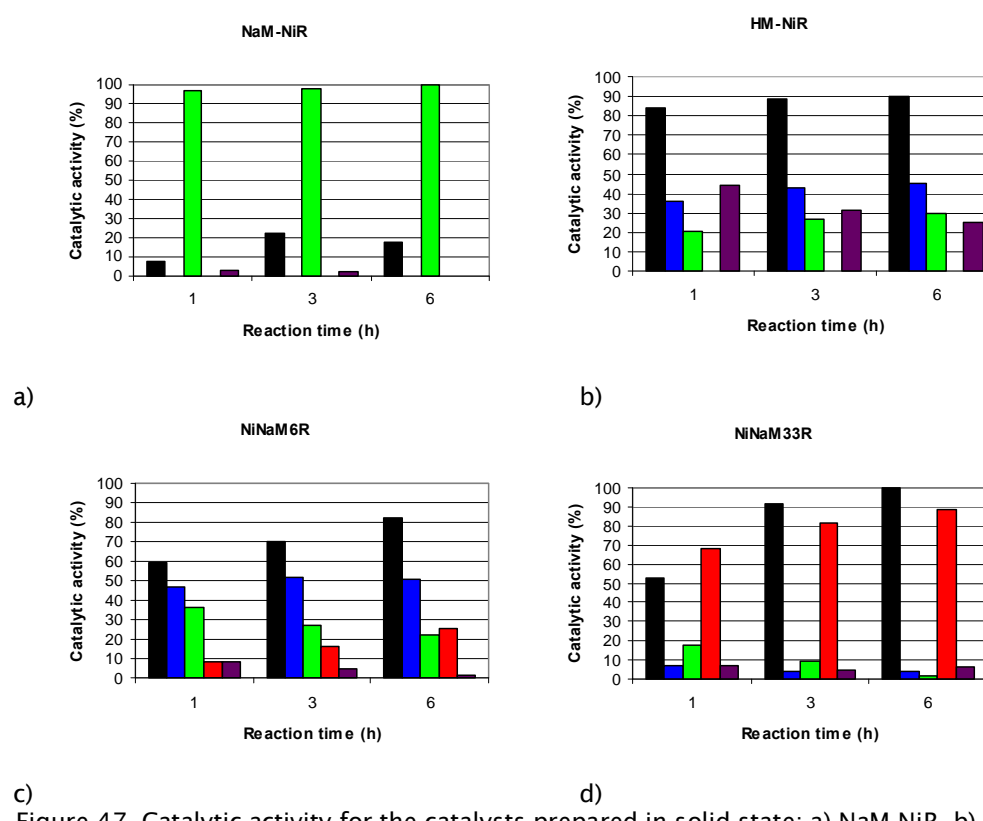


Figure 47. Catalytic activity for the catalysts prepared in solid state: a) NaM-NiR, b) HM-NiR, c) NiNaM6R and d) NiNaM33R.

- Conversion (%), ■ Selectivity to 2-ethoxy-2-phenylethanol (%), ■ Selectivity to β -phenylacetraldehyde (%), ■ Selectivity to 2-phenylethanol (%), ■ Selectivity to Condensation products (%).

The catalytic results of the catalysts NaM-Ni and HM-Ni, used as references, are shown in Fig. 47a and Fig. 47b, respectively. Catalyst NaM-Ni has very low activity giving to β -phenylacetraldehyde as a main product (around 95 %), whereas catalyst HM-Ni presents higher activity (90 % of

conversion at 6 hour of reaction). We detected a mixture of reaction products for this catalyst. However, we do not detect 2-phenylethanol in any of them. It seems that the Brønsted acid sites win in the competition between the nickel metallic sites and the Brønsted acid sites due to the very low metallic area of these samples. The lower selectivity to 2-ethoxy-2-phenylethanol observed for catalyst HM-Ni respect to sample HM (Fig. 44) should be explained by the use of half amount of HM for its preparation.

In contrast, catalysts NiNaM6R and NiNaM33R present different catalytic activity respect to all the catalysts presented until now (Fig. 47c and 47d). At 6 hours of reaction, catalyst NiNaM6R has 80 % of conversion whereas catalyst NiNaM33R shows total conversion. On one hand, catalyst NiNaM6R gives to 2-ethoxy-2-phenylethanol and β -phenylacetaldehyde in higher amounts, and to 2-phenylethanol and condensation products in small amounts. On the other hand, catalyst NiNaM33R shows the highest amount of 2-phenylethanol (90 % of selectivity at 6 hours of reaction). The rest of by-products observed for the other catalysts are detected in very small amounts in this catalyst.

Samples NaM-NiO, HM-NiO and NiNaM33 have similar micropore areas (Table 11) so they should have similar availability the acid sites in their corresponding catalysts. Interestingly, catalyst NiNaM33R shows the highest metallic area value ($5.7\text{ m}^2/\text{g}$ sample) and gives to high amounts of 2-phenylethanol. Therefore, we can conclude that there is a competition between the two reactions: the hydrogenation of styrene oxide catalysed by metallic sites and the styrene oxide ring-opening catalysed by Brønsted and Lewis acid sites. The higher amount of metallic nickel sites favours the hydrogenation of styrene oxide to give selectively 2-phenylethanol and minimize other side reactions. This also explains the fact that catalyst NiNaM6R, which has slight higher metallic area than catalysts NaM-Ni and HM-Ni but much lower metallic area than catalyst NiNaM33R, gives to small amounts of 2-phenylethanol.

4.3.4 Conclusions

We obtained around 47 % of exchanged Ni^{2+} mordenite using a microwave oven with the best conditions (50 ml $\text{Ni}(\text{NO}_3)_2 \cdot 6\text{H}_2\text{O}$ 1 M at 333 K for 15 minutes). Similar values of exchanged Ni^{2+} were obtained by conventional exchanging but needing much longer time (24 hours).

Interestingly, we obtained 84 % of exchanged Ni^{2+} when we submit the sample exchanged under microwaves at the best conditions to a thermal treatment under microwaves followed by a second exchange process at the same conditions than the first exchange. This treatment could favour the migration of the nickel cations located in the main channels to other positions less accessible of mordenite. However, microwaves, especially at harder conditions, can cause some local overheating that gives to punctual modifications in the mordenite structure. This agrees with NH_3 -TPD and catalytic activity results.

The exchanged Ni^{2+} mordenites present different acid properties depending on the Ni^{2+} exchange degree and the procedure used in the exchange process. The acidity has been evaluated by testing five mordenites in two reactions catalysed by different acid sites. (NaM (commercial mordenite), M9 (47 % Ni^{2+} , one exchange under microwaves), M12 (33 % Ni^{2+} , one exchange by conventional method), M13 (52 % Ni^{2+} , two exchanges under microwaves with an intermediate thermal treatment in an oven) and M14 (84 % Ni^{2+} , two exchanges under microwaves with an intermediate thermal treatment under microwaves). The catalytic behaviour of these samples has been correlated with the NH_3 -TPD results. Samples M9 and M12 have higher amounts and stronger Brønsted acid sites than the rest of samples, as observed by NH_3 -TPD. This explains the high yields to β -phenylacetaldehyde obtained in the isomerization of styrene oxide, and the important amounts of condensation products formed in the styrene oxide ring-opening reaction for these catalysts. On the other hand, the highest yields in the styrene ring-opening reaction achieved by samples M13 and M14 have been related to the

presence of weaker acid sites (peaks 1 and 2), some of which (peak 1) only appear in the samples exchanged under microwaves. These weakest acid sites only can be explained by some local overheating caused by the microwaves action that could cause some local modifications in the mordenite structure.

The catalysts obtained for the samples exchanged by microwaves or by conventional method do not show metallic areas for all reduction temperatures tested. This can be due to the strong interaction between the nickel cations with the mordenite structure. However, the catalysts obtained from the samples prepared in solid state have metallic areas.

For the hydrogenation of styrene oxide, the catalysts which become from the samples exchanged by ion exchange method (M9R, M12R, M13R and M14R) give to similar catalytic behaviour to that obtained for their precursors for the styrene oxide ring-opening (2-phenylethanol or other hydrogention products were not detected). This fact together with the null metallic areas obtained for these catalysts indicate that reduction is not achieved and similar acid sites are present. However, the catalytic activity of the Ni-Mordenite catalysts prepared in solid state (NiNaM33R and NiNaM6R) shows the formation of 2-phenylethanol which is detected in higher amounts for the catalyst with higher metallic area. This confirms that there is a competition between the styrene oxide ring-opening catalysed by acid sites and the hydrogenation of styrene oxide catalysed by metallic sites.

5. CONCLUSIONES

Debido a que cada apartado de discusión de resultados contiene sus conclusiones, en esta sección se expondrán las conclusiones finales generales resumiéndolas en dos apartados.

Preparación de precursores y catalizadores

- El uso de microondas en la preparación de hidrotalcitas de Ni/Mg/Al ($\text{Ni}^{2+}/\text{Al}^{3+}$, 4:1 $\text{Ni}^{2+}/\text{Mg}^{2+}$, 6:1) en autoclave permite obtener hidrotalcitas más cristalinas en tiempos de envejecimiento más cortos que mediante métodos convencionales. No obstante, se produce una cierta desaluminación que es muy importante cuando se utiliza una temperatura de 453 K en el tratamiento térmico (45 % Al perdido) y a mayores tiempos. Al aumentar la temperatura de tratamiento se obtienen hidrotalcitas que junto a una mayor cristalinidad, presentan mayor área BET y un cierto incremento en su basicidad.
- Los catalizadores obtenidos a partir de las hidrotalcitas envejecidas en microondas tienen unas áreas metálicas mayores que los obtenidos a partir del resto de hidrotalcitas preparadas. Este resultado es consecuencia de una mejor dispersión de la fase níquel en el catalizador.
- Se ha obtenido NaMordenita intercambiada con un 84 % de Ni^{2+} mediante un doble intercambio iónico a 333 K y un tratamiento térmico intermedio a 453 K, utilizando en todos los casos un horno microondas.
- La presencia de Ni^{2+} en la mordenita induce la formación de centros de Brønsted fuertes. La utilización de microondas en los procesos de intercambio y tratamientos térmicos intermedios favorece la formación de nuevos centros ácidos débiles de Lewis y/o de Brønsted como consecuencia de la acción de las microondas sobre la superficie de la mordenita.

Conclusiones

Actividad catalítica en la hidrogenación del óxido de estireno para la obtención selectiva de 2-feniletanol

- Los catalizadores de níquel másicos preparados por diferentes procedimientos presentan todos una elevada selectividad hacia 2-feniletanol (60-85 % a las 6 horas de reacción), aunque la actividad es diferente para cada uno de ellos, hecho que se puede relacionar con la morfología y tamaño de las partículas metálicas, resultando ser el más activo el que tiene mayor área metálica (NiB). Partículas de níquel metálico más pequeñas y con una morfología octaédrica definida (NiC) favorecen la formación de productos de condensación que desactivan el catalizador.
- La presencia de MgO en los catalizadores de níquel ha implicado un aumento importante del rendimiento en el producto de interés (2-feniletanol). La cantidad de magnesia y el procedimiento de preparación son determinantes en la actividad del catalizador. El NiMgO es el que presenta una mayor conversión (100 %) y selectividad a 2-feniletanol (100 %), a las 3 horas de reacción. La influencia de los centros básicos en el níquel metálico así como, una limitada disponibilidad de los mismos, favorece la rápida formación del 2-feniletanol y minimiza la formación de productos de condensación.
- Los catalizadores de níquel con propiedades básicas que han resultado ser los más activos (100 % de conversión, 1 hora de reacción), manteniendo una alta selectividad en el 2-feniletanol (95 %) y que presentan mayor resistencia a la desactivación, son los preparados a partir de los precursores tipo hidrotacita de Ni/Mg/Al ($\text{Ni}^{2+}/\text{Al}^{3+}$, 4:1 $\text{Ni}^{2+}/\text{Mg}^{2+}$, 6:1), debido a las elevadas áreas metálicas que presentan ($\approx 47 \text{ m}^2/\text{g muestra}$) y a su idónea basicidad.
- De los catalizadores de Ni-Mordenita preparados el que presenta una mayor conversión (100 % a las 6 horas de reacción) y mayor selectividad a 2-feniletanol (90 % a las 6 horas de reacción) es NiNaM33R, cuyo

precursor se ha preparado en estado sólido con un mayor porcentaje de níquel, presentando después de la reducción una mayor área metálica.

- A partir de los resultados catalíticos obtenidos para los catalizadores preparados utilizando precursores de Ni-Mordenita (por intercambio iónico y en estado sólido) se ha podido establecer que existe una competición entre los centros ácidos, que catalizan la reacción de apertura del anillo del óxido de estireno, y los centros metálicos, que catalizan la hidrogenación del óxido de estireno.

6. REFERENCIAS BIBLIOGRÁFICAS

- [1] S. Arctander, Perfume and Flavour Chemical, Montclair, NJ, 1969.
- [2] B. D. Mookherjee, R. A. Wilson, Kirk-Othmer Encyclopedia of Chemical Technology, 4 ed., vol. 4, John Wiley & Sons, New York, 1996.
- [3] K. Bauer, D. Garbe, H. Surburg, Common Fragrance and Flavour Materials, New York, 1990.
- [4] R. A. Wilson, Kirk-Othmer Encyclopedia of Chemical Technology, Jonh Willey, New York, 1991.
- [5] H. O. House, Modern Synthetic Reactions, W. A. Benjamin, Menlo Park, 1972.
- [6] F. A. Carey, R. J. Sundberg, Advanced Organic Chemistry, Plenum Press, New York, 1977.
- [7] M. Bartok, K. L. Lang, The Chemistry of Heterocyclic Compounds-Small Ring Heterocycles, ed. A. Weissberger and E. C. Taylor, Wiley, New York, 1985.
- [8] R. Sreekumar, R. Padmakumar, P. Rugmini, Tetrahedron Lett. 39 (1998) 5515.
- [9] G. Smith, Synthesis. 8 (1984) 629.
- [10] C. Bonini, Tetrahedrom. 45 (1989) 2895.
- [11] M. Hudlicky, Reductions in Organic Chemistry, Ellis Horwood Chichester, England, 1984.
- [12] E. L. Eliel, D. W. Delmonte, J. Am. Chem. Soc. 78 (1956) 3226.
- [13] M. L. Mihaolovic, V. Andrejevic, J. Milovanoic, Helv. Chim. Acta. 69 (1976) 2305.
- [14] A. Ookawa, H. D. Soai, Bull. Chem. Soc. Jpn. 60 (1987) 1813.
- [15] S. Krishnamurthy, R. M. Shubert, H. C. Brown, J. Am Chem. Soc. 95 (1973) 8486.
- [16] R. O. Hutchings, I. M. Taffer, W. Burgoyne, J. Org. Chem. 46 (1981) 5214.
- [17] W. B. Smith, J. Org. Chem. 49 (1984) 3219.
- [18] Y. Fort, R. Vanderesse, P. Caubere, Tetrahedron Lett. 26 (1985) 3111.
- [19] B. C. Ranu, A. R. Das, J. Chem. Soc., Chem. Commun. 19 (1990) 1334.

Referencias bibliográficas

- [20] J. M. Campelo, R. Chekraborty, J. M. Marinas, *Synth. Commun.* 26 (3) (1996) 415.
- [21] J. S. Cha, J. H. Park, *Bull. Korean Chem. Soc.* 23 (2002) 1377.
- [22] K. Weissermel, H. J. Arpe, *Química Orgánica Industrial*. Ed. Reverté, S. A., 1981.
- [23] M. P. De Frutos, J. A. Delgado, I. Vic, EP 0943611, 1999.
- [24] H. Fujitsu, S. Shirahama, E. Matsumura, K. Takeshita, I. Mochida, *J. Org. Chem.* 46 (1981) 2287.
- [25] R. A. Grey, G. P. Pez, A. Wallo, *J. Am. Chem. Soc.* 103 (1981) 7536.
- [26] I. Mochida, S. Shirahama, H. Fujitsu, K. Takeshita, *Chem. Lett.* 4(1977) 421.
- [27] U. Matteoli, G. Menchi, M. Bianchi, F. Piacenti, S. Ianelli, M. J. Nardelli, *J. Organomet. Chem.* 498 (1995) 177.
- [28] T. Ohta, M. Kamiya, K. Kusui, T. Michibata, M. Nobutomo, I. Furukawa, *Tetrahedron Lett.* 40 (1999) 6963.
- [29] K. Nomura, H. Ogura, Y. Imanishi, *J. Mol. Catal. A: Chem.* 166 (2001) 345.
- [30] C. Bellefon, N. Tanchoux, S. Caravieilhes, *J. Organomet. Chem.* 567 (1998) 143.
- [31] O. Loehr, U. S. Pat 1787205, 1930.
- [32] T. F. Wood, N. J. Clifton, U. S. Pat 2524096, 1950.
- [33] H. Hopff, H. Kuhn, U. Hoffmann, B. Hamburg, U. S. Pat. 2822403, 1958.
- [34] S. Mitsui, S. Imaizumi, M. Hisashige, Y. Sugi, *Tetrahedron Lett.* 29 (1973) 4093.
- [35] C. A. Gibson, L. F. Theiling, U. S. Pat. 4064186, 1977.
- [36] V. G. Yadav, S. B. Chandalia, *Org. Process Res. & Dev.* 2 (1998) 294.
- [37] R. V. Chaudari, M. M. Telkar, Ch. V. Rode, U. S. Pat. 6166269, 2000.
- [38] I. Kirm, F. Medina, X. Rodríguez, Y. Cesteros, P. Salagre, J. E. Sueiras, *J. Mol. Catal. A: Chem.* 239 (2005) 215.
- [39] I. Kirm, F. Medina, J. E. Sueiras, P. Salagre, Y. Cesteros, *J. Mol. Catal. A: Chem.* 261 (2007) 98.
- [40] R. Ravichandran, S. Divakar, *J. Mol. Catal. A: Chem.* 137 (1999) 31

- [41] R. Dimitrova, V. Minkov, N. Micheva, *Appl. Catal. A.* 145 (1996) 49.
- [42] M. Steilemann, J. N. Armor, W. F. Hölderich., *Chemm. Commun.* 8 (1999) 697.
- [43] C. V. Rode, M. M. Telkar, R. Jaganathan, R. V. Chaudhari, *J. Mol. Catal. A: Chem.* 200 (2003) 279.
- [44] K. Tanabe, *Solid Acid and Bases their catalytic properties*, Academic Press, New York, London, 1979.
- [45] W. H. Hölderich, U. Barsnick, in: S.A. Sheldon, H. van Bekkum (Eds.) *Fine Chemicals though Heterogeneous Catalysis*, Wiley-VCH, Weinheim, 2001.
- [46] I. Salla, O. Bergada, P. Salagre, Y. Cesteros, F. Medina, J. E. Sueiras, T. Montanari, *J. Catal.* 232 (2005) 239.
- [47] N. K. Kotsev, I. L. Ilieva, *Catal. Lett.* 18 (1993) 173.
- [48] P. Bukovec, N. Bukovec, B. Orel, K. S. Wissiak, *J. Therm. Anal.* 40 (1993) 1193.
- [49] R. I. Razhork, R. S. Mikhail, *J. Phys. Chem.* 63 (1959) 1050.
- [50] P. N. Rylanda, *Ullmann's Encyclopedia of Industrial Chemistry*, Vol. A.13, VCH, Veinheim, 1989.
- [51] Y. Cesteros, R. Fernández, J. Estellé, P. Salagre, F. Medina, J. E. Sueiras, J. L. G. Fierro, *Appl. Catal., A.* 152 (1997) 249.
- [52] M. Raney, U.S. Patents 1,563,587 (1927), 1,628,190 (1927), 1,915,473 (1933).
- [53] Y. C. Kang, S. B. Park, Y. W. Kang, *Nanostruct. Mater.* 5 (1995) 777.
- [54] J. Estellé, P. Salagre, Y. Cesteros, M. Serra, F. Medina, J. E. Sueiras, *Solid State Ionics.* 156 (2003) 4968.
- [55] P. J. Anderson, R. F. Hohrlock, *Trans. Faraday Soc.* 58 (1962) 1993
- [56] M. Serra, P. Salagre, Y. Cesteros, F. Medina, J. E. Sueiras, *Phys. Chem. Chem. Phys.* 6 (2004) 858.
- [57] P. L. Lewellyn, V. Chevrot, J. Ragai, O. Cerclier, J. Estienne, R. Rouquerol, *Solid State Ionics* 101-103 (1997) 1293.
- [58] M. A. A. Elmasry, A. Gaber, E. M. H. Khater, *J. Therm. Anal.* 52 (1998) 489.
- [59] H. Hattori, *Appl. Catal., A.* 222 (2001) 247.

Referencias bibliográficas

- [60] M. L. Bailly, C. Chizallet, G. Costentin, J. M. Krafft, H. Lauron-Pernot, M. Che, *J. Catal.* 25 (2) (2005) 413.
- [61] O. Sidjabat, D. L. Trimm, *Top. Catal.* 11-12 (2000) 279.
- [62] M. Serra, P. Salagre, Y. Cesteros, F. Medina, J. E. Sueiras, *J. Catal.* 197 (2001) 210.
- [63] M. Serra, P. Salagre, Y. Cesteros, F. Medina, J. E. Sueiras, *J. Catal.* 209 (2002) 202.
- [64] H. Schaper, J. J. Berg-Slot, V. H. J. Stork, *Appl. Catal.* 54 (1989) 79.
- [65] S. Sato, R. Takahashi, T. Sodesawa, F. Nozaki, X. Z. Jin, S. Suzuki, T. Nakayama, *J. Catal.* 191 (2000) 261.
- [66] S. Takenaka, S. Sato, R. Takahashi, T. Sodesawa, *Phys. Chem. Chem. Phys.* 5(21) (2003) 4968.
- [67] T. Borowiecki, *Appl. Catal.* 10 (1984) 273.
- [68] T. Borowiecki, *Appl. Catal.* 31 (1987) 207.
- [69] N. Takezawa, H. Terumura, M. Shimokawabe, H. Kobayashi, *Appl. Catal.* 23 (1986) 291.
- [70] A. Parmaliana, F. Arena, F. Frusteri, S. Coluccia, L. Marchese, G. Martra, A. L. Chuvalin, *J. Catal.* 141 (1993) 34.
- [71] J. R. Rastrup-Nielsen, *Steam Reforming Catalysts*; Danish Technical: Copenhagen, 1975.
- [72] A. Parmaliana, F. Arena, F. Frusteri, N. Giordano, *J. Chem. Soc. Faraday Trans.* 86 (1990) 2663.
- [73] F. Arena, B. A. Horrell, D. L. Cocke, A. Parmaliana, N. Giordano, *J. Catal.* 132 (1991) 58.
- [74] G. C. Bond, S. P. Sarsam, *Appl. Catal.* 38 (1988) 365.
- [75] M. Serra, P. Salagre, Y. Cesteros, F. Medina, J. E. Sueiras, *Solid State Ionics.* 134 (2000) 229.
- [76] L. Xiancai, W. Min, L. Zhihua, H. Fei, *Appl. Catal., A.* 290 (2005) 81.
- [77] D. Tichit, A. Vaccari, *Appl. Clay Sci.* 13 (1998) 311.
- [78] V. Rives, M. A. Ulibarri, *Coord. Chem. Rev.* 181 (1999) 61.
- [79] F. Cavani, F. Trifiró, A. Vaccari, *Catal. Today.* 11 (1991) 173.

- [80] C. N. Perez, C. A. Perez, C. A. Henriques, J. L. F. Monteiro, *Appl. Catal., A.* 272 (2004) 229.
- [81] S. Abelló, F. Medina, D. Tichit, J. Pérez-Ramírez, X. Rodríguez, J. E. Sueiras, P. Salagre, Y. Cesteros, *Appl. Catal., A.* 281 (2005) 191.
- [82] I. Kirm, F. Medina, X. Rodríguez, Y. Cesteros, P. Salagre, J. E. Sueiras, *Appl. Catal., A.* 272 (2004) 175.
- [83] S. Velu, C. S. Swamy, *Catal. Lett.* 40 (1996) 265.
- [84] F. Basile, G. Fornasari, V. Rosetti, F. Trifirò, A. Vaccari, *Catal. Today.* 91-92 (2004) 293.
- [85] K. M. Lee, W. Y. Lee, *Catal. Lett.* 83 (2002) 65.
- [86] A. Morato, C. Alonso, F. Medina, J. E. Sueiras, D. Tichit, B. Coq, *Appl. Catal., B.* 32 (2001) 167.
- [87] Y. Cesteros, P. Salagre, F. Medina, J. E. Sueiras, D. Tichit, B. Coq, *Appl. Catal., B.* 32 (2001) 25.
- [88] A. Chen, H. Xu, Y. Yue, W. Shen, W. Hua, Z. Gao, *Appl. Catal., A.* 274 (2004) 101.
- [89] F. Medina, D. Tichit, B. Coq, A. Vaccari, N. T. Dung, J. *Catal.* 167 (1997) 142.
- [90] D. Tichit, M. H. Lhouty, A. Guida, B. H. Chinche, F. Figueras, A. Auroux, D. Bartalini, E. Garonne, *J. Catal.* 151 (1995) 50.
- [91] S. Abelló, F. Medina, D. Tichit, J. Pérez-Ramírez, Y. Cesteros, P. Salagre, J. E. Sueiras, *Chem. Commun.* 11 (2005) 1453.
- [92] S. Abelló, F. Medina, D. Tichit, J. Pérez-Ramírez, J. C. Groen, J. E. Sueiras, P. Salagre, Y. Cesteros, *Chem. Eur. J.* 11 (2005) 728.
- [93] T. Sato, H. Fujita, T. Endo, M. Shimada, *Reactivity of Solids.* 5 (1988) 219.
- [94] S. Miyata, *Clays Clay Miner.* 23 (1975) 369.
- [95] T. López, P. Bosch, E. Ramos, R. Gómez, O. Novarro, D. Acosta, F. Figueras, *Langmuir.* 12 (1996) 189.
- [96] D. M. P. Mingos, D. R. Baghurst, *Chem. Soc. Rev.* 20 (1991) 1.

Referencias bibliográficas

- [97] H. M. Kingston, S. J. Haswell, *Microwave-Enhanced Chemistry Fundamentals, Sample Preparation and Applications*, American Chemical Society: Washington, DC, 1997.
- [98] G. Fetter, F. Hernández, A. M. Maubert, V. H. Lara, P. Bosch, *J. Porous Mater.* 4 (1997) 27.
- [99] S. Komarneni, Q. H. Li, R. Roy, *J. Mater. Res.* 11 (1996) 1866.
- [100] P. Benito, F. M. Labajos, V. Rives, *J. Solid State Chem.* 179 (2006) 3784.
- [101] P. Benito, F. M. Labajos, J. Rocha, V. Rives, *Microporous Mesoporous Mater.* 94 (2006) 148.
- [102] P. Benito, F. M. Labajos, V. Rives, *Cryst. Growth and Des.* 6 (2006) 1961.
- [103] E. Dumitriu, V. Hulea, C. Chelaru, C. Catrinescu, D. Tichit, R. Durand, *Appl. Catal., A*. 178 (1999) 145.
- [104] E. López-Salinas, M. García-Sánchez, M.A. E. Llanos-Serrano, J. Navarrete-Bolañoz, *J. Phys. Chem. B*. 101 (1997) 5112.
- [105] P. Benito, F. M. Labajos, J. Rocha, V. Rives, *Microporous Mesoporous Mater.* 94 (2006) 148.
- [106] J. A. Rivera, G. Fetter, P. Bosch, *Microporous. Mesoporous. Mater.* 89 (2006) 306.
- [107] M. J. Climent, A. Corma, S. Iborra, K. Epping, A. Velty, *J. Catal.* 225 (2004) 316.
- [108] D. Tichit, A. Rolland, F. Prinetto, G. Fetter, M. J. Martínez-Ortíz, M. A. Valenzuela, P. Bosch, *J. Mater. Chem.* 12 (2002) 3832.
- [109] G. Fetter, A. Botello, V. H. Lara, P. Bosch, *J. Porous Mater.* 8 (2001) 227.
- [110] S. Möhmel, I. Kurzawski, D. Uecker, D. Müller, W. Gebner, *Cryst. Res. Technol.* 37 (2002) 359.
- [111] J. I. Di Cosimo, C. R. Apesteguía, M. J. L. Ginés, E. Iglesia, *J. Catal.* 190 (2000) 261.
- [112] Z. Pál, P. G. Menon, *Cat.Rev.-Sci.Eng* 25(2) (1983) 229.
- [113] Z. Paál, P. G .Menon, *Hydrogen Effects in Catalysis*, CRC, Press, New York, 1987.
- [114] C. H. Bartholomew, *Catal.Lett.* 7 (1990) 27.

- [115] S. Smeds, T. Salmi, L. P. Lindfors, O. Krause, *Appl.Catal.*, A. 144 (1996) 177.
- [116] P. Kramer, M. Andre, *J. Catal.* 58 (1979) 287.
- [117] G. D. Weatherbee, C. H. Bartholomew, *J. Catal.* 87 (1984) 55.
- [118] Y. Cesteros, P. Salagre, F. Medina, J. E. Sueiras, *Appl. Catal.*, B. 22 (1999) 135.
- [119] Y. Cesteros, P. Salagre, F. Medina, J. E. Sueiras, *Appl. Catal.*, B. 25(4) (2000) 213.
- [120] I. E. Maxwell, *Catal. Today.* 1 (1987) 385.
- [121] C. E. Webster, A. Cottone, R. S. Drago, *J. Am. Chem. Soc.* 121 (1999), 12127.
- [122] P. Canizares, A. De Lucas, F. Dorado, A. Duran, I. Asencio, *Appl. Catal.* 169 (1998) 137.
- [123] R. M. Barrer, *Zeolites and Clay Materials*, Academic Press, London, 1979.
- [124] J. Dedecek, B. Wichterlova, *J. Phys. Chem. B.* 103 (1999) 1462.
- [125] H. G. Karge, H. K. Beyer, *Molecular Sieves*, vol.3, Springer, Berlin, 2002.
- [126] J. Scherzer, A. J. Gruia, *Hydrocracking Science and Technology*, Marcel Dekker, New York, 1996.
- [127] A. Lugstein, A. Jentys, H. Vinek, *J. Chem. Soc. Faraday Trans.* 93 (1997), 1837.
- [128] A. Lugstein, A. Jentys, H. Vinek, *Appl. Catal. A: Gen.* 176 (1999) 119.
- [129] A. de Lucas, J. L. Valverde, F. Dorado, A. Romero, I. Asencio, *J. Mol. Catal.*, A. 225 (2005) 47.
- [130] B. I. Mosqueda-Jiménez, A. Jentys, K. Seshan, J. A. Lercher, *Appl. Catal.*, B. 43 (2003) 105.
- [131] M. B. Chanaa, M. Lallement, M. H. Simonot-Grange, G. Bertrand, *Thermochim. Acta.* 115 (1987) 317.
- [132] B. I. Whittington, N. B. Milestone, *Zeolites.* 12 (1992) 815.
- [133] A. Arafat, J. C. Jansen, A. R. Ebaid, H. van Bekkum, *Zeolites.* 13 (1993) 162.

Referencias bibliográficas

- [134] C. Chang, W. F. Zhang, L. H. Zhang, R. S. Li, M. W. Tian, X. W. Yang, L. Hou, *Chem. J. Chinese Univ.* 17 (1996) 1914.
- [135] Y. Kuroda, T. Okamoto, R. Kumashiro, Y. Yoshikawa, M. Nagao, *Chem. Comm.* 2002, 1758.
- [136] F. S. Xiao, W. G. Xu, S. L. Qiu, R. R. Xu, *Catal. Lett.* 26 (1994) 209.
- [137] F. S. Xiao, W. G. Xu, S. L. Qiu, R. R. Xu, *J. Mater. Chem.* 4 (1994) 735.
- [138] M. D. Romero, G. Ovejero, M. A. Uguina, A. Rodríguez, J. M. Gómez, *Catal. Commun.* 5.(2004) 154.
- [139] M. Zendehdel, M. Kooti, M. M. Amini, *J. Porous Mater.* 12 (2005) 143.
- [140] S. Kieger, G. Delahay, B. Coq, B. Neveu, *J. Catal.* 183 (1999) 276.
- [141] M. Suzuki, K. Tsutsumi, H. Takahashi, *Zeolites.* 2 (1982) 51.
- [142] T. T. Meek, R. D. Blake, J. D. Katzs, J. R. Bradbury, M. H. Brooks, *J. Mater. Sci. Lett.* 7 (1988) 311.
- [143] C. Gibson, I. Matthews, A. Samuel, *J. Microwave Power Electromag. Energy.* 23 (1988) 17.
- [144] M. Niwa, N. Kertada, *Catal. Surv. Jpn.* 1 (1997) 215.